COMMONWEALTH OF KENTUCKY
DEPARTMENT OF TRANSPORTATION
Division of Research
533 South Limestone
Lexington, KY 40508

CALVIN G. GRAYSON
SECRETARY

JULIAN M. CARROLL
GOVERNOR

H-2-72

August 29, 1978

MEMORANDUM TO: G. F. Kemper
State Highway Engineer
Chairman, Research Committee

SUBJECT: Research Report 502; "Determination of Rutting in Asphaltic Concrete Pavements: Field Instrumentation and Laboratory Characterizations;" KYHPR-72-72; HPR-PL-1(14), Part II.

Report 502 relates progress toward solving an old, enigmatic problem: rutting in asphaltic concrete pavements. Some 14 miles of I 75 in Rockcastle County were milled (1977) to re-smooth the surface, which had become uneven because of ruts. Ruts develop more on upgrades than on downgrades. Dwell-time, or speed of travel, load on the wheels, and number of wheel passes are the combined, forcing factors. Stiffness and thicknesses of the pavement layers combine to resist deformation. Rutting without attendant cracking is interpreted as viscous and(or) plastic shear. Rutting interferes with the normal runoff of water from pavements and increases the hazards of wet-weather driving. In effect, rutting caused by deformation is not unlike rutting caused by wear -- that is, like wear induced by studded tires.

Our pavement studies in 1957 (Report 135) involved trenching across wheel paths to expose a cross section for inspection and measurement of rutting in the layers and subgrade. It appeared that about 85 percent of the rutting was in the subgrade. Only a slight amount was attributed to thinning of the asphaltic concrete. Then, thicknesses of asphaltic concrete in pavements were somewhat less than they are now. Studies by others, elsewhere, have attributed rutting principally to thinning of the asphalt layer in the wheel paths.

The timeliness of these studies is apparent in the design strategies coming under consideration for the KY 80 reconstruction in eastern Kentucky (Hazard-Watergap). To provide further reassurances that rutting occurs largely in the subgrade material, a truck lane on the Daniel Boone Parkway, westward from the toll plaza at Hyden, will be trenched and examined this season. It is planned also to scribe lines (in the surface) transversely across the wheel paths in order to detect any movement downgrade which would be attributable to traction of drive-wheels. Descriptions and photos, there, may precede issuance of this report.

Respectfully submitted,

Jas. H. Havens

Jas. H. Havens
Director of Research

gd
Encl.
cc's: Research Committee

Technical Report Documentation Page

1. Report No.	2. Government Accession No.	3. Recipient's Catalog No.

4. Title and Subtitle
Determination of Rutting in Asphaltic Concrete Pavements: Field Instrumentation and Laboratory Characterizations

5. Report Date
August 1978

6. Performing Organization Code

7. Author(s)
David L. Allen

8. Performing Organization Report No.
502

9. Performing Organization Name and Address
Division of Research
Kentucky Department of Transportation
533 South Limestone
Lexington, KY 40508

10. Work Unit No. (TRAIS)

11. Contract or Grant No.
KYHPR-72-72

12. Sponsoring Agency Name and Address

13. Type of Report and Period Covered
Interim

14. Sponsoring Agency Code

15. Supplementary Notes
Prepared in cooperation with the US Department of Transportation, Federal Highway Administration
Study Title: Determination of Flexible Pavement Rutting Behavior

16. Abstract

This report describes a number of gages developed to measure the location and magnitude of ruts. These were installed in a newly constructed asphaltic concrete pavement. They measure lateral deflections and transient and permanent vertical deflections. Some preliminary vertical deflections are reported. An investigation of materials is also reported. The asphalt concrete base, dense-graded aggregate base, and subgrade material were characterized by (1) shear strength (triaxial tests), (2) rheologic behavior (creep tests), (3) permanent deformation characteristics (repeated-load and creep tests), (4) Young's modulus (resonant column tests), and (5) resilient properties (repeated-load tests). Empirical functions were formulated to describe the permanent deformation characteristics of all three materials.

17. Key Words	18. Distribution Statement
pavement rutting flexible pavement material characterization permanent deformation resonant column repeated-load tests Young's Modulus resilient properties	

19. Security Classif. (of this report)	20. Security Classif. (of this page)	21. No. of Pages	22. Price
Unclassified	Unclassified		

Research Report
502

DETERMINATION OF RUTTING IN ASPHALTIC CONCRETE PAVEMENTS: FIELD INSTRUMENTATION AND LABORATORY CHARACTERIZATIONS

Interim Report
KYHPR-72-72; HPR-PL-1(14), Part II

by

David L. Allen
Research Engineer Chief

Division of Research
Bureau of Highways
DEPARTMENT OF TRANSPORTATION
Commonwealth of Kentucky

in cooperation with the
US Department of Transportation
Federal Highway Administration

August 1978

INTRODUCTION

The behavior of asphalt-bound layers, unbound aggregate bases, and foundation soil (subgrade) can be affected by such variables as gradation, asphalt and(or) moisture content, type of aggregate, density, method of compaction, temperature, magnitude and frequency of loading, duration of each load cycle, and other less significant variables. The complex interaction of all these variables will yield a composite behavior for a particular pavement structure that could become manifest in some form of distress or even complete "failure".

Flexible pavements are known to be highly susceptible to rutting. It is not well known where and to what extent rutting takes place within a pavement structure. Rutting is a result of wheel passes recurring in paths within a lane. The distribution or scatter of wheel passes will generally approximate a normal distribution curve. Figure 1, taken from P. J. Van de Loo *(37)*, is an example of a typical wheel distribution pattern. It shows that a large percentage of wheel passes will occur within relatively narrow paths on the pavement surface. It is this distribution of traffic that causes accumulated deformations to occur, producing ruts. If these ruts are to be estimated or predicted, for design purposes, the behavior of the materials under consideration must be known or "parameterized".

BACKGROUND

Pagen *(26)* indicated that the mechanical properties of dense bituminous concrete mixtures may be expressed by linear viscoelastic theory to a useful degree of approximation. However, Lai and Anderson *(16)* suggested that nonlinear viscoelasticity is a much better indicator of behavior. Monismith and Secor *(21)* gave a detailed discussion of the viscoelastic response of asphaltic paving slabs under creep loading. Tons, et al., *(36)* have studied extensively the flow properties of aggregate-binder mixtures. Saal and Labout *(28)* described the rheological properties of asphalts as affected by temperature and stress level. Van der Poel *(38)* has shown the effects of time and temperature on the deformation of asphaltic bitumens and bitumen-mineral mixtures under various experimental conditions.

Many researchers including Witczak and Root *(39)*, Saraf and Majidzadeh *(29)*, Kallas and Riley *(15)*, Terrel, et al., *(34)*, and Monismith, et al., *(22)* have reported on the dynamic responses of bituminous concretes. Others including Morris and Haas *(23)*, Mclean and Monismith *(20)*, Terrel, et al., *(35)*, and Barksdale and Miller *(5)* have studied the permanent deformation characteristics of bituminous concretes.

Much has been done on determining the resilient properties and the permanent deformation characteristics of untreated, granular, base-course materials. Smith and Nair *(32)*, Hicks *(11)*, and Barksdale *(4)* reported that the resilient modulus can be considered a function of the average principal stresses and can be represented mathematically by a power law function. Smith and Nair *(32)* showed that the resilient Poisson's ratio can be considered a constant value, independent of stress state. The same authors stated that a value of 0.35 is a reasonable, average Poisson's ratio for partially saturated material.

Drake and Havens *(8)* reported the results of surface rutting measurements on 94 bituminous concrete pavements in Kentucky. Eight locations having medium to severe rutting were opened by careful trenching methods. It was then noted that only four percent of the rutting was in the bituminous layer and 72 percent in the base, consisting of water-bound macadam. They concluded the "deformations must result primarily from particle rearrangement and movement and must be the combined result of upheaval and subsidence."

Barenberg and Thompson *(3)* included pavement structures in a circular test track that were identical to some sections of the AASHO Road Test pavements. Pavements tested had surface-base-subbase thicknesses (in inches) of (1) 2-3-0, (2) 3-0-0, (3) 2-3-0, and (4) 1-6-0. Generally, those pavement structures suffered very little rutting damage until the subgrade, granular layers, and surface were saturated to duplicate spring-thaw conditions. Upon completion of saturation and drainage, resumption of loading produced severe rutting. After opening the sections, it was found that most of the rutting occurred in the granular base materials. It was concluded that "distress is probably caused by inadequate stability of the granular materials -- a condition greatly aggrevated by excess water in the pavements. The only way in which water in the subgrade had any apparent effect is by the creating of a weakened plane at the interface between the subgrade and the granular layers."

The cited studies suggest that when the granular layers were saturated, wheel loads cause sufficient pore pressures to reduce particle friction, allowing particle reorientation. The net result is a possible combination of dilation and shear failure.

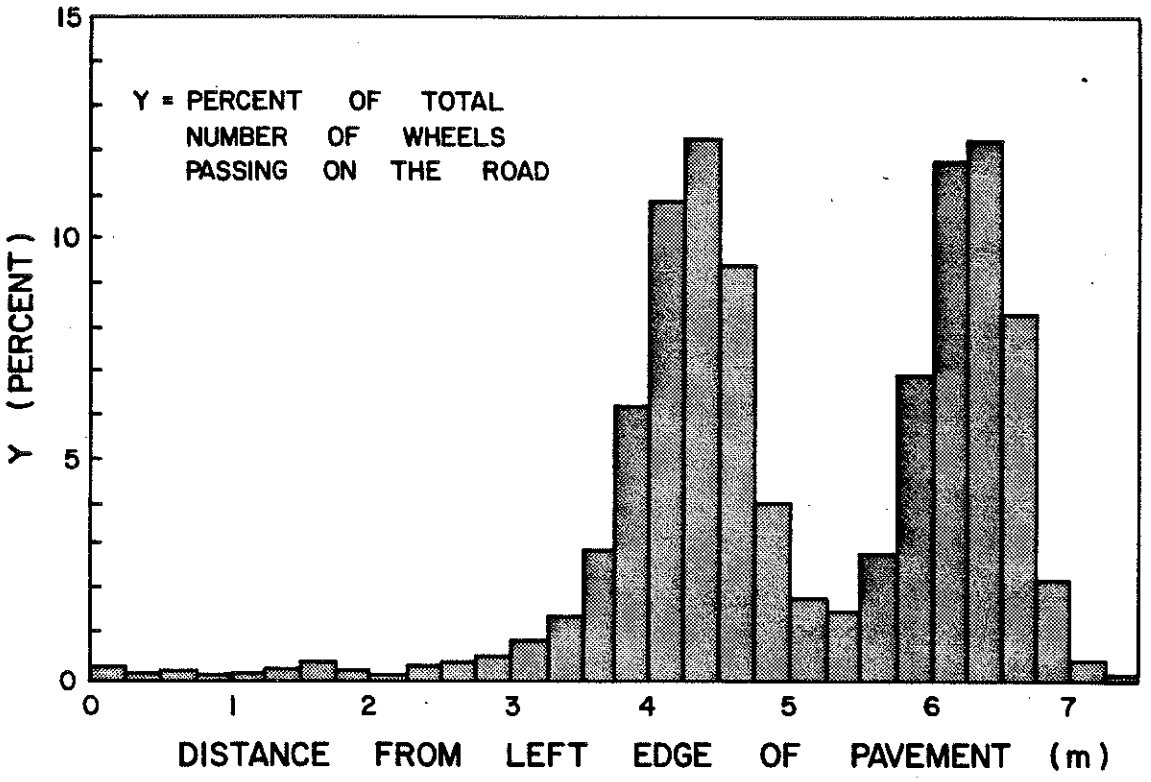

Figure 1. **Typical Distribution of Wheel Passes Across a Pavement Cross-Section (Reference 37).**

INVESTIGATIVE APPROACH

Objectives of this study are as follows:

1. to develop or adapt instrumentation to determine where and to what extent rutting occurs within a pavement system,
2. to formulate or describe the mechanistic behavior of rutting, and
3. to correlate laboratory data with actual field measurements.

The first objective was to measure lateral movement throughout the entire pavement structure and into the subgrade. Transient and permanent vertical displacements would be measured at each interface and at the pavement surface.

To fulfill the second objective, the pavement materials were tested for their shear strength (triaxial tests), rheologic behavior (creep tests), permanent deformation characteristics (repeated-load and creep tests), Young's modulus (resonant column tests) and resilient properties (repeated-load tests). Tests for the resilient Poisson's ratio were not attempted. Barksdale *(4)* had indicated that moderate changes in mixture variables do not greatly affect rutting characteristics; therefore, it was decided not to "parameterize" the materials according to these variables; an extremely large volume of testing would have been required. Also, the sand-asphalt surface course was not tested.

The third objective required summaries or models of traffic and environmental conditions experienced in the field. Therefore, temperature distributions, moisture contents, and traffic characteristics were determined.

Figure 2 is a simplified flow chart of this study, showing the anticipated lines of investigation. The shaded portions indicate those items completed. This report is largely concerned with the design and installation of field instrumentation and with results of the laboratory investigation.

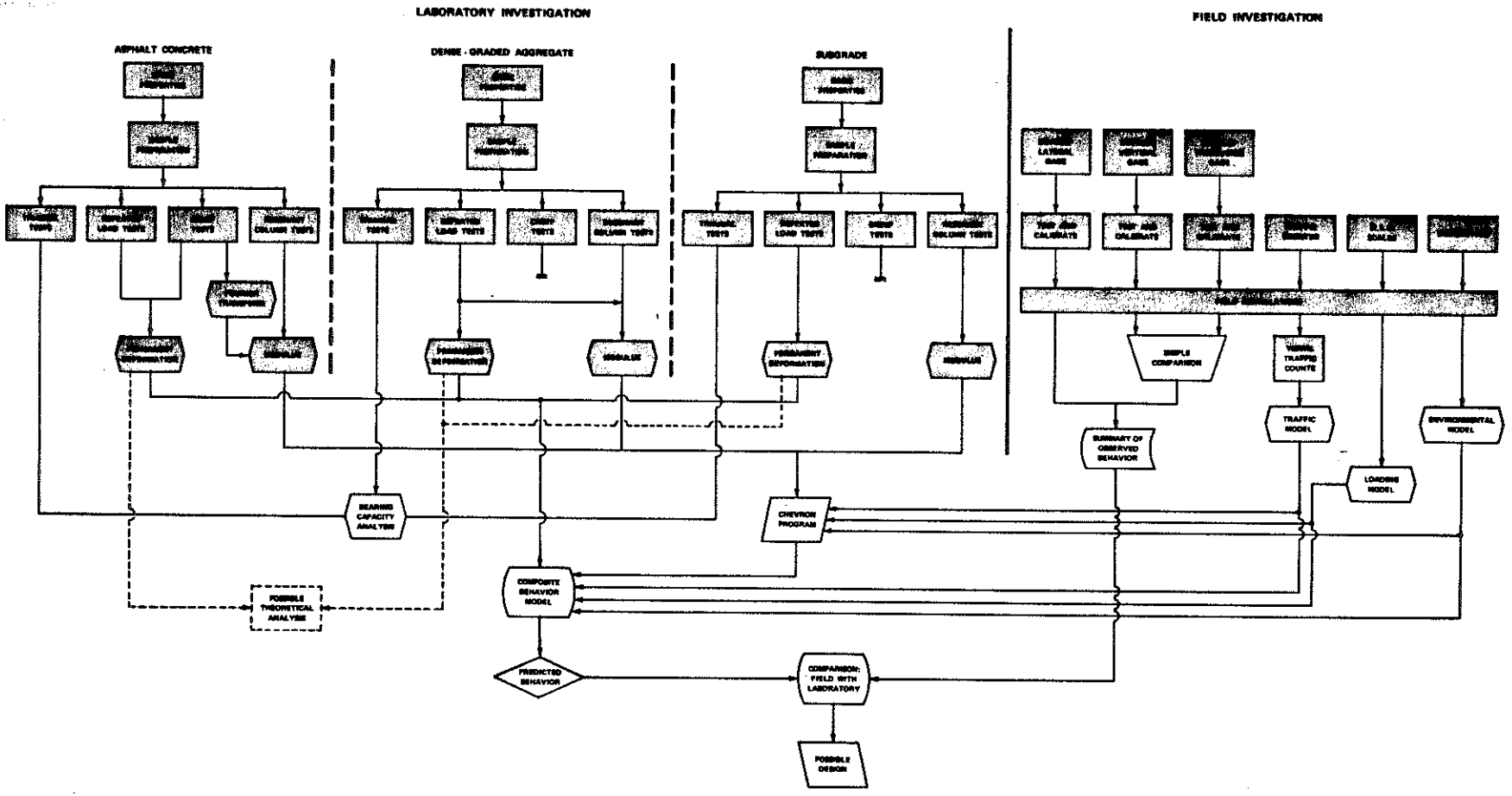

Figure 2. Simplified Flow Chart of Research Study KYHPR-72-72.

FIELD INVESTIGATION

The field instrumentation is located on a rural, two-lane highway (KY 627) in Clark County. The site (Station 141 + 50) is on a grade of +0.80 percent and a 45-minute curve. The roadway is in transition from a small cut to a small fill section. Figure 3 is a general view of the site.

The subgrade is constructed of "shot" rock indigenous to the area. The rock is composed chiefly of stone from the Tanglewood and Branon members of the Lexington Limestone Group. These members are largely thick beds of highly fossiliferous limestone, interbedded with thin layers of clay shales. The clay shales comprise 20 to 30 percent of the material and are highly susceptible to mechanical breakdown and weathering.

The remainder of the pavement section is constructed of 9.5 inches (241 mm) of dense-graded aggregate (gradation shown in Figure 40), 5.5 inches (140 mm) of asphaltic concrete base (gradation shown in Figure 26) and 0.75 inch (19 mm) of sand asphalt. Details of construction are being reported by Newberry *(25)*.

This site was chosen for the following reasons: (1) its accessibility, (2) the geometrics were such that speeds would probably be normal for an "open" highway, (3) no cross roads or entrances were close, (4) drainage appeared to be good, (5) traffic volumes were moderate (ADT $\approx$ 2,000), and (6) the percentage of heavily loaded truck traffic appeared to be high.

To determine the types and, hopefully, the magnitude of movements within the pavement structure, a number of gages were developed and installed.

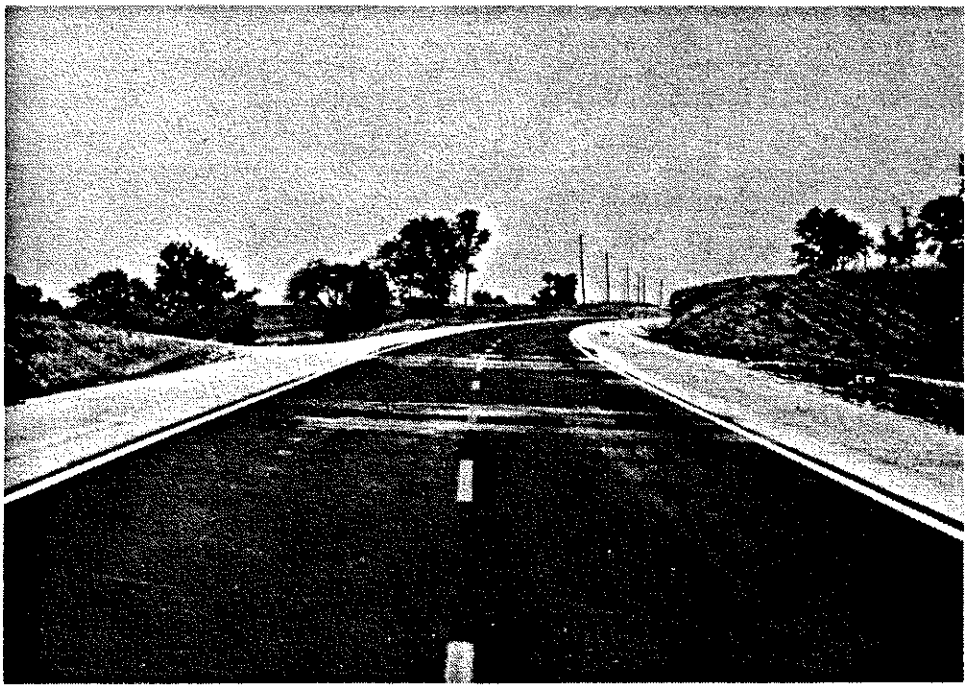

Figure 3. General View of Instrumentation Site at Station 141 + 50 on KY 627, Clark County.

LATERAL DEFLECTION GAGE

The principle and design of this unit are based upon the larger slope inclinometers sold commercially and used to measure deflections in earth structures. This unit consists primarily of an accelerometer glued in the end of a 0.25-inch (6.4-mm) O.D. polyethylene tube, as shown in Figures 4 and 5. The accelerometer, Model No. EGAL-125-5, was purchased from Entran Devices, Inc., Little Falls, New Jersey. The accelerometer is basically a mass mounted at the end of a cantilever beam. The beam is equipped with four semiconductor strain gages mounted at the point of maximum bending (Figure 4). As the accelerometer is held vertically, the force of the mass acts along the axis of the beam; and the accelerometer reading is zero. However, as the unit is tilted from the vertical, gravity causes the mass to bend the beam and produce a readout from the strain gages. The required accelerometer excitation is 15 volts DC and the output is read from a DC recorder or a DC voltmeter.

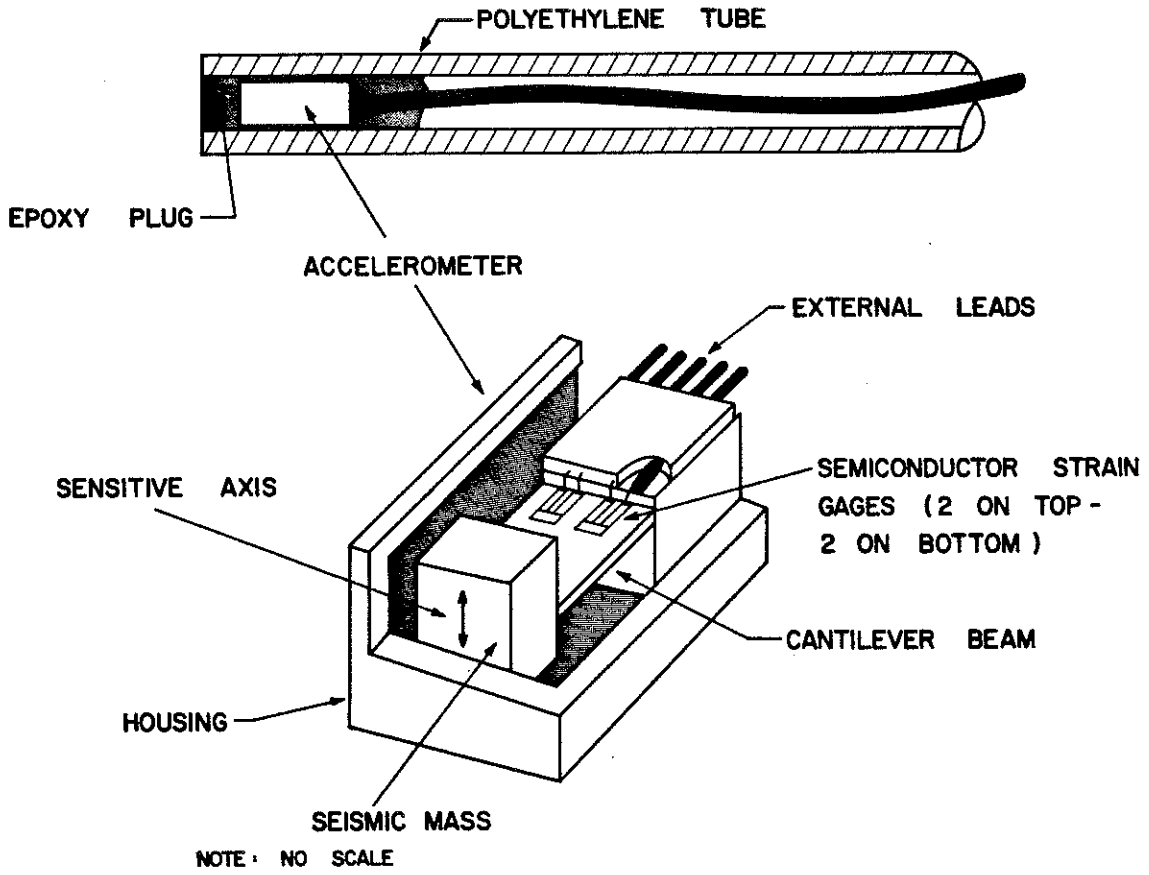

Figure 4. Schematic Diagram of the Accelerometer in the Lateral Deflection Gage and a Sketch Showing Its Installation in the Polyethylene Tube.

Figure 5. An Assembled Lateral Deflection Gage.

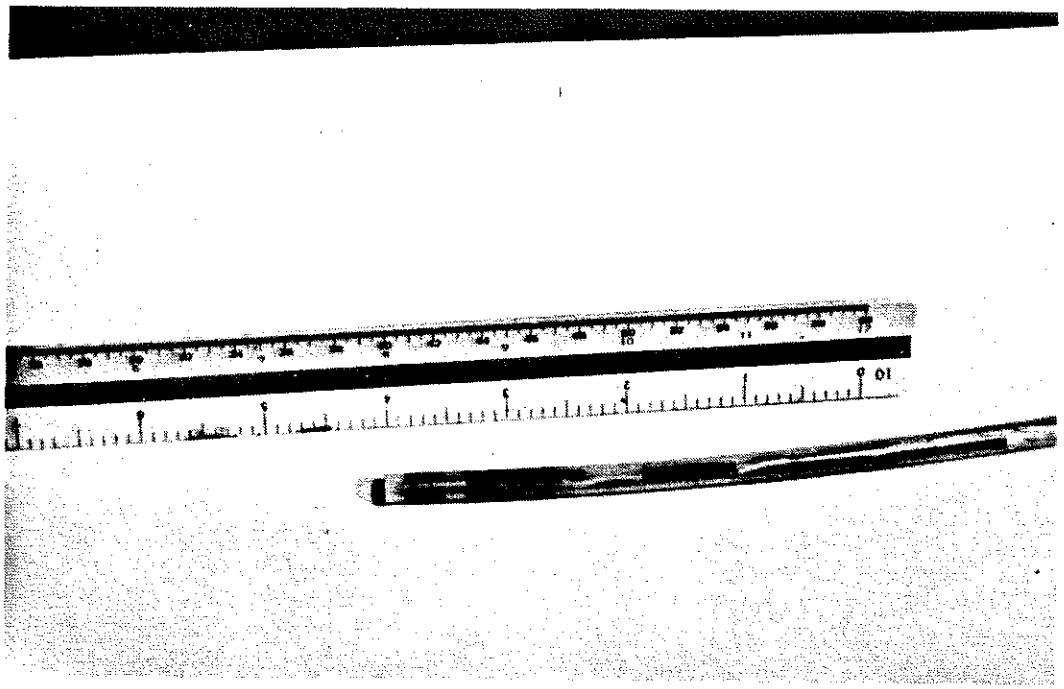

A 24-inch (610-mm) piece of polyethylene tubing, 0.38 inch (9.5 mm) O.D., serves as a "casing" for this gage. Four small cuts approximately 0.5 inch (12.7 mm) long are made at the top end of the casing tube and the four resulting "flaps" are folded outward. The "flaps" are fastened between two stainless steel washers, and a steel cover is placed over the steel washers to prevent foreign matter from entering the "casing" tube. A detailed drawing of this assembly is shown in Figure 6. The casing tube is installed after completion of the pavement. A hole, large enough to accommodate the tube, is drilled vertically through the pavement and several inches into the subgrade. (In this case, it was approximately 8 inches (200 mm) into the subgrade.) The hole is then "backfilled" with an asphalt emulsion to eliminate voids that might remain between the hole wall and the tube. Afterwards, the top cap assembly is set flush with the pavement surface and sealed with epoxy. Figure 6 shows how an installation is made, and Figure 7 is a closeup of one of the units installed.

To read this gage, the 0.25-inch (6.4-mm) O. D. tube containing the accelerometer is inserted to the bottom of the casing tube and is then withdrawn 1 inch (25.4 mm) at a time for reading. After one axis has been read, the accelerometer is turned 90 degrees and reinserted into the casing tube and the reading process is repeated. It appears that the accelerometer tube does not "twist" but that the axes of the two tubes remain properly aligned during insertion. However, to insure against twisting and, consequently, an improper accelerometer reading, each axis is read three times and an average value is computed and recorded.

Figure 8 illustrates how horizontal displacement at any point along the casing is calculated. The accelerometer can be calibrated to read any predetermined voltage at the maximum deflection of 90 degrees from vertical (in this case 1.0 volt). The sine of the angle, ζ, being read is then directly proportional to, and linear with, the voltage output. For example, if the angle is 45 degrees, the sine would be 0.707; therefore, the output would read 0.707 volt. The horizontal deflection, δ_i, is then calculated by multiplying the sine of the angle by the distance between readings or slope distances, x_i. In this case, the slope distance, x_i, was 1 inch (25.4 mm). The total horizontal displacement at some point on the casing is the sum of all δ_i's from the bottom of the casing.

The locations of the top caps were surveyed very accurately. More surveys will be made in the future and compared with the initial survey. The difference between these surveys will equal the displacement of the top cap. This displacement will be compared to that calculated using the accelerometer, and the difference, if any, will be assumed to be movement of the bottom of the casing.

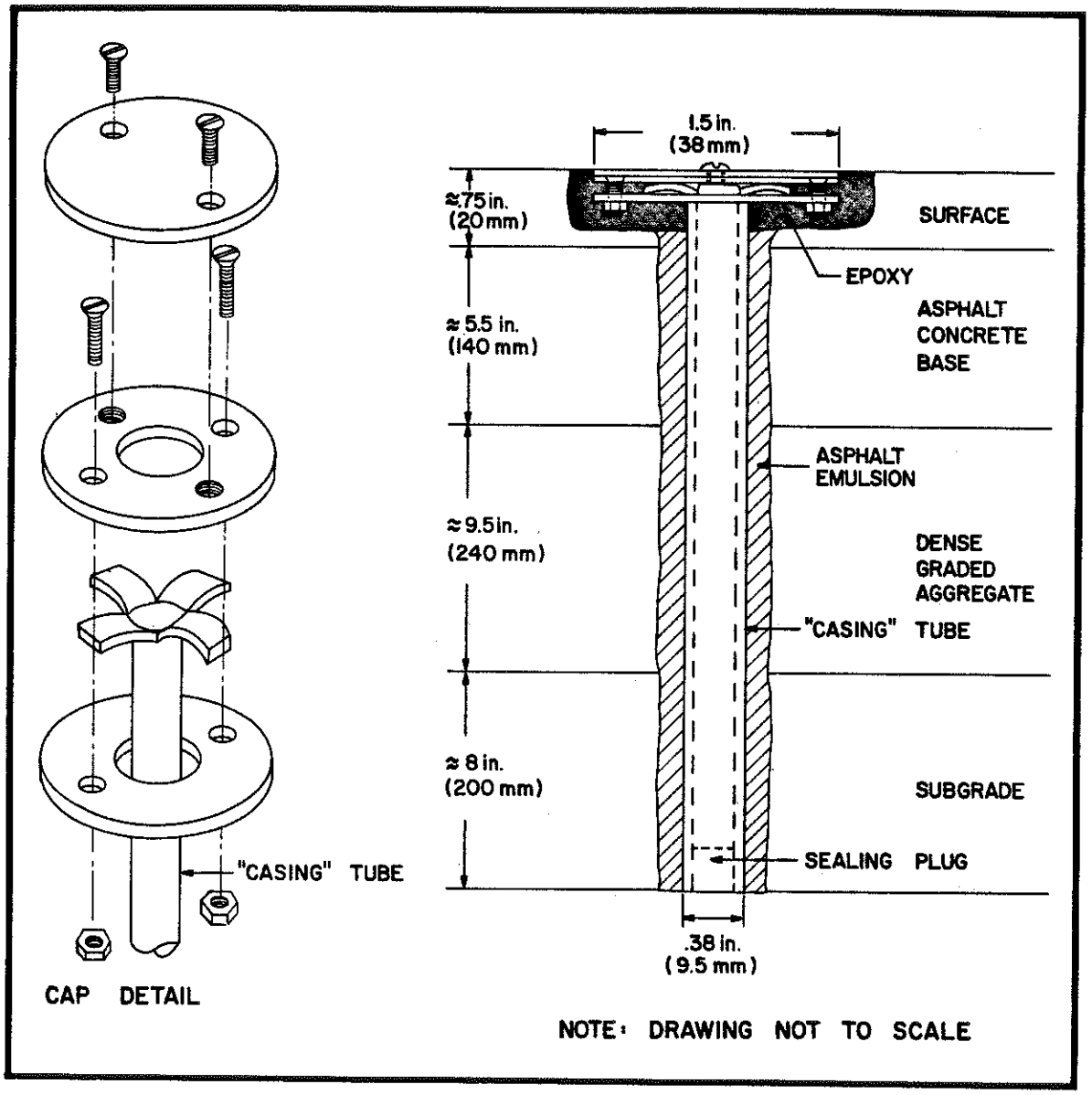

Figure 6. **Cap Detail for "Casing" Tube and a Typical Installation of "Casing" Tube.**

Figure 7. Photograph of a Lateral Deflection Gage Installation.

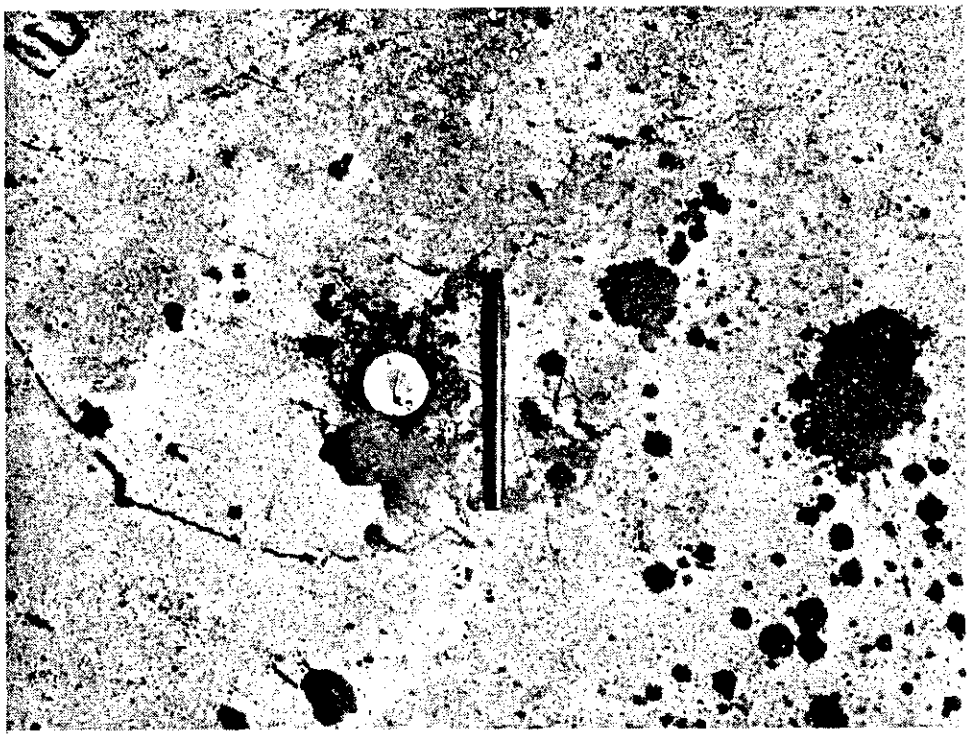

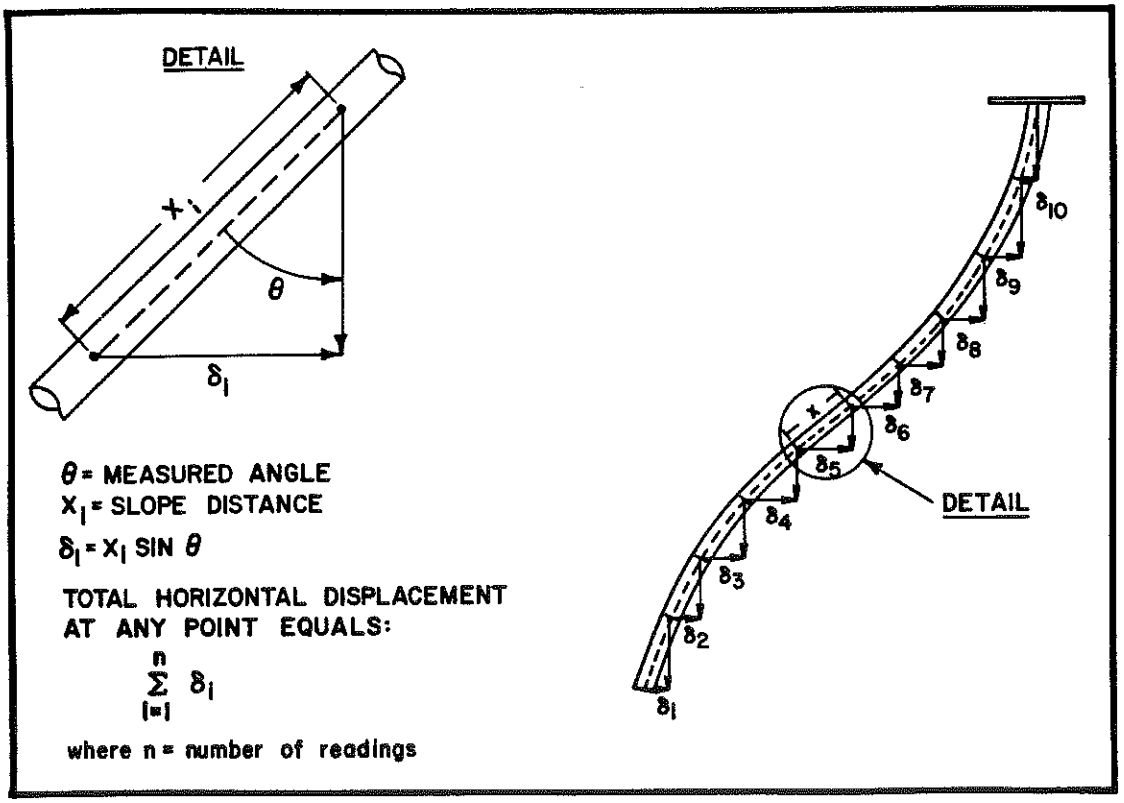

Figure 8. Detail of Horizontal Displacement Calculations from the Lateral Deflection Gage.

Six lateral deflection gages were installed in Clark County in the configuration shown in Figure 9. It is expected that these will detect any lateral movement at any depth greater than 1 inch (25.4 mm). The rigidity of the tube near the top cap will not permit sufficient bending to read deflections at depths of less than 1 inch (25.4 mm).

PERMANENT DEFLECTION GAGE

Four of these gages were installed. Two were placed transversely the entire width of the roadway at the interface between the subgrade and the dense-graded aggregate; the remaining two were similarly placed at the interface between the dense-graded aggregate and the asphaltic concrete base. A companion gage was installed at each interface to serve as a "back-up", in case the other gage failed to operate.

The principle of these gages is the same as that of the mercury-filled settlement gage. In fact, these are merely miniaturized settlement gages. They consist of two 0.063-inch (1.6 mm) O.D. polyethylene tubes -- one for air and one for mercury. The mercury line is cut every 12 inches (305 mm) and rejoined with a stainless steel union. A wire is soldered to each union and is run to an electrical plug at the end of each gage. The two small tubes, the steel unions, and the electrical wires are then pulled into a 0.63-inch (16.0 mm) O.D. polyethylene tube and sealed at both ends with epoxy. Figure 10 is a close-up view of a steel union on the mercury tube. Figure 11 shows a completed gage before installation. The wires from each steel union and the electrical plug may be seen in the lower right-hand corner of the photograph.

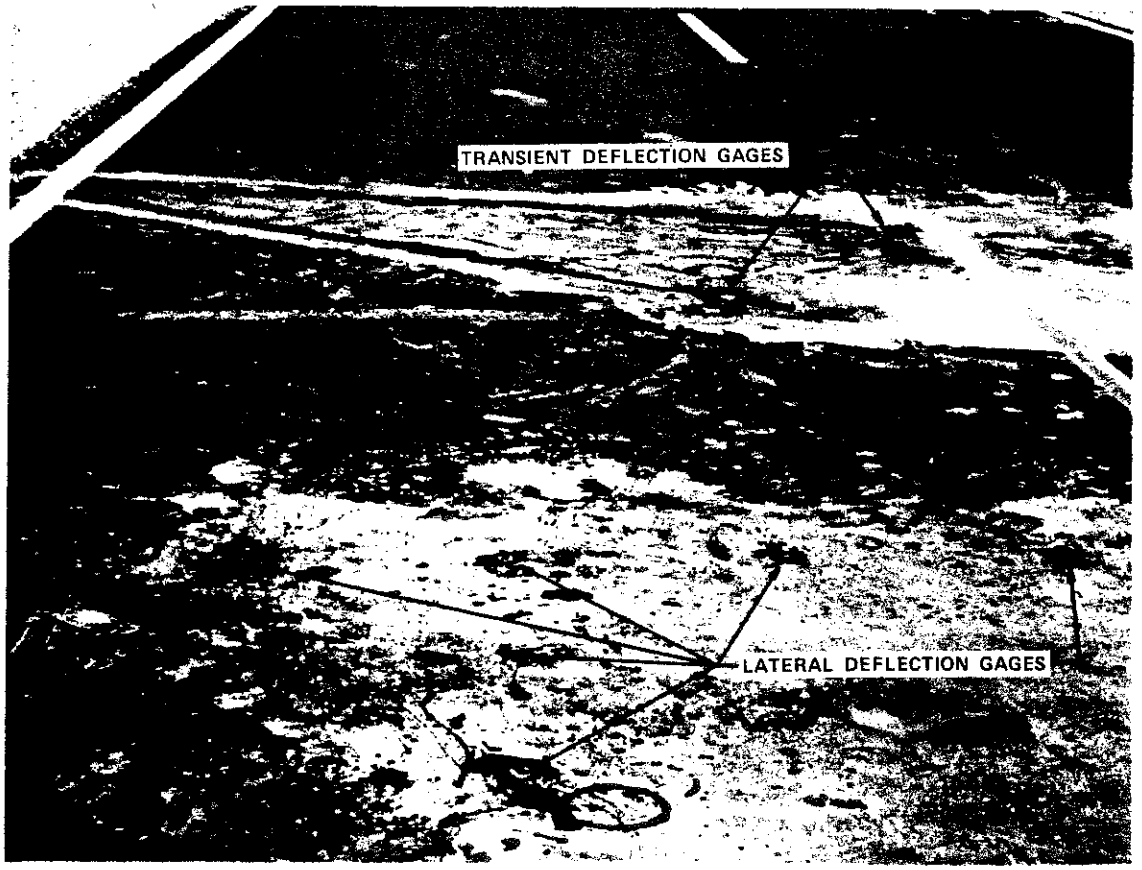

Figure 9. Installation Configurations of the Lateral Deflection Gages and the Transient Deflection Gages.

Figure 10. Close-Up View of a Steel Union on a Permanent Deflection Gage.

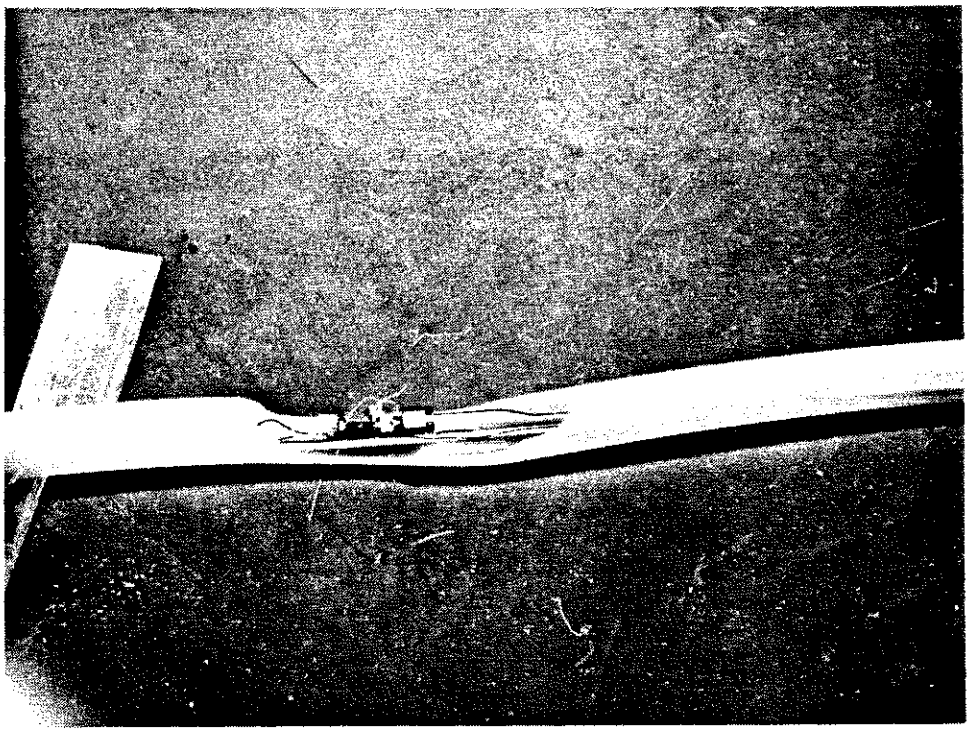

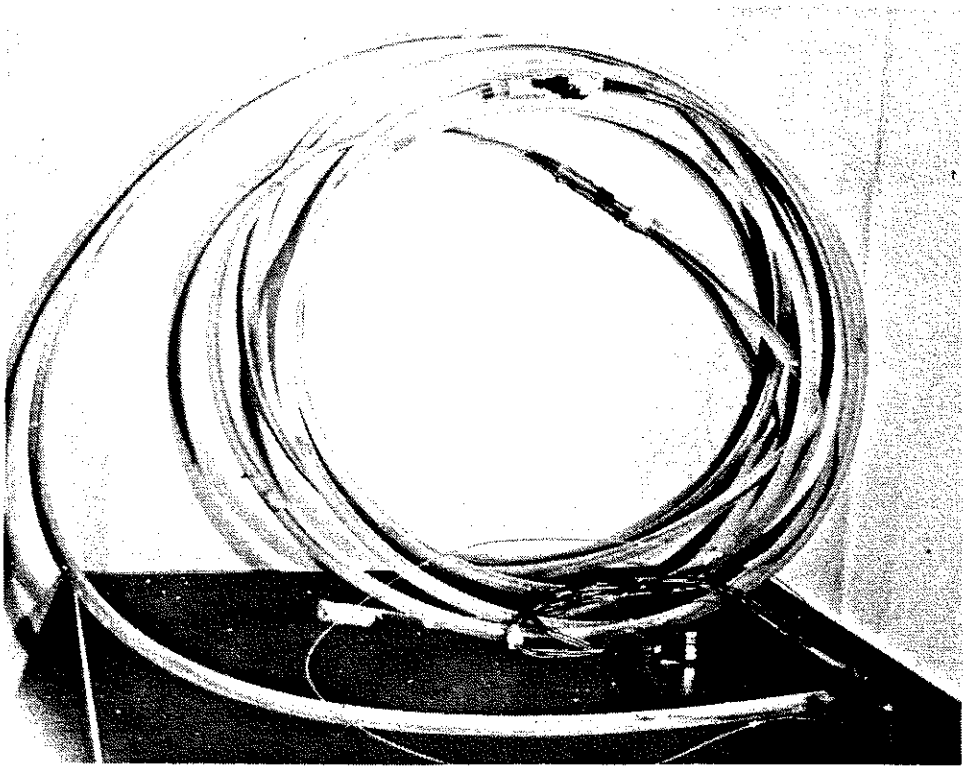

Figure 11. An Assembled Permanent Deflection Gage.

The ends of all four gages were brought to a common point approximately 13 feet (4 m) from the edge of the pavement. They were set in a concrete slab approximately 2 feet by 2 feet (0.61 m by 0.61 m). They were then protected by a weathertight steel cover approximately 2 inches (51 mm) high (Figure 15).

Briefly, the settlement gage is read by pouring a calculated quantity of mercury (determined by the length of the gage) into one tube until it is filled. Some mercury is then allowed to flow out, under pressure, until electrical contact is broken at the most remote point (steel union) on the gage. This is indicated on an ohm meter. The pressure necessary to hold the column of mercury between this point and a point of known elevation (initial point) at the remote end of the gage is read from a manometer. This pressure is converted to an elevation difference using the density of mercury. A detailed discussion of the theory and operation of mercury-filled settlement gages was reported by Hopkins and Deen *(13, 14)* in 1972.

TRANSIENT DEFLECTION GAGE

This gage was designed to measure transient deflections within individual pavement layers produced by moving vehicles. It is based on a gage developed and reported by the Road Research Laboratory in England *(19)*. Figure 12 is a schematic drawing of the gage. The outer casing consists of polyvinyl chloride tubing approximately 2 inches (51 mm) in diameter, with brass caps at the bottom and top. The center of the tube is constructed with a slip joint and a compressible rubber ring. This allows the gage to compress and rebound with the pavement layers. A brass ring, constructed to hold a LVDT, is threaded into the top portion of the gage. The LVDT probe rests upon a brass, adjustable, datum rod threaded into the bottom cap. Figure 13 is a photograph of an assembled gage before installation.

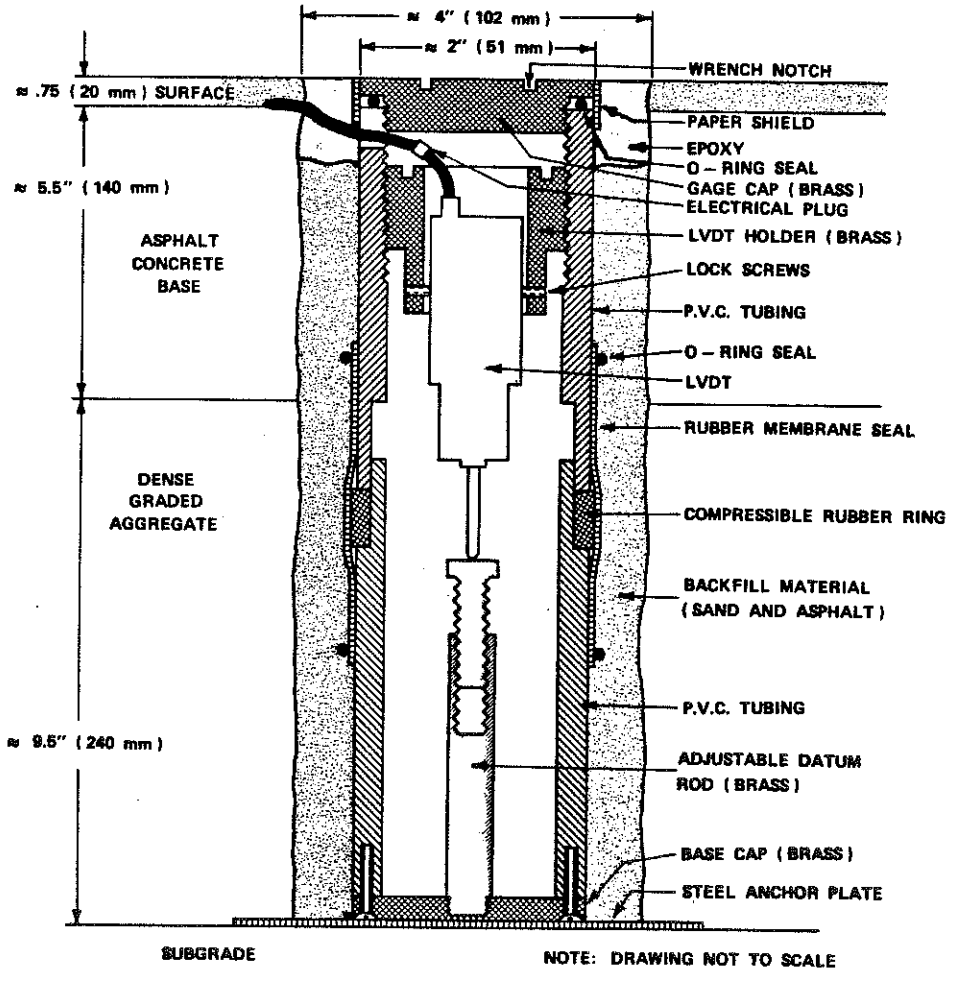

Figure 12. Schematic Diagram of a Transient Deflection Gage.

To measure the combined compression of the surface, asphaltic concrete base, and dense-graded aggregate layers, collectively, a steel plate is placed on the subgrade just before the dense-graded aggregate is placed. After the surface is completed, a hole 4 inches (102 mm) in diameter is drilled through these layers to the plate. The gage is set on the plate, and the hole is backfilled with a sand-asphalt mixture. The top inch (25.4 mm) of the hole is then sealed with epoxy. A groove is sawed in the pavement from the gage to the readout box at the edge of the shoulder (Figure 15). The same readout box is used for the permanent deflection gage. The electrical lead for the LVDT is laid in the groove, and the groove is sealed with an asphalt emulsion. Figure 14 shows a completed installation.

To measure compression of only the surface and the asphaltic concrete base, a gage similar to the one just described is installed on a plate placed, during construction, on the surface of the dense-graded aggregate. Unlike the first gage, the second one does not have an adjustable stem, but the LVDT probe rests on the bottom brass cap. Otherwise, the construction, installation, and operation of the second gage is identical to the first. Figure 9 shows a close-up view of the locations of the transient deflection gages.

To read the gage, the top cap is removed from the gage and the LVDT is inserted and locked into place. It is then "zeroed" by adjusting the height of the brass LVDT holder. The top cap is replaced and traffic is allowed to pass over it. The output is recorded on an ocillographic recorder at the readout box located at the edge of the shoulder.

The transient compression, or deflection, if any, in the dense-graded aggregate layer is simply the difference in the deflections of the two gages. The difference between the total surface deflection and the deflection of the first gage (the gage that is anchored on the top of the subgrade) is equal to the deflection of the subgrade.

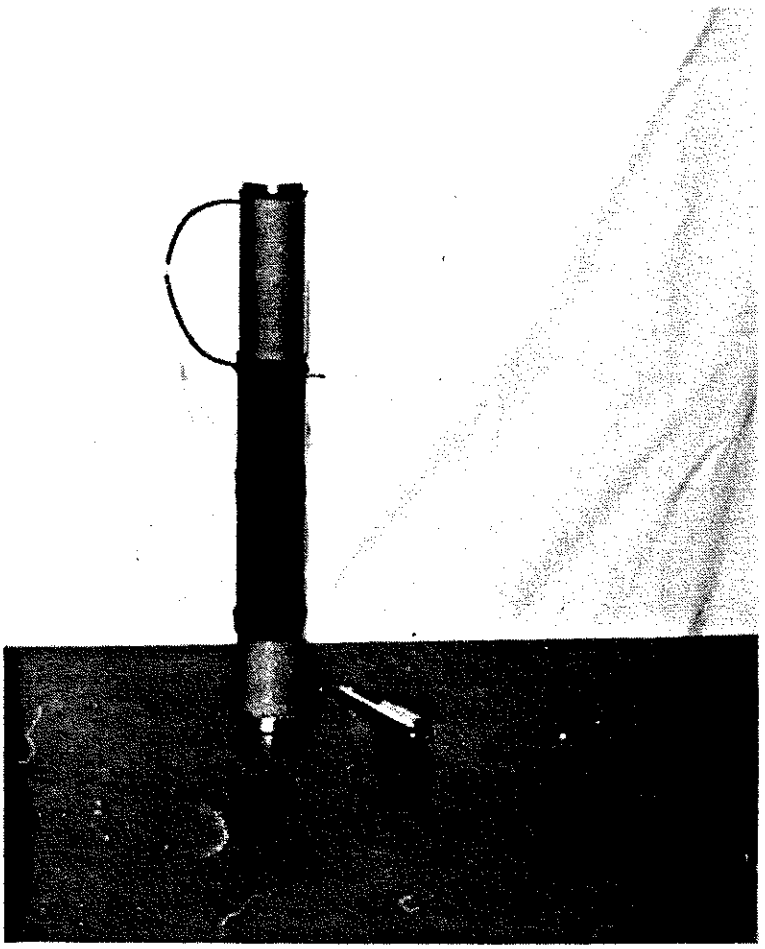

Figure 13. An Assembled Transient Deflection Gage.

Figure 14. An Installed View of a Transient Deflection Gage.

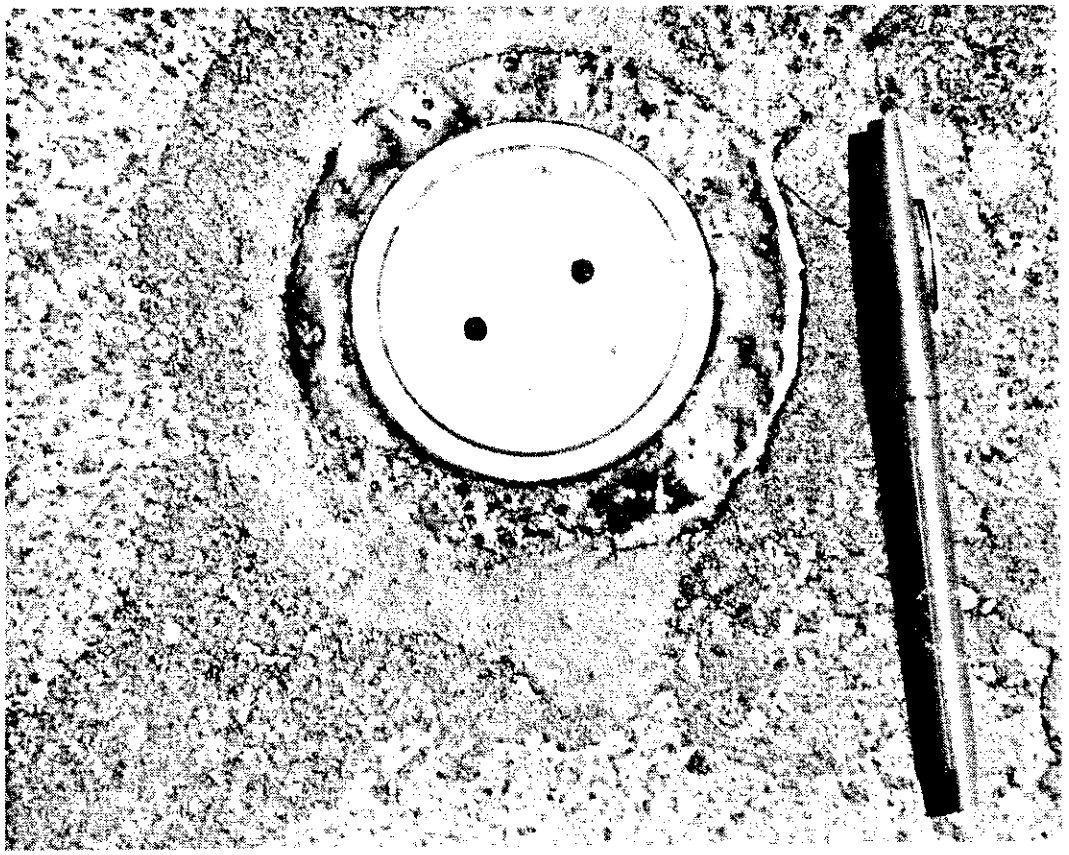

OTHER INSTRUMENTATION

To determine patterns of loading on the pavement, it is necessary to know characteristics of the traffic stream. For this purpose, two permanent traffic counters were installed to determine volume. Also, visual counts have been and will be made to determine the characteristics of the traffic stream such as average speed, vehicle spacing, and percentage of trucks.

"Weighing-In-Motion" scales were installed to determine vehicle weights. However, at the time of this writing, the scales are inoperable; and no usable data have been obtained.

Additionally, to determine the temperature distribution throughout the asphalt-bound layers, continuously recording thermistors were installed at every 0.5 inch (12.6 mm) of depth. Figure 15 shows the location of all instrumentation.

PRELIMINARY RESULTS

Figures 16 through 18 show some very preliminary results from the permanent deflection gages. These data had not been checked or thoroughly analyzed, therefore, they are presented here with only one comment. It does appear that some "rutting" may be developing at the site. The magnitudes of the "rutting" and the changes in elevation of the surface and interfaces are presently inexplicable.

Figure 15. General View of Instrumentation Site Showing Locations of All Instrumentation.

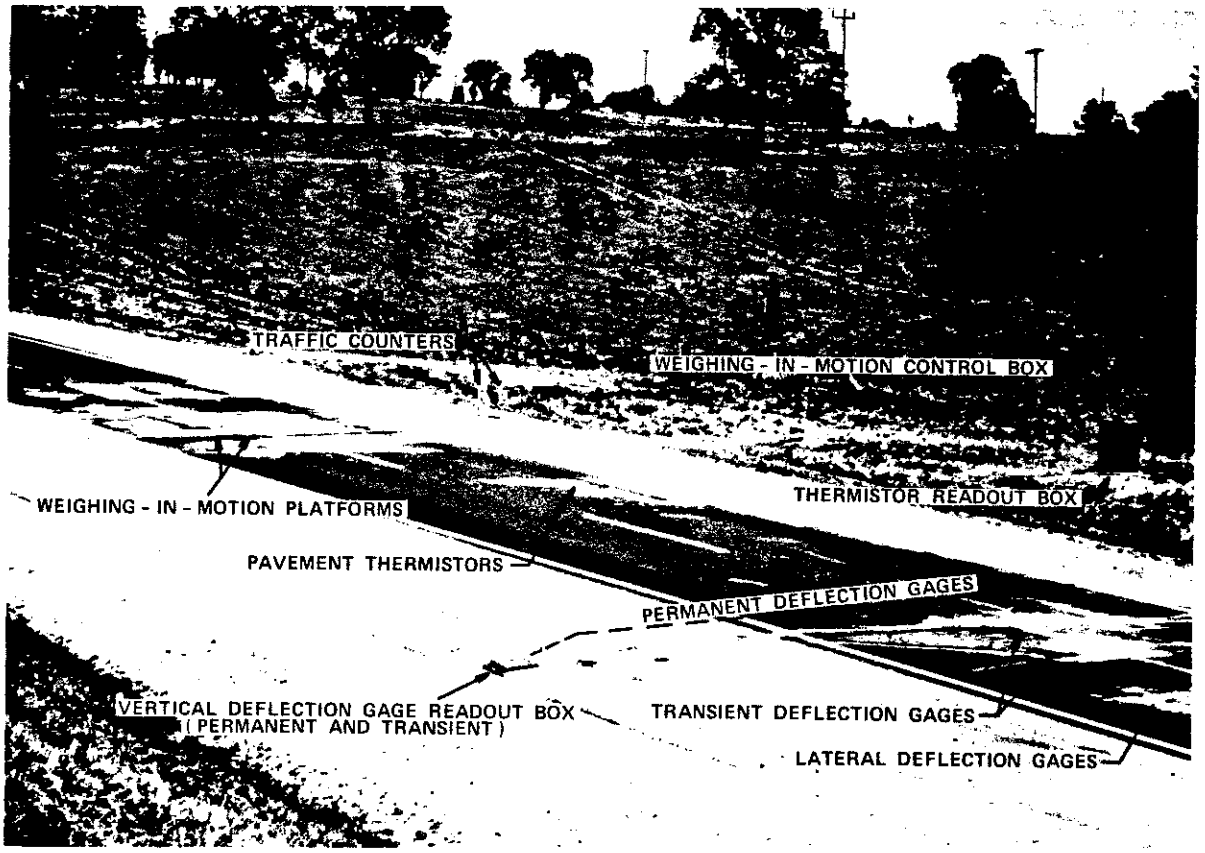

Figure 16. Apparent Rutting of Roadway Surface at Station 141 + 50 on KY 627, Clark County.

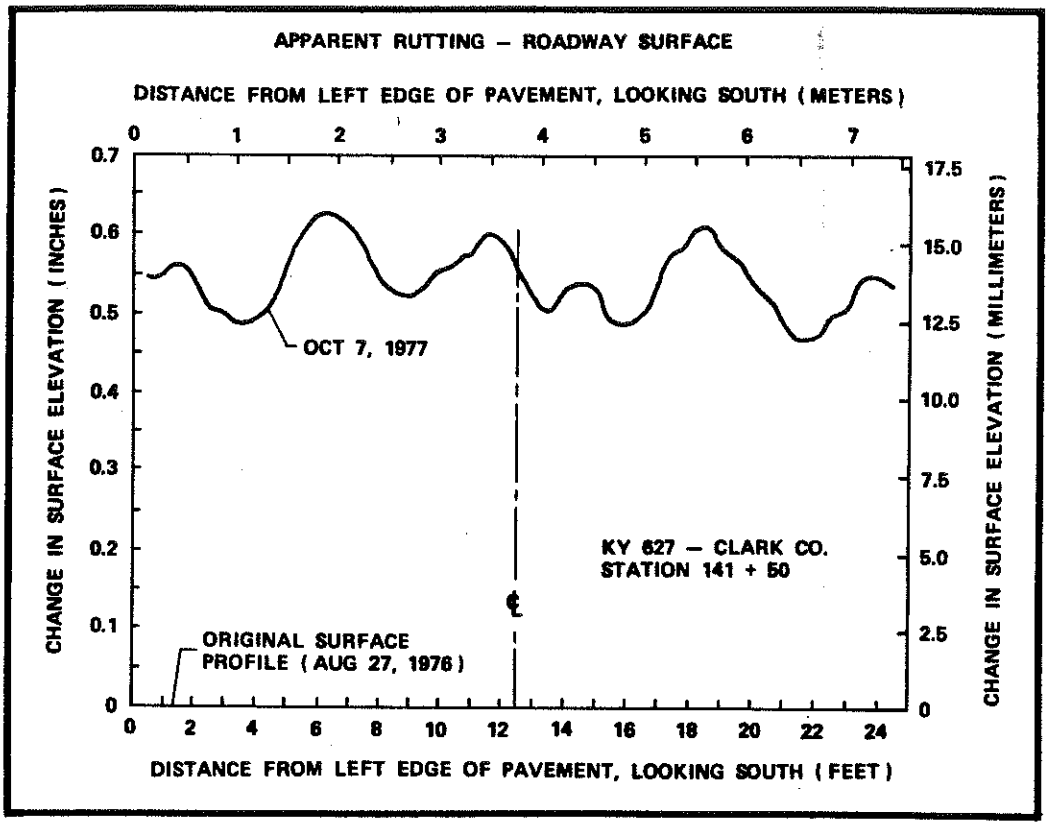

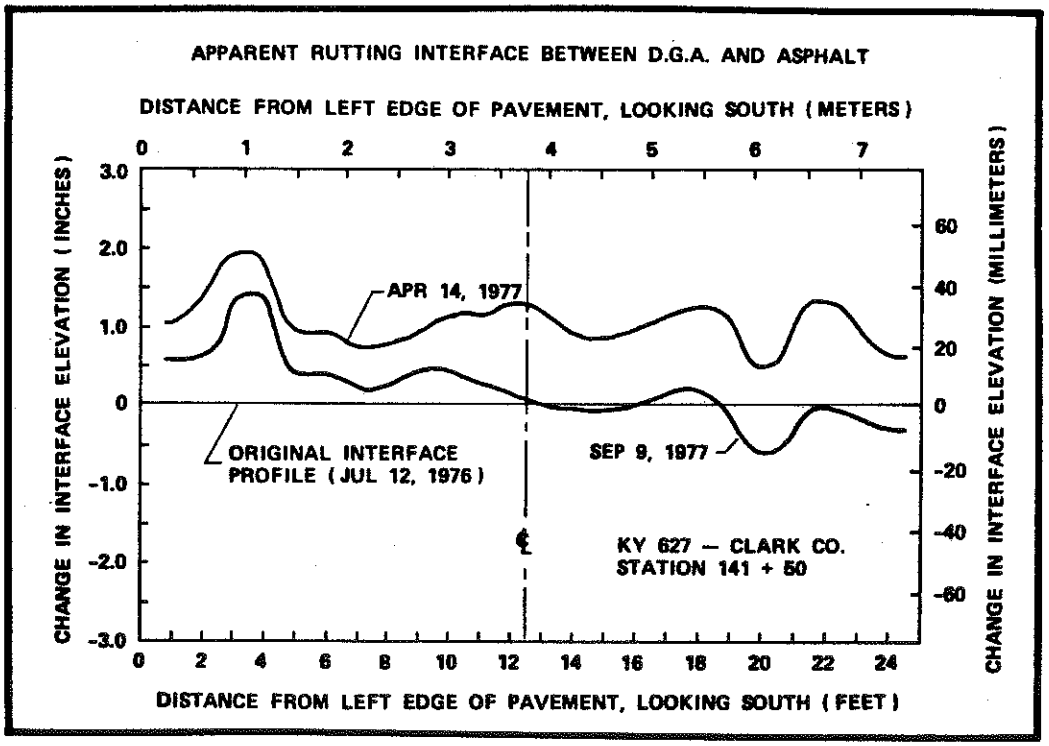

Figure 17. Apparent Rutting of Interface between Dense-Graded Aggregate and Asphalt Concrete at Station 141 + 50 on KY 627, Clark County.

Figure 18. Apparent Rutting of Interface between Subgrade and Dense-Graded Aggregate at Station 141 + 50 on KY 627, Clark County.

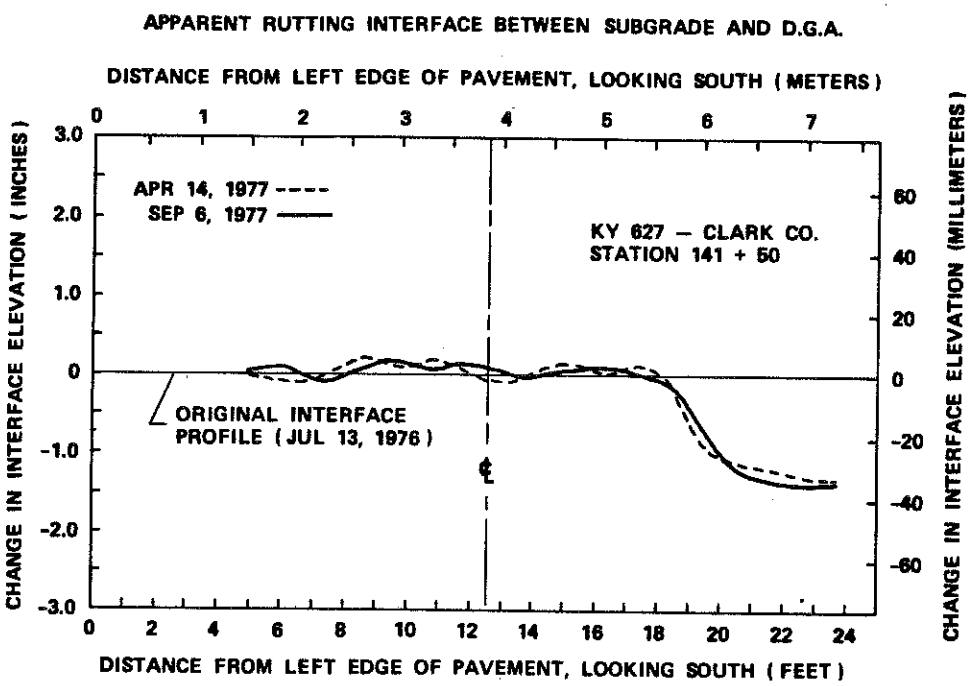

LABORATORY INVESTIGATION

EQUIPMENT

Triaxial Test Equipment

Triaxial tests were performed using a Model 530, Karol-Warner, triaxial loading frame and chamber. The confining fluid was water; and a regulated, compressed air system provided ambient pressures. The sample pedestal was 2 inches (51 mm) in diameter and was fitted with a porous stone; pore pressure measurements were made at the bottom of the test specimen. Pore pressures and load were measured using a strain-gage-type transducer, and both were recorded on an oscillographic recorder. Sample strains were measured using a dial extensometer having a resolution of 0.0001 inch (0.025 mm). For temperature control when testing asphaltic samples, the triaxial chamber was fitted with a copper heating coil. Water from a constant temperature bath was circulated through the coil heating (or cooling) the confining fluid and, consequently, the sample. An ASTM thermometer was mounted on the sample to measure its temperature.

A more detailed description of triaxial equipment, procedures and theory has been reported by Scott *(30)*.

Creep Test Equipment

Creep tests were performed on a modified Soiltest consolidation frame, Model No. C-280. The complete testing apparatus was housed in an environmental room capable of controlling temperature and humidity. The test specimen was loaded and unloaded manually by a weight and lever system. Strains in the specimen were measured by linear variable differential transformers and by SR-4 strain gages glued to the specimen. Strains were monitored on an oscillographic recorder.

Repeated-Load Test Equipment

The repeated-load test is used primarily to measure the fatigue or permanent deformation characteristics of material. The basic repeated-load apparatus (Model STD-1000) was purchased from Structural Behavior Engineering Laboratories in Phoenix, Arizona. The unit is capable of loading to 1,250 pounds (568 kg). Stress intensity, duration of stress, and frequency of stress can be varied. Load and unload times can be varied continuously from 0.03 second to 10 seconds. Strains were measured by two LVDT's mounted on opposite sides of the sample and were recorded on an oscillographic recorder. Stress was measured with the same equipment used in the triaxial test and was also recorded on an oscillographic recorder. Figure 19 is a typical example of the stress wave form at longer stress durations (1 to 10 seconds). It appears to approximate a square wave; however, at stress durations of less than 1 second, the wave form more closely approximates a triangular wave.

Figure 19. Typical Waveform Patterns of the Repeated-Load Apparatus.

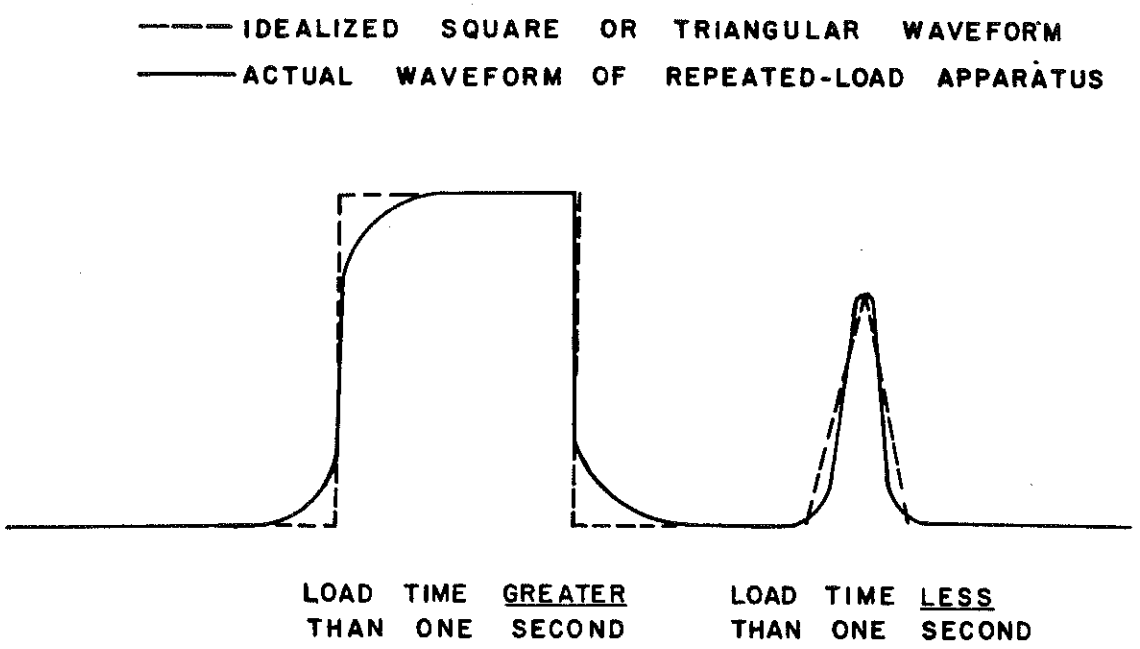

Figure 20 is a photograph of a complete set-up of the repeated-load test. The sample chamber, the pore pressure device, and the temperature control apparatus are the same as that used in the triaxial test.

Resonant Column Test Equipment and Theory

The resonant column test, a relatively nondestructive test employing wave propagation in cylindrical specimens, is used to obtain the modulus and damping of soils, asphalts, and other materials as functions of vibratory strain amplitude and other factors such as ambient confining stress, density, and moisture content. Figure 21 is a schematic representation of the resonant column device used in this study, and many of the symbols used in the following brief discussion of theory and operation are defined in that figure.

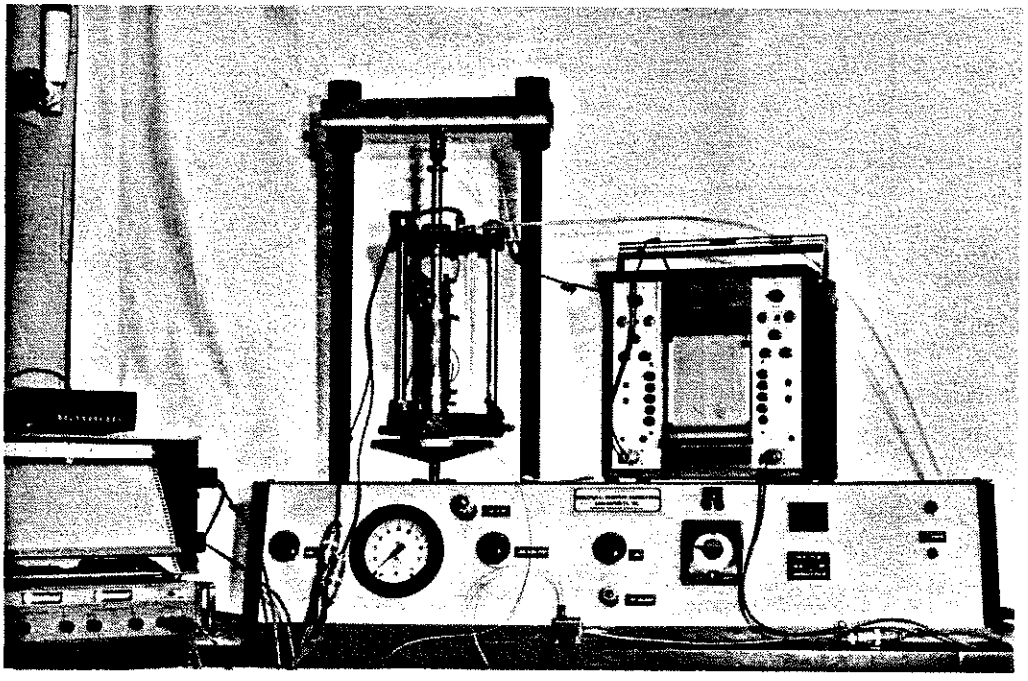

Figure 20. Photograph of Repeated-Load Apparatus.

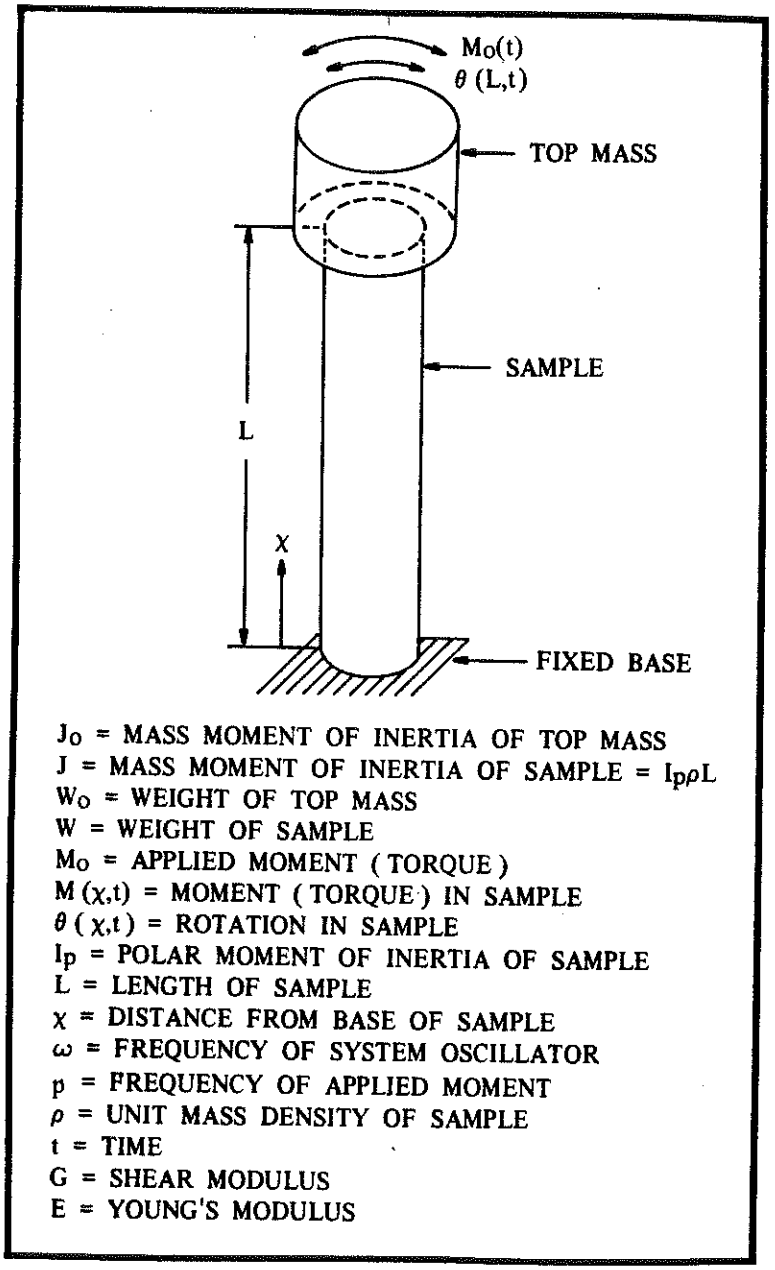

J_O = MASS MOMENT OF INERTIA OF TOP MASS
J = MASS MOMENT OF INERTIA OF SAMPLE = $I_p \rho L$
W_O = WEIGHT OF TOP MASS
W = WEIGHT OF SAMPLE
M_O = APPLIED MOMENT (TORQUE)
$M(\chi,t)$ = MOMENT (TORQUE) IN SAMPLE
$\theta(\chi,t)$ = ROTATION IN SAMPLE
I_p = POLAR MOMENT OF INERTIA OF SAMPLE
L = LENGTH OF SAMPLE
χ = DISTANCE FROM BASE OF SAMPLE
ω = FREQUENCY OF SYSTEM OSCILLATOR
p = FREQUENCY OF APPLIED MOMENT
ρ = UNIT MASS DENSITY OF SAMPLE
t = TIME
G = SHEAR MODULUS
E = YOUNG'S MODULUS

Figure 21. A Simplified Schematic Diagram of a Fixed-Base Resonant Column with End Mass Attached, Including Definitions of Nomenclature.

Given an elastic rod or test specimen (the assumption of elasticity holds because the values of damping are small), fixed at the bottom and having a mass at the top that is free to vibrate either longitudinally or torsionally, the shear modulus or Young's modulus and damping can be calculated. If the mass fixed to the top of the specimen is oscillated torsionally with sinusoidal motion, the equation of motion can be written as follows:

$$\partial^2\theta/\partial t^2 = (G/\rho)(\partial^2\theta/\partial x^2). \quad 1$$

Consideration of the boundary conditions at both ends of the specimen yields

$$\theta(0,t) = 0, \quad 2$$

or the motion at the base of the specimen must be zero, and

$$M_o(t) + M(L,t) = -J_o[\partial^2\theta(L,t)/\partial t^2]$$
$$= J_o\omega^2\theta(L,t), \quad 3$$

which says that the moment, or torque, at the top of the specimen equals the mass moment of inertia of the top mass multiplied by the sinusoidally varying force. In addition, only steady-state motion is considered, i.e. $\omega = p$.

Equation 1 can now be solved by the method of separation of variables to obtain the "frequency equation" for the resonant column:

$$\Psi_s \tan \Psi_s = J/J_o, \quad 4$$

where Ψ_s = root of frequency equation.
However, Equation 4 is a transcendental equation and must, therefore, be solved graphically for a series of J/J_o ratios as shown in Figure 22. Ψ_s is then used to solve for the shear modulus.

The basic expression for shear modulus is

$$G = \rho V_s^2, \quad 5$$

where V_s = shear wave propagation velocity.
For a solid cylindrical specimen,

$$\rho = (W/V)/g \quad 6$$

where V = volume of specimen and
g = acceleration of gravity.
The propagation velocity of the shear wave in the specimen is calculated as follows:

$$V_s = 2\pi f_n L/\Psi_s, \quad 7$$

where f_n = undamped natural frequency of the specimen.
Therefore,

$$G = (2\pi f_n L/\Psi_s)^2\rho; \quad 8$$

however, the quantity $(2\pi L\Psi_s)^2\rho$ is essentially constant for any given test, therefore,

$$G = \text{constant} \times f_n^2. \quad 9$$

The theory and calculations for determining Young's modulus are basically the same as for shear modulus except Equation 4 becomes

$$\Psi_L \tan \Psi_L = W/W_o, \quad 10$$

and Equation 5 becomes

$$E = \rho V_c^2, \quad 11$$

where V_c = rod wave propagation velocity.

Figure 22. **A Graphical Solution to Find the Root of the Frequency Equation, Ψ, for the Resonant Column.**

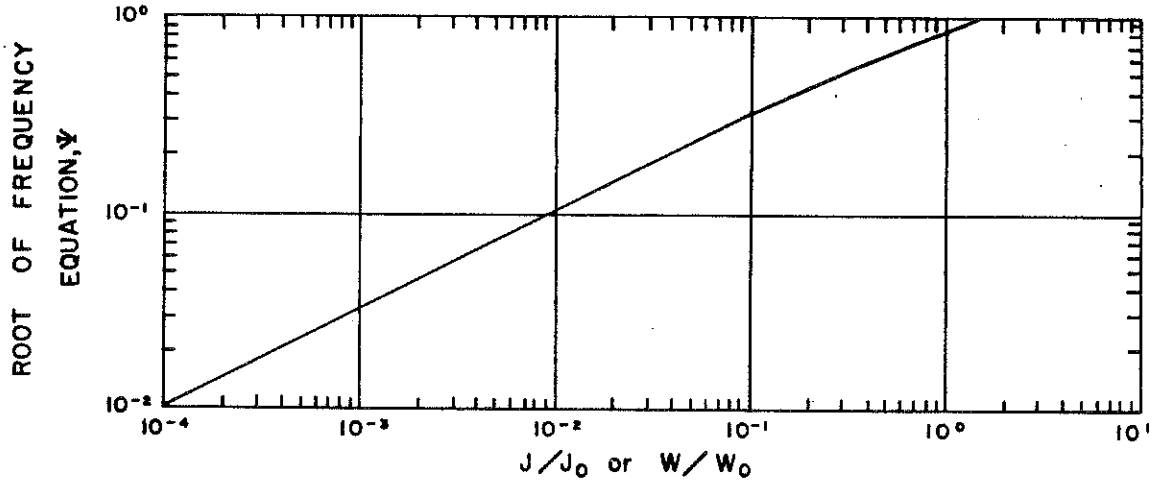

The resonant column test is used to obtain the natural frequency, f_n, of the test specimen (Equation 7). The equipment used in this study was the Drnevich Longitudinal-Torsional Resonant Column, designed by V. P. Drnevich of the University of Kentucky, and manufactured and sold by Soil Dynamics Instruments, Inc. of Lexington, Kentucky. Figure 23 is a photograph showing the basic unit, without any of the supporting electronics. To vibrate the sample either longitudinally (axially) or torisonally, a sinusoidal (AC) current is sent through the single longitudinal coil or four torisonal coils, respectively, thus sending a longitudinal or torsional wave through the sample.

Figure 24 is a schematic diagram of the supporting electronic equipment. The sinusoidal excitation is generated by a variable oscillator, amplified to drive the electromagnetic transducers which vibrate the column. Frequency is monitored by two accelerometers (one each for longitudinal and torsional motions) mounted on the oscillating top cap. Output from the power amplifier (driving force) and output from the accelerometers are monitored on an X-Y oscilloscope. The resulting patterns are defined as Lissajous' figures *(18)*. Lissajous' figures represent the vector sum of two perpendicular sine waves (the driving force and the acceleration induced). During a test, as the oscillator is advanced through a range of frequencies, the figure suddenly grows in size, and the major and minor axes of the elipse align themselves with the horizontal and vertical axes of the screen. When this occurs, the acceleration of the vibrating assembly (including the test specimen) is 90° out of phase with the driving force. The frequency at which the lag angle is 90° is the natural frequency of the test specimen assembly.

To test stiffer asphaltic samples, the Drnevich resonant column was modified considerably. The aluminum base plate, which was supported on three aluminum legs, was replaced by a base plate of solid steel. This prevented undesirable vibrations in the base. The top mass assembly was also redesigned to reduce internal vibrations. Figure 25 shows the modified apparatus with the heating coil installed for temperature control on asphalts.

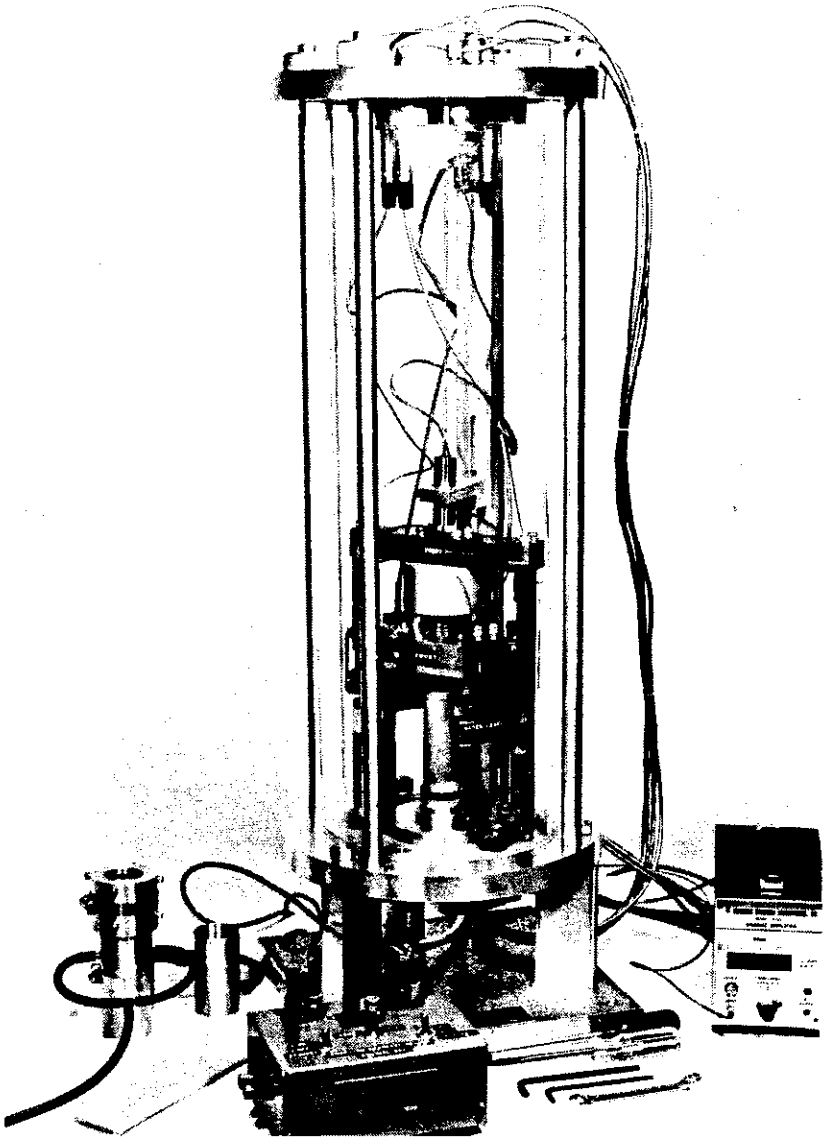

Figure 23. **The Drnevich Longitudinal-Torsional Resonant Column, without Electronics.**

Figure 24. Schematic Diagram of the Electronics for the Resonant Column.

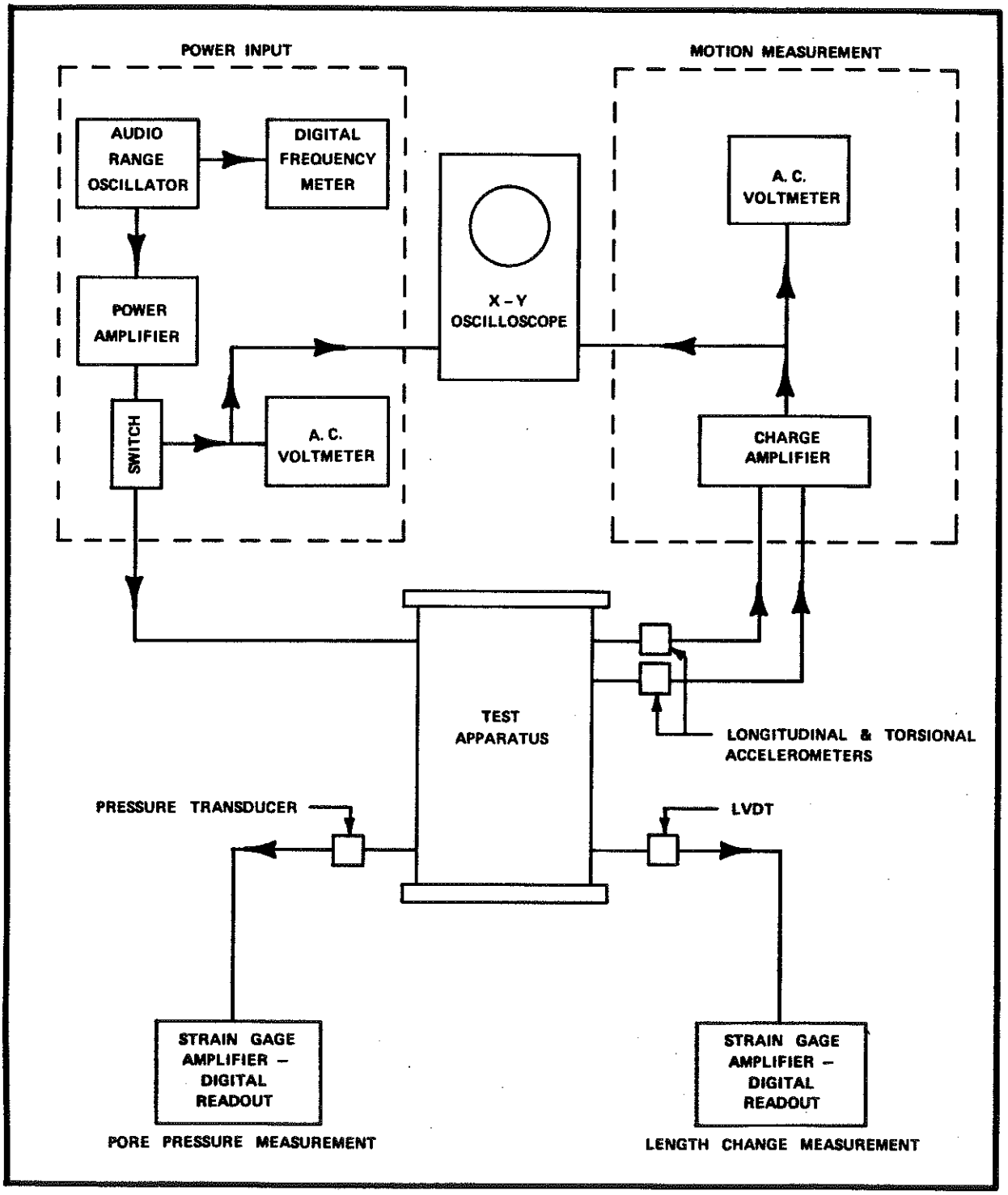

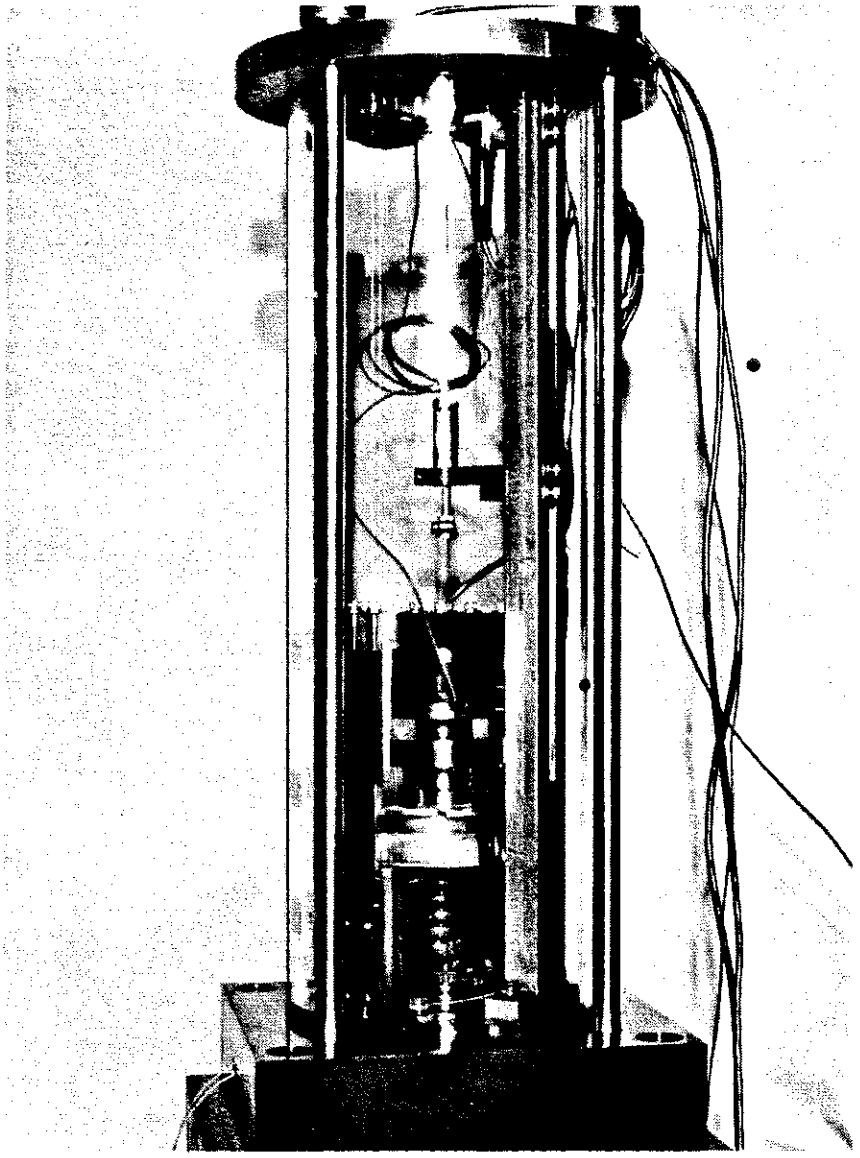

Figure 25. **The Drnevich Longitudinal-Torsional Resonant Column, without Electronics, as Modified for this Study.**

MATERIALS CHARACTERIZATION

Asphaltic Concrete Base

The base course mixture used in this study was collected from the hopper of the paver as it passed over the instrumentation site in Clark County. The material was stored in air-tight, metal containers and transported to the laboratory where the samples were compacted. The mixture contained crushed limestone aggregate and was graded as shown in Figure 26. It contained 5.2 percent asphalt. Samples were compacted in a split mold having a double plunger (top and bottom). The material was reheated to 300°F (149°C), and the proper quantity of material was weighed into a heated mold. The material was compressed under a 5,000-pound (2,273-kg) load for 2.5 minutes. The average temperature at the time of compaction was 280°F (138°C). The average height was 3.0 inches (76 mm) and the average diameter was 2.0 inches (51 mm). The samples were capped with a sulfur-base capping compound to insure smooth, uniform ends.

Nine triaxial tests were performed. The tests were run at three temperatures 32°F (0°C), 77°F (25°C), and 100°F (38°C) to approximate the range of in-service conditions. A series of tests at a temperature higher than 100°F (38°C) would have been preferred inasmuch as pavement temperatures exceed this value in the summer; however, equipment limitations prevented this. In addition, at each temperature, a test was run at each of the following confining pressures: (1) unconfined, (2) 30 psi (207 kPa), and (3) 60 psi (413 kPa). Each triaxial sample was allowed to "heat" or "cool" a minimum of 16 hours before testing to insure temperature equilibrium. The samples were tested at a strain rate of 0.03 percent per minute.

Figure 27 shows the Mohr's failure envelopes for the nine tests. As expected, the values for the internal friction angle, ϕ, appeared to be relatively independent of temperature. However, cohesion increased rapidly as temperature decreased. Figure 28 shows the relationships between cohesion and internal friction angle and temperature. The values given in Figure 28 will be used in a bearing-capacity analysis of the pavement in Clark County (see Figure 2).

To predict the accumulation of rutting in the field, due to repeated service loads, it is necessary to determine the susceptibility of the mixture to deformation. Twenty-seven unconfined, repeated-load tests were used to determine this parameter. The tests were run at three temperatures: 45°F (7°C), 77°F (25°C), and 100°F (38°C). Three deviator stresses (or vertical loads) were used at each temperature: 80 psi (551 kPa), 50 psi (345 kPa), and 20 psi (138 kPa). In addition, three loading times, 0.5 second, 1.0 second and 2.0 seconds, were used at each deviator stress. Relaxation time (time between each load) was 1.0 second for all 27 tests.

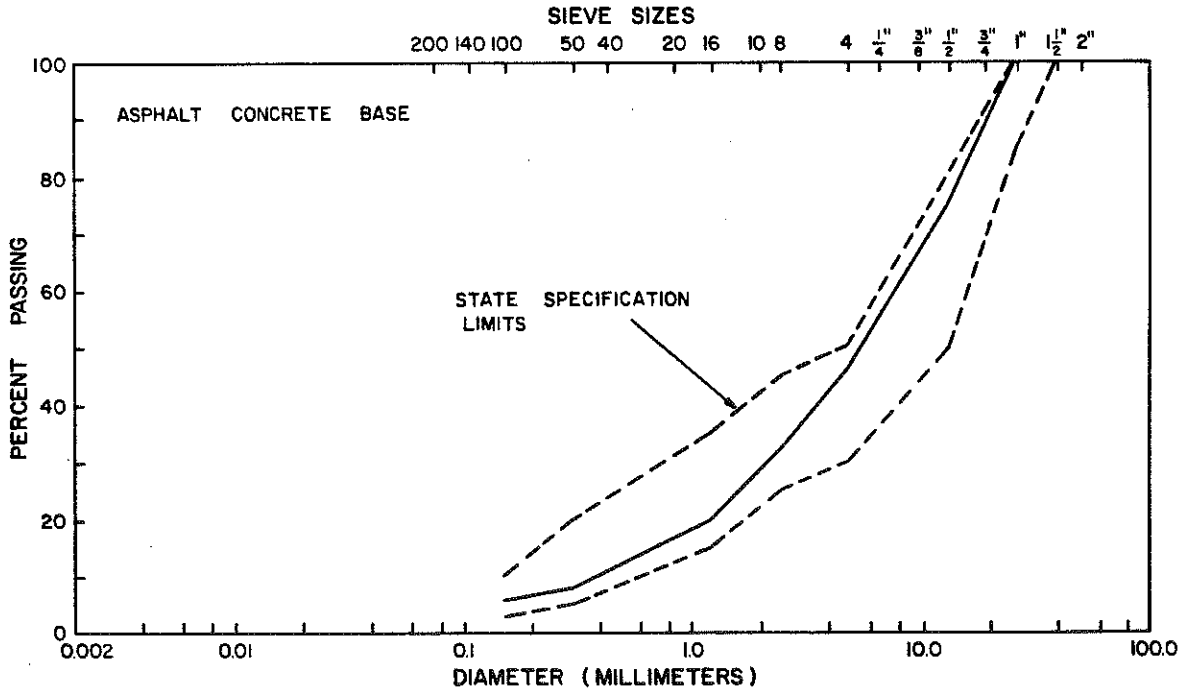

Figure 26. Gradation of the Asphaltic Concrete Base Tested and Used on KY 627, Clark County.

Figure 27. Mohr's Failure Envelopes, Asphaltic Concrete Base.

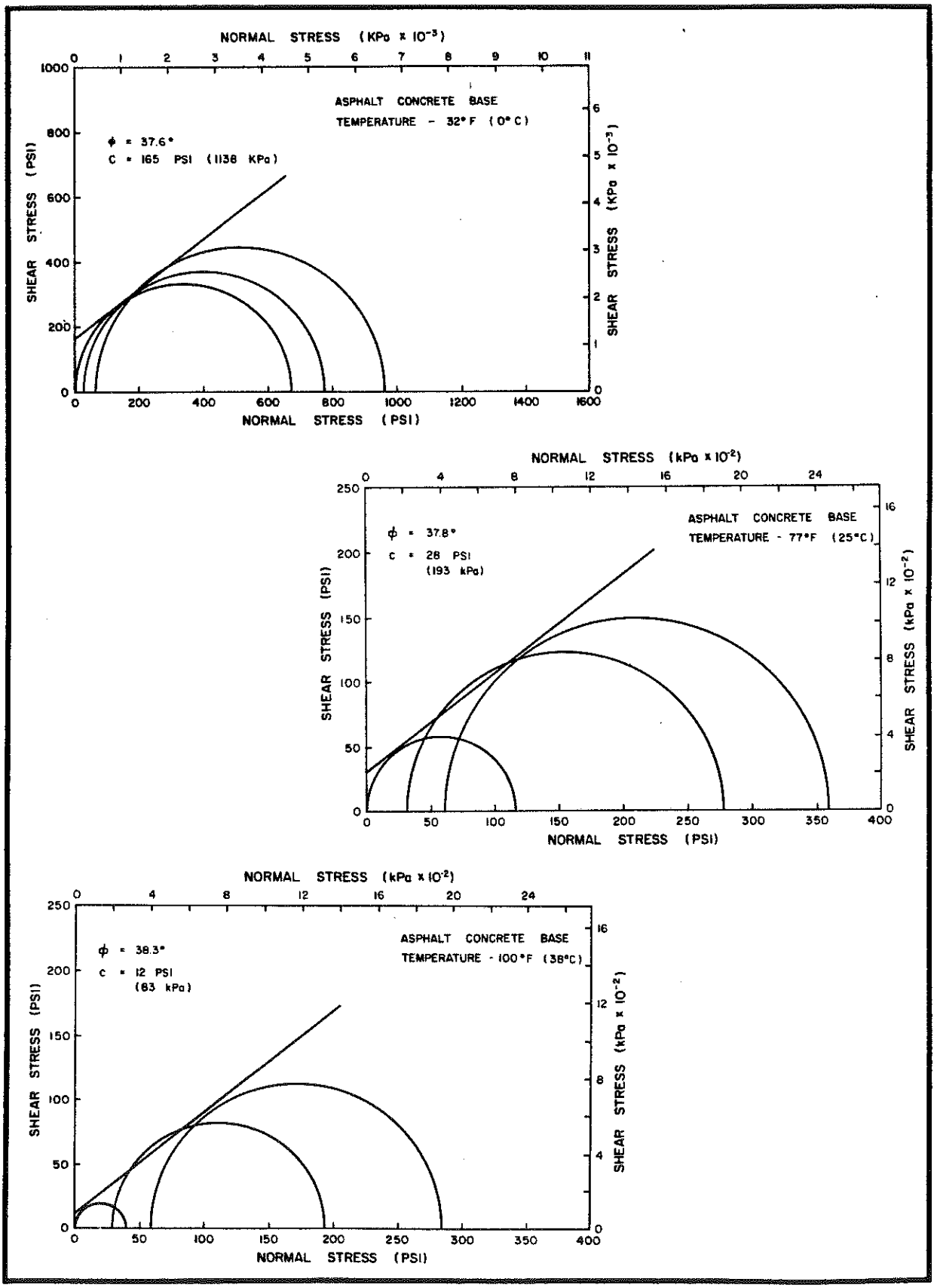

Figure 28. **Effect of Temperature on Cohesion and the Internal Angle of Friction, Asphaltic Concrete Base.**

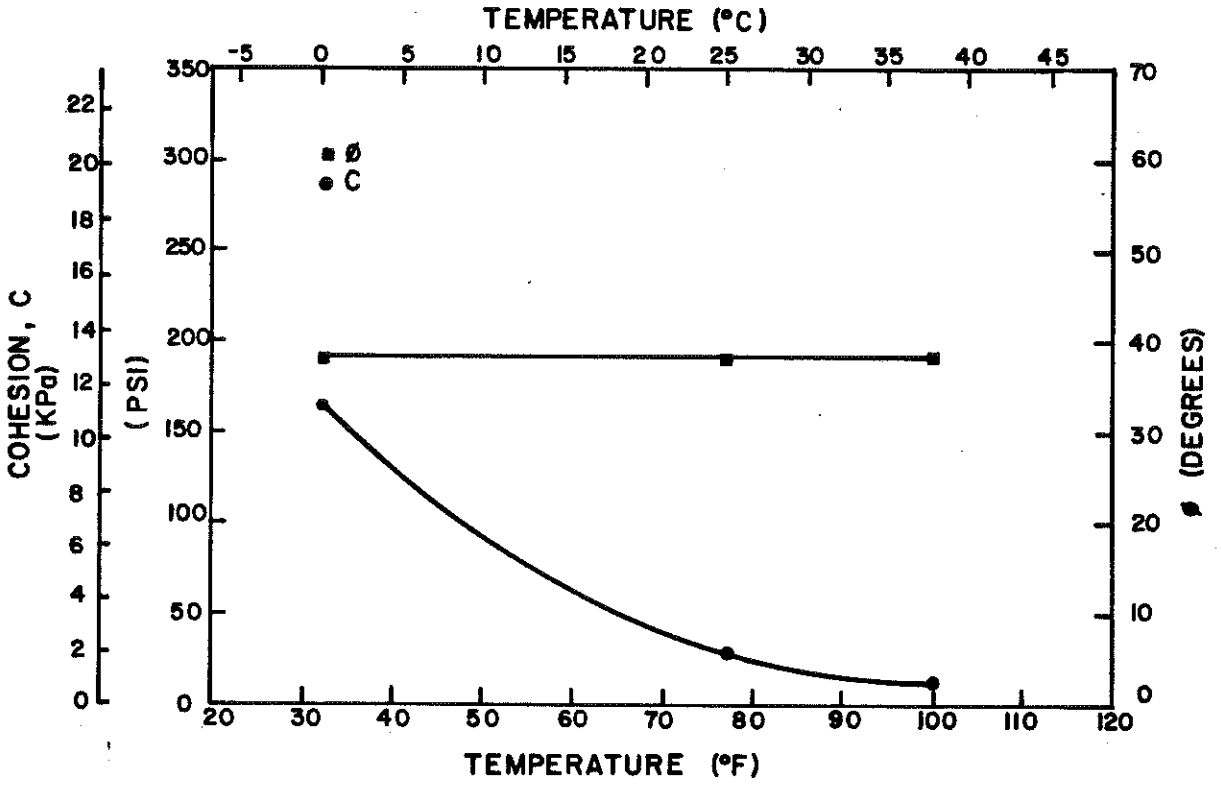

Figure 29 shows the results of the repeated load tests. The data indicated that samples at the same temperature and under the same deviator stress will have the same amount of permanent deformation, assuming the **total** loading times are equivalent. For example, one sample could receive 10 cycles of an 80-psi (551-kPa) stress where each cycle had a load duration of 1.0 second. This would give a total loading time of 10 seconds. A second sample could receive 20 cycles of the same stress for 0.5 second per cycle and also have a total loading time of 10 seconds. Therefore, their permanent deformations will be equal. To simplify the analyses, it was assumed that this relationship was valid for the loading times used in this study. For this reason, only the data from the tests that had load durations of 1.0 second are shown in Figure 29. In Figure 29 , the data for the test at 45°F (7°C) and 20 psi (138 kPa) deviator stress are not shown because of equipment malfunction during the test.

Figure 29. **Relationship between Permanent Strain and Number of Deviator Stress Repetitions (Load Cycles), Asphaltic Concrete Base.**

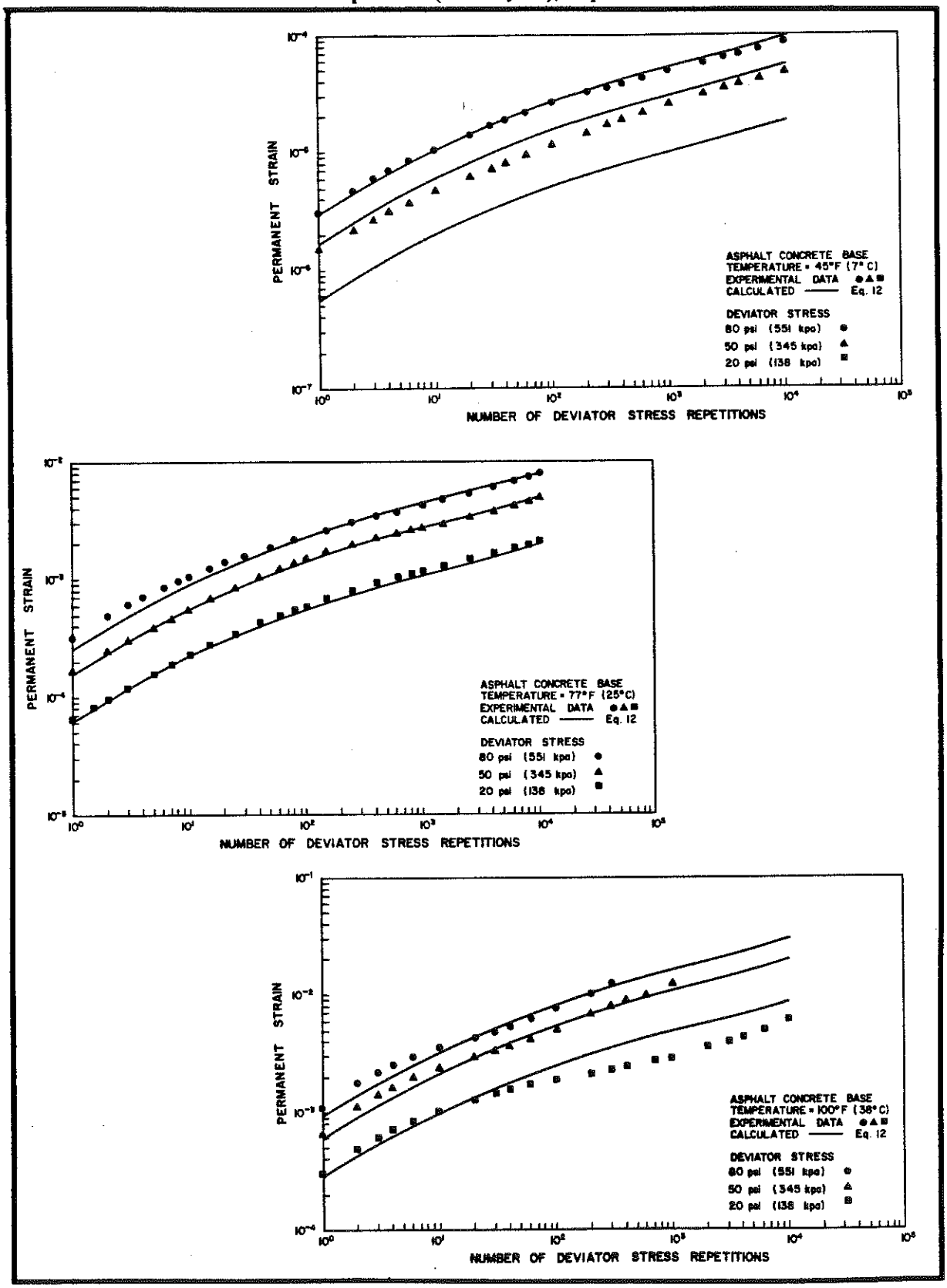

A linear regression analysis was run on the data from all tests shown in Figure 29. The following third-order polynomial resulted:

$$\log \epsilon_p = C_0 + C_1(\log N) - C_2 (\log N)^2 + C_3(\log N)^3, \quad 12$$

where ϵ_p = permanent strain (change in length/initial length),
N = number of deviator stress repetitions,
C_3 = 0.00938,
C_2 = 0.10392,
C_1 = 0.63974,
C_0 = $[-0.000663\ T^2 + 0.1521\ T - 13.304] + [(1.46 - 0.00572\ T)(\log \sigma_1)]$,
T = temperature (°F), and
σ_1 = deviator stress (psi).

This empirical equation is similar to one reported by McLean and Monismith *(20)*; however, the form of the function representing C_0 differs considerably from theirs. It is evident from Equation 12 that the logarithm of the relationship between the first load cycle and any subsequent cycle is simply a function of the number of cycles applied and is independent of temperature and stress. Conversely, Equation 12 indicates that only the logarithm of the magnitude of the initial cycle is affected by temperature and stress. Therefore, given any unique set of conditions (temperature, stress, and number of cycles), the accumulated permanent strain may be calculated. Equation 12 has been programmed.

This model (Equation 12) should be used with caution when strains approach or exceed 0.01. In the repeated load tests and also the creep tests, to be discussed later, all samples began to approached failure rapidly at this strain value. The model does not predict strains approaching failure. However, the model does predict acceleration in the rate of strain between 5,000 and 10,000 seconds of total loading time (5,000 to 10,000 cycles of 1.0-second loading).

Approximately 60 creep tests were performed on the asphaltic base material. They were run at three temperatures; 32°F (0°C), 77°F (25°C), and 100°F (38°C). Also, three stress levels were run at each temperature: 90 psi (620 kPa), 50 psi (345 kPa), and 10 psi (69 kPa). Most of the creep tests were unconfined; however, a small number were run with confining pressures as high as 50 psi (345 kPa). It appeared that confining pressure had very little effect on the results, and it was considered negligible in all analyses.

Creep specimens were prepared in the environment room and allowed to remain there overnight to reach thermal equilibrium. The next day the specimen was loaded for a predetermined number of seconds (either 15, 60, or 300), and the load was then removed. Two tests, at 77°F (25°C), were loaded for 20,000 seconds. The strain was recorded throughout the loading and rebound portions of the test until a constant strain was reached in the rebound portion.

Whenever a "viscoelastic-plastic" material, such as an asphalt-aggregate mixture, is loaded and rebounded, a strain-time curve similar to the one shown in Figure 30 results ideally. The strain for this type of material has three components: (1) elastic, (2) retarded elastic or viscoelastic, and (3) plastic. When the load is removed, all strains are eventually recovered except the plastic component.

In Figure 30, the plastic component of strain was shown to be lineraly proportional to time. However, in in plastic component of strain exhibited nonlinear behavior. Lai and Anderson *(16)* also reported nonlinear plastic behavior in asphaltic concrete mixtures. The following function describes the nonlinear behavior generally observed here:

$$C_1 (1 - e^{-C_2 t}), \quad 13$$

where C_1, C_2 = constants,
e = base of the natural logarithm, and
t = time.

Equation 13 may also be used to describe the viscoelastic portion of strain; however, the constants would be different.

Figure 30. "Typical" Creep Curve for Asphaltic Concrete.

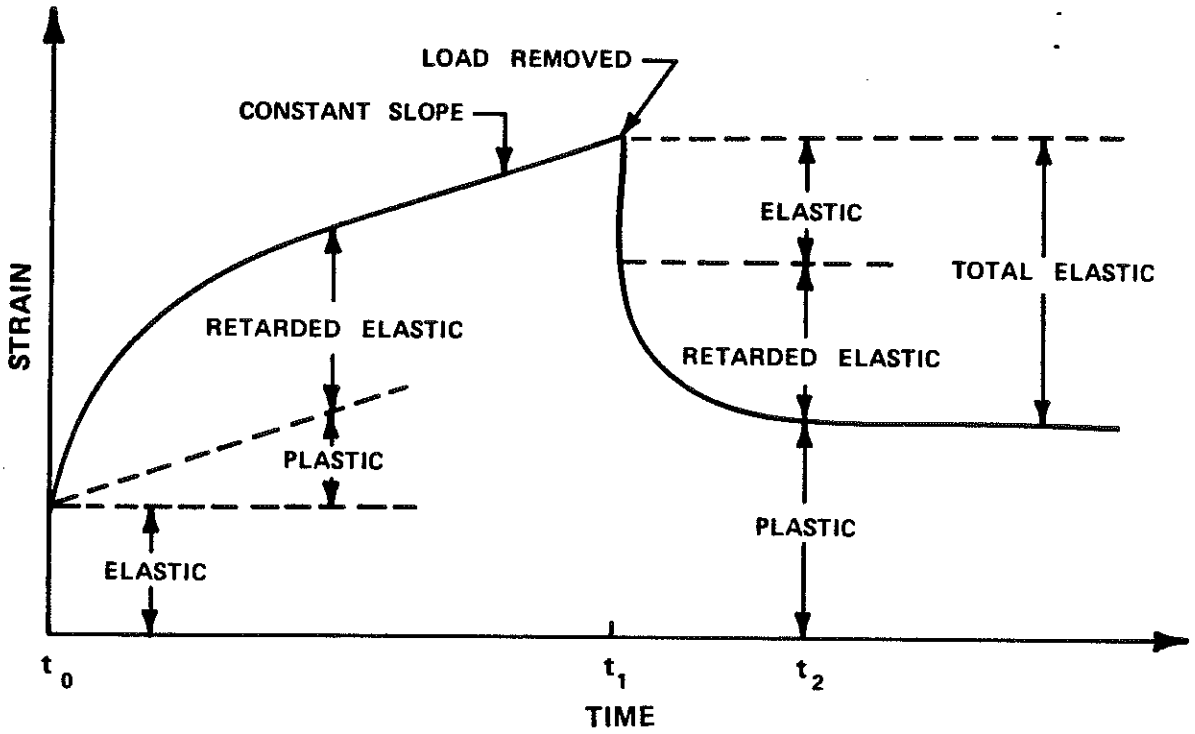

This presents a dilemma. A constant slope in the creep curve, as shown in Figure 30, will not be reached with nonlinear plasticity. Therefore, how are the viscoelastic and elastic components separated from the plastic component? Figure 31 provided an easy solution to the problem. This is a plot of total (peak) strain at time t_1 in Figure 30 versus ultimate residual (plastic) strain at time t_2 or greater. A somewhat surprising relationship developed. Figure 31 shows that for all tests used in this study, the average ratio between peak strain and plastic strain was approximately 4:3. This may also be stated as

$$\epsilon_T = 1.33\ \epsilon_p, \qquad 14$$

where ϵ_T = peak strain or total strain at any time, t, and
ϵ_p = plastic strain.

Therefore, to find plastic strain, ϵ_p, for the mixture used in this study, at any time during the creep test, simply read ϵ_T and solve Equation 14 for ϵ_p. The sum of the elastic and viscoelastic components of strain, ϵ_E, can now be calculated:

$$\epsilon_E = \epsilon_T - \epsilon_p. \qquad 15$$

There is one factor which will cause a small percentage of error when using Equation 14. The ratio between peak and plastic strain differed slightly for tests having different durations of loading. For instance, the coefficient of ϵ_p in Equation 14 for the 15-second dwell times was 1.40 and for the 60-second and the 300-second times the coefficients were 1.38 and 1.28, respectively. However, for purposes of analysis, the average value of 1.33 was used.

The elastic compliance, J_E, is defined as follows:

$$J_E = \epsilon_E/\sigma_1, \qquad 16$$

where σ_1 = deviator stress.

Figure 32 presents all of the data from the unconfined creep tests. The points were calculated using Equation 16. The points include data from three stress levels: 10 psi (69 kPa), 50 psi (345 kPa), and 90 psi (620 kPa). Due to the relatively small range in the data, the viscoelastic component of strain was assumed to be linear with stress. If the viscoelastic component were perfectly linear and there were no experimental errors, all of the points, at each temperature, would have fallen on the same curve. The average of the logarithm of the maximum and minimum values of the range of data was calculated at several different times and was plotted on the data. A line was constructed through these points to give the "range median curve".

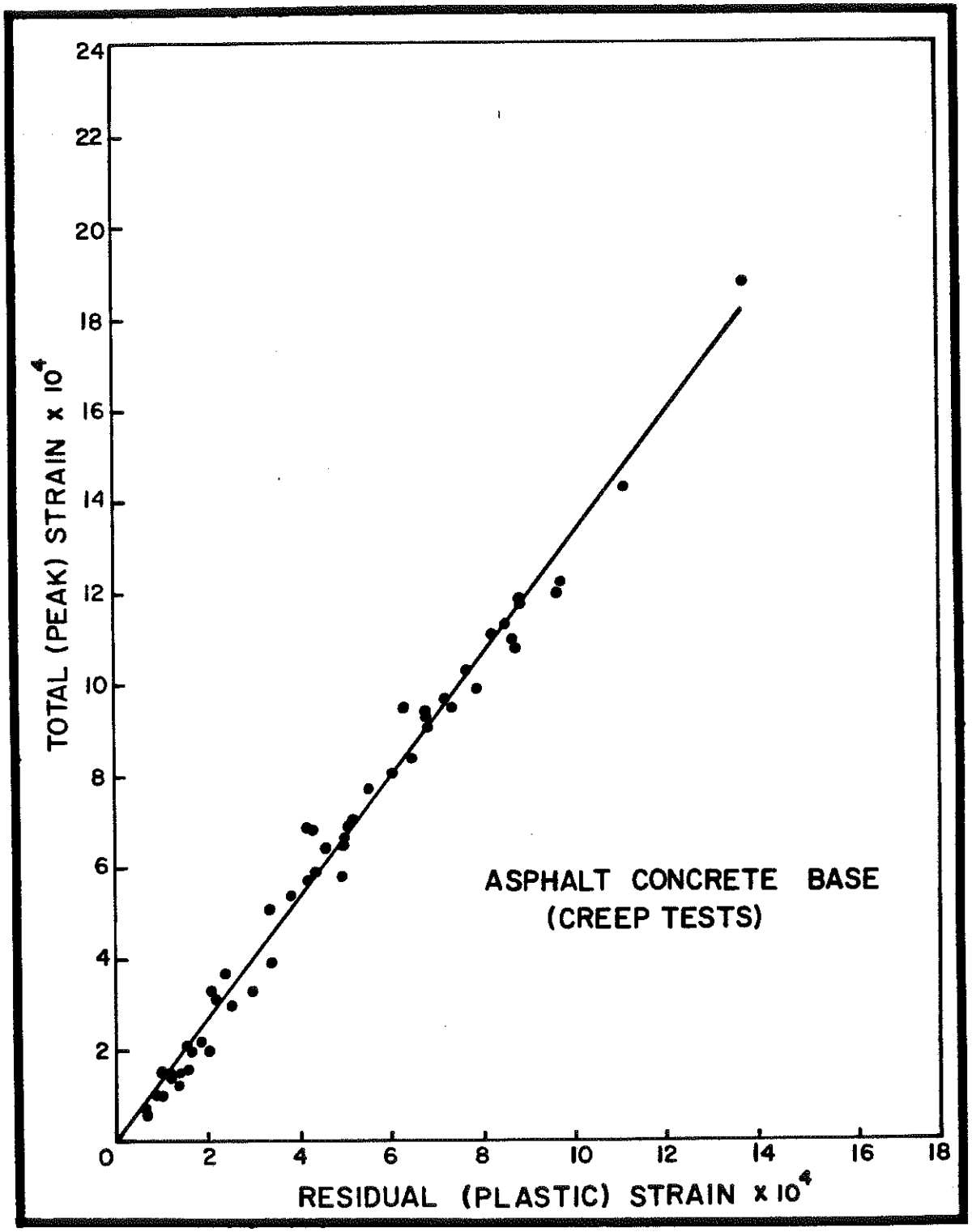

Figure 31. Relationship between Peak Strain and Plastic Strain, Creep Tests on Asphaltic Concrete Base.

Figure 32. Elastic Compliance as a Function of Time, Asphaltic Concrete Base.

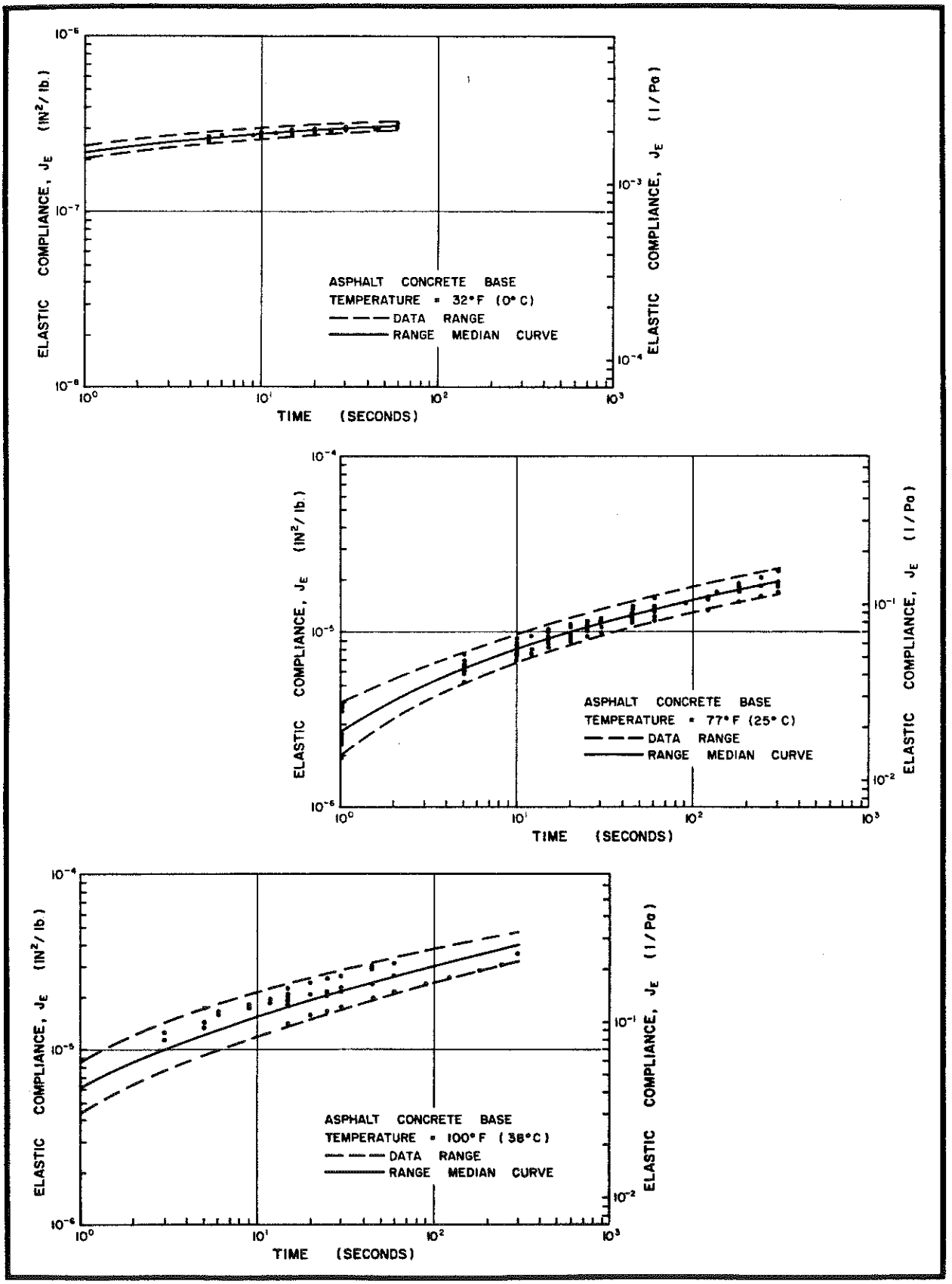

The elastic compliance curve can be represented by a number of Voigt elements in series. A Voigt element is shown in Figure 33 and can be represented mathematically according to

$$\Psi(t) = J_i [1 - \exp(-t/\tau_i)], \quad 17$$

where J_i = elastic creep compliance for any particular element,

τ_i = N_i/G_i = ratio of viscosity (dashpot) to shear rigidity (spring), and

t = time.

Therefore, the elastic compliance for any set of data can be represented by

$$\Psi(t) = \sum_{i=1}^{n} J_i [1 - \exp(-t/\tau_i)], \quad 18$$

where n = number of elements used.

J_i and τ_i for each element and n, the number of elements used to describe a particular set of data, can be determined graphically by a procedure reported in detail by Allen *(1)*, Mossbarger *(24)*, and Papazian *(27)*.

The elastic compliance of Equation 18 can now be transformed to the complex elastic compliance (from a time domain to a frequency domain) by using the following equations:

$$J_1(\omega) = J_i/(1 + \omega^2\tau_i^2), \quad 19$$

$$J_2(\omega) = J_i\omega\tau_i/(1 + \omega^2\tau_i^2), \quad 20$$

where ω = frequency of oscillation (radians per second).

$J_1(\omega)$ is defined as the storage compliance (real component) and $J_2(\omega)$ is the loss compliance (imaginary component). Therefore, J^*, the complex elastic compliance can be calculated by

$$J^* = [J_1(\omega)^2 + J_2(\omega)^2]^{1/2} \quad 21$$

As the data in Figure 32 are assumed to be elastic, the complex elastic modulus, E^*, is simply defined as the inverse of Equation 21:

$$E^* = 1/J^*. \quad 22$$

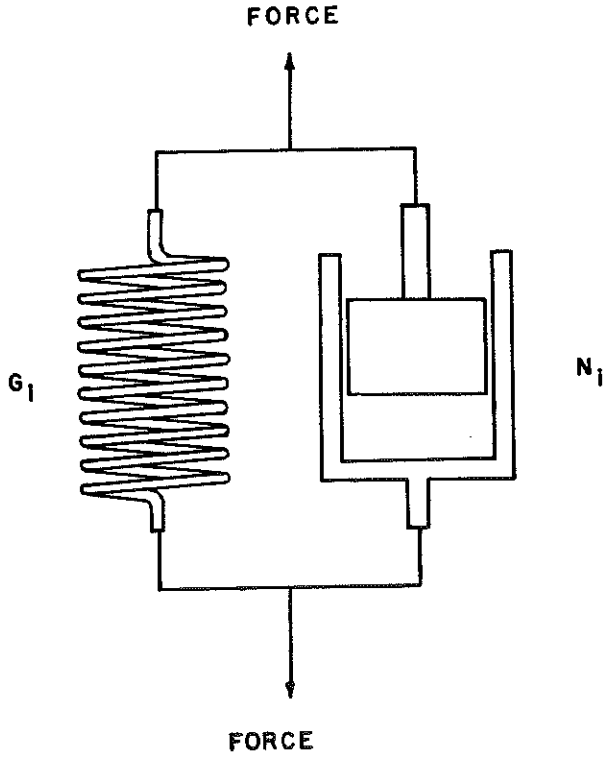

Figure 33. Voigt Element.

The complex elastic modulus curves, calculated from the elastic compliance curves in Figure 32, are shown in Figure 34. A more detailed derivation of Equations 17 through 22 has been reported by Allen *(1)* and published by Ferry *(10)*.

Using the principles of time-temperature superposition, the three curves in Figure 34 are reducible to a "master modulus curve". This is accomplished by graphically "shifting" the 77°F (25°C) curve to the right until it matches the 100°F (38°C) curve. Likewise, the 32°F (0°C) curve is "shifted" until it converges with the 77°F (25°C) curve. The numbers of logarithmic decades each curve was shifted, a_ω, is plotted as a function of temperature (Figure 35). A reference temperature is chosen; in this case, it was 70°F (21°C), and the plot is shifted until a_ω for 70°F (21°C) equals zero. New a_ω's are calculated for the three test temperatures, as shown in Figure 35. The master modulus curve in Figure 36 is now constructed by multiplying the frequencies for each curve in Figure 34 by their respective a_ω in Figure 35 to obtain a reduced frequency, (ω/a_ω). Mossbarger *(24)* reported, in detail, on the principles of time-temperature superposition.

Figure 37 is a comparison of elastic modulus calculated from Figure 36 with elastic modulus derived from AASHO Road Test data and reported by Southgate *(33)*. The comparison is made at a frequency of one-half cycle per second. The comparison appears reasonable, although vastly different methods were used, and lends support to the validity of this method for estimating modulus.

Figure 38 is a comparison of permanent deformation from the creep test with Equation 12 (repeated-load tests). There is good agreement between the two, emphasizing the fact that creep tests, alone, appear to be sufficient to estimate modulus and permanent deformation characteristics of asphaltic concrete.

Two samples were tested in the resonant column. They were prepared in the same manner as all other test specimens. The samples were 3.25 inches (82.6 mm) in height and 1.41 inches inches (35.8 mm) in diameter. One sample was tested at temperatures of 45°F (7.2°C) and 77°F (25.0°C); the second sample was tested at 40°F (4.4°C), 50°F (10.0°C), and 100°F (37.8°C). The force applied to the samples was less than 1 pound (0.454 kg).

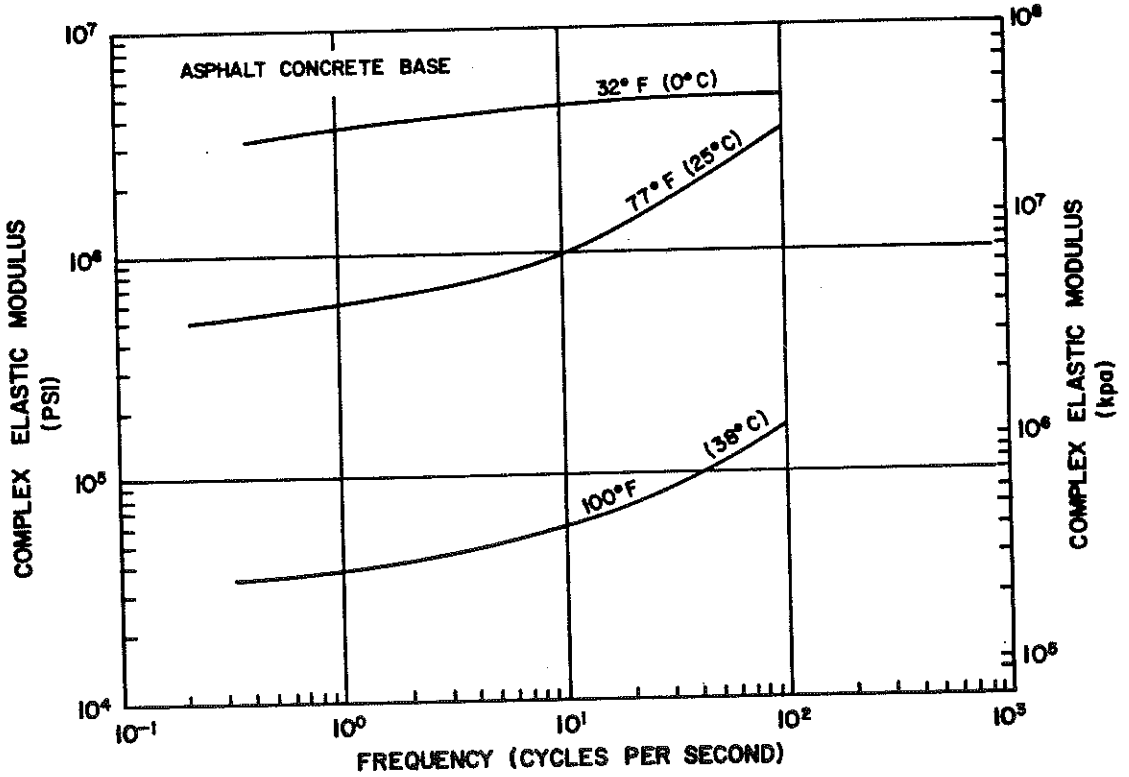

Figure 34. Transformed Complex Elastic Modulus as a Function of Frequency, Asphaltic Concrete Base.

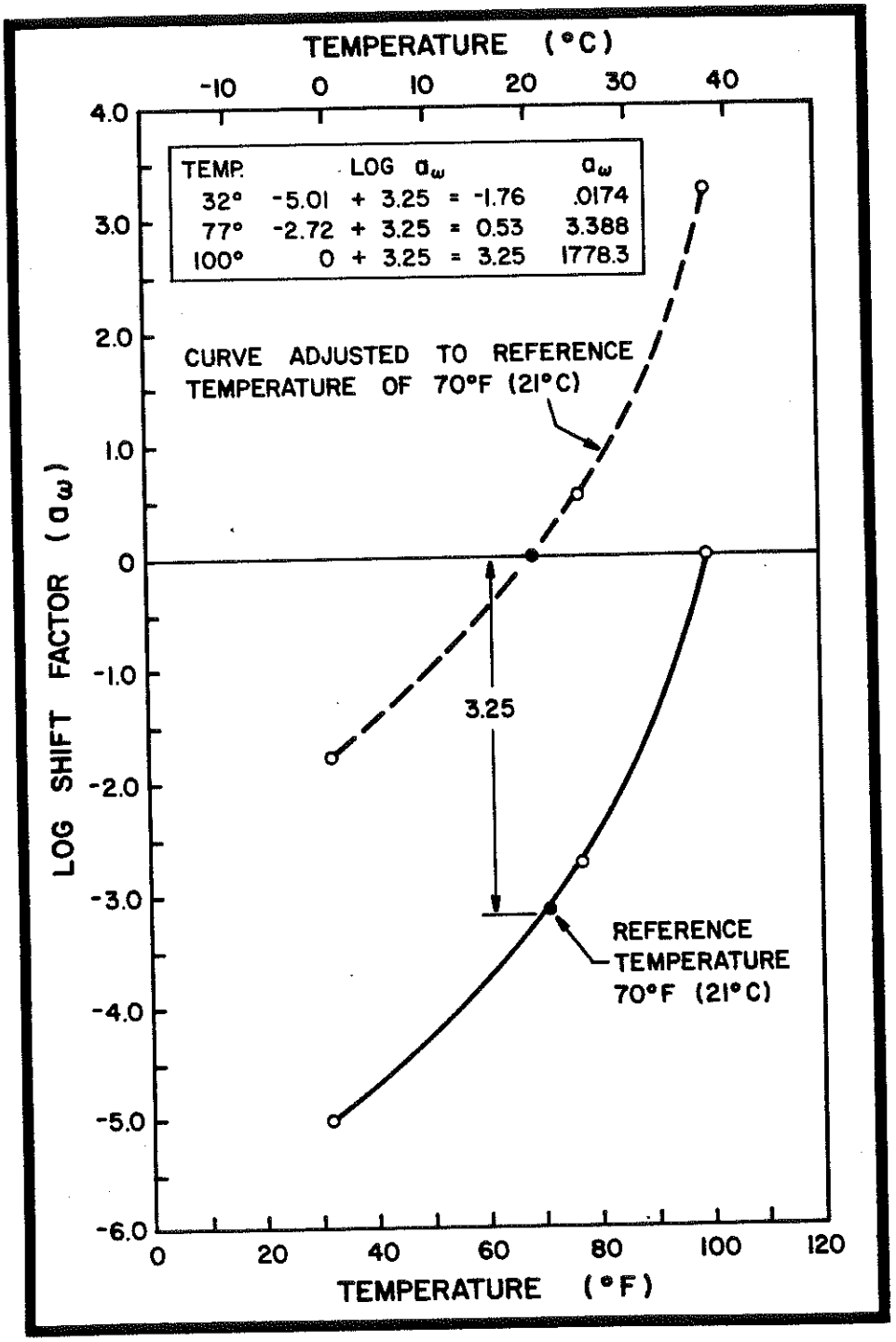

Figure 35. Shift Factor, a_ω, as a Function of Temperature.

Figure 36. The Reduced Complex Modulus Curve, Asphaltic Concrete Base.

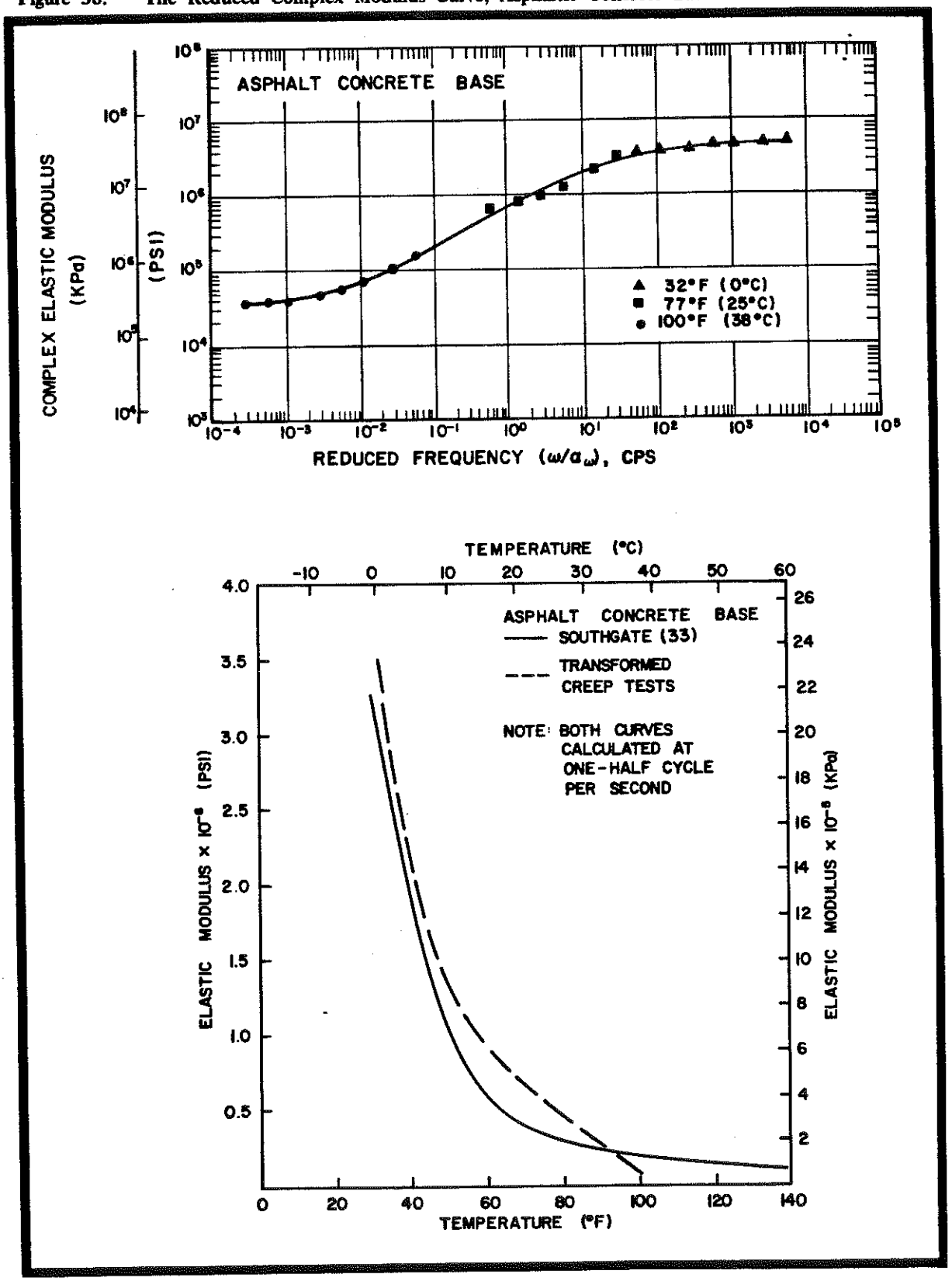

Figure 37. Elastic Modulus versus Temperature at One-Half Cycle Per Second, Asphaltic Concrete Base.

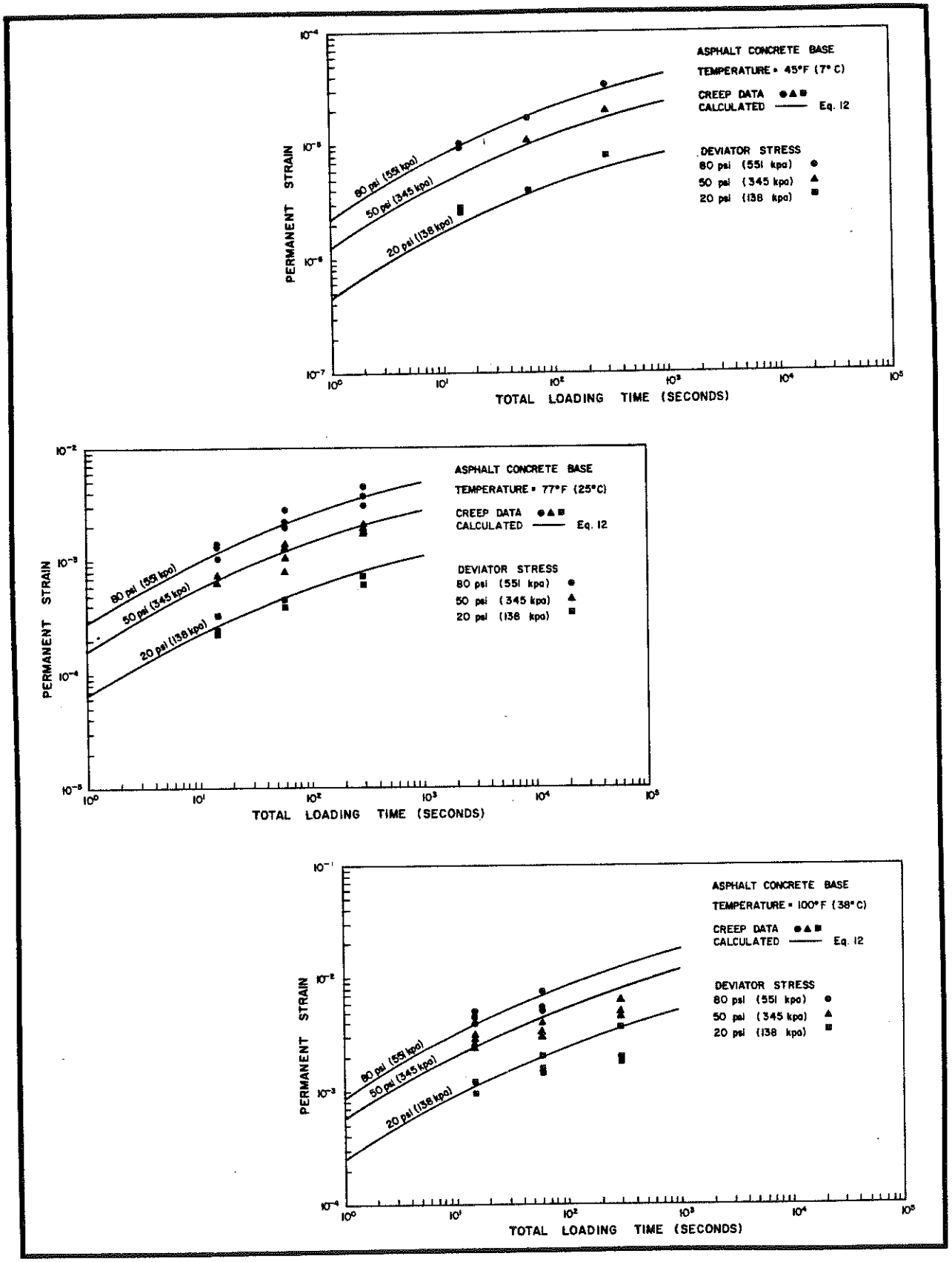

Figure 38. Comparison of Permanent Strain Calculated from Creep Tests and Repeated-Load Tests, Asphaltic Concrete Base.

Young's modulus, calculated as described in the section on the resonant column, is plotted in Figure 39 as a function of temperature. The modulus values at 77°F (25°C) and 100°F (37.8°C) appear valid; however, at 50°F (10.0°C) and below, the measured values are probably lower than the actual material modulus because the resonant frequency of the samples (approximately 1,300 cps) began to approach the resonant frequency of the testing system (1,400 to 1,500 cps). When this situation begins to occur, improper accelerometer readings are displayed as the accelerometers begin to detect spurious vibrations in the system.

Dense-Graded Aggregate

The dense-graded aggregate was crushed limestone from the Tyrone and Oregon (Ordovician) deposits. The gradation of laboratory aggregate and the gradation of aggregate placed at the instrumentation site, in the field, are shown in Figure 40. The laboratory gradation is somewhat finer because particles larger than 0.75 inch (19 mm) could not be accommodated in the equipment. Therefore, particles larger than 0.75 inch (19 mm) were discarded. Intuitively, these gradations would exhibit some differences in behavior; however, in view of data to be reported by Newberry *(25)*, this difference would appear to be very small. All data and properties reported herein refer to the laboratory gradation.

To prepare samples at various moisture contents, it was necessary to determine the moisture-density relationship according to AASHTO Standard T-180. The maximum dry density was 150 pounds per cubic foot (2403 kg/m^3); optimum moisture content was 4.7 percent (Figure 41).

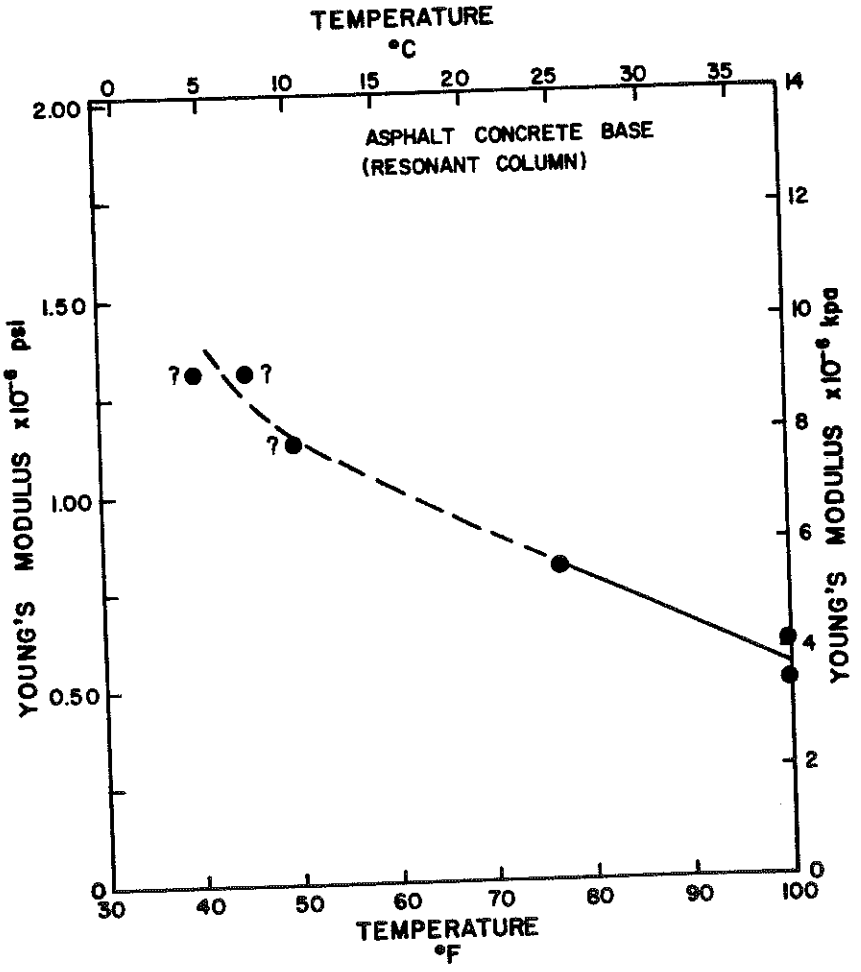

Figure 39. Young's Modulus as a Function of Temperature from the Resonant Column, Asphaltic Concrete Base.

Figure 40. Gradation of the Dense-Graded Aggregates Used in this Study.

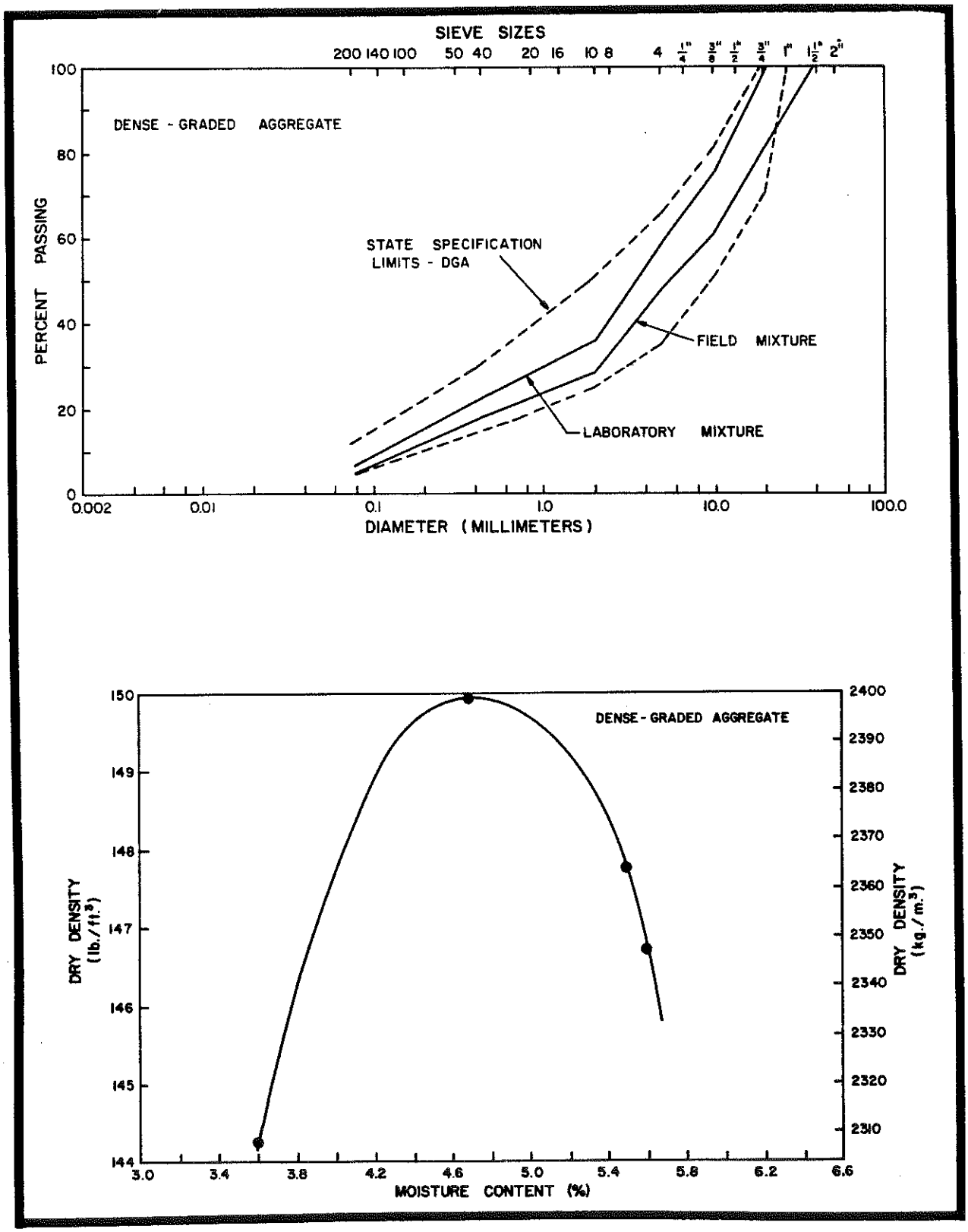

Figure 41. Moisture-Density Relationship, Dense-Graded Aggregate.

Although most base courses do not appear to fail by the Mohr-Coulomb theory of shear failure *(32)*, nine triaxial tests were run at a strain of 0.03 percent per minute to determine shear strength parameters for a bearing capacity analysis. Three moisture contents (1.7, 3.6, and 5.3 percent) were tested. Also, three confining pressures of 10 psi (69 kPa), 20 psi (138 kPa), and 30 psi (207 kPa) were tested at each moisture content. All specimens were compacted in a split mold at optimum moisture content (AASHTO T-180). The samples were 3 inches (76.2 mm) in height by 2 inches (50.8 mm) in diameter.

Triaxial samples which were to be tested at moisture contents less than optimum were air dried and weighed periodically until the desired moisture content was reached. The specimens tested at moisture contents higher than optimum were placed in the test chamber immediately after compaction. Attempts were made then to "de-air" the "wet" samples and to increase the degree of saturation by drawing water into the specimen through pore-pressure lines located at the base of the specimen. Figure 42 shows the relationship between moisture content and degree of saturation for all the specimens tested. The points shown are for all tests at the moisture content immediately after testing.

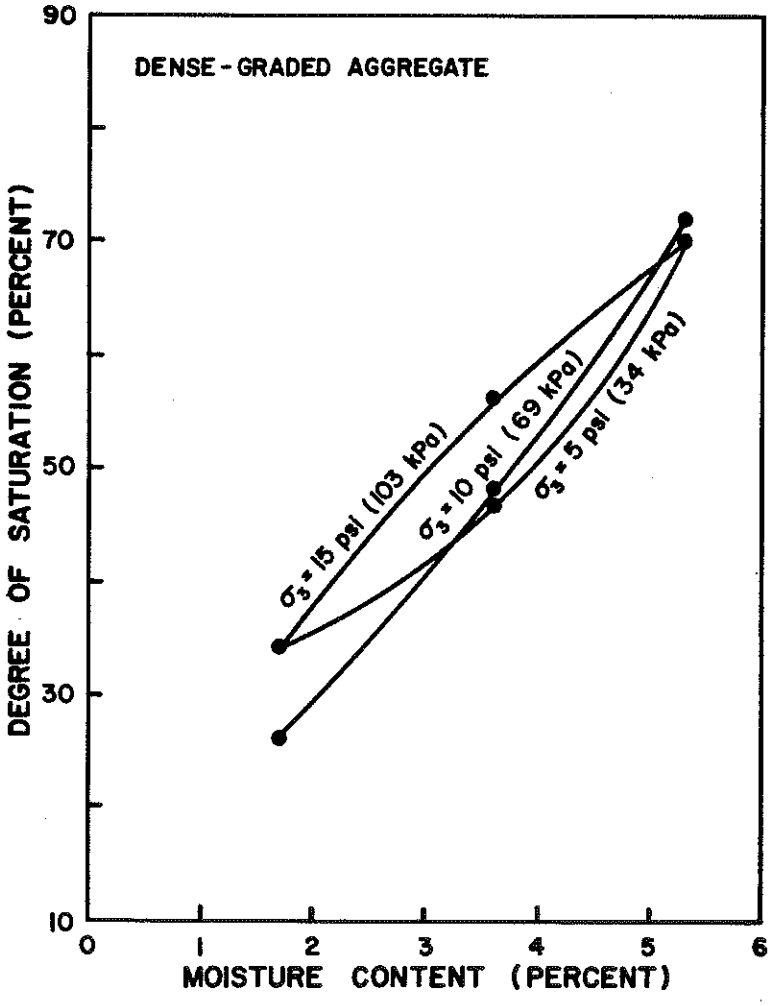

Figure 42. Relationship between Degree of Saturation and Moisture Content, Dense-Graded Aggregate.

As Figure 42 indicates, the triaxial tests were run on partially saturated samples. This complicates the analysis considerably inasmuch as the shear strength is related to the effective stress. This holds true for drained and undrained loading. However, "effective stress" is defined as the "total stress" minus the pore pressure. In a test on partially saturated material, the pore pressure cannot be measured; therefore, effective stress cannot be calculated. The triaxial tests were run unconsolidated-undrained, to approximate field loading conditions, and it is obvious from Figure 43 that a total stress ($\phi = 0$) analysis of triaxial data does not apply to a partially saturated material. Lambe and Whitman *(17)* stated that at lower ranges of confining pressure the material remains partially saturated and effective stress will increase as confining pressure increases. This phenomenon is evident in Figure 44. However, as confining pressure continues to increase, the specimen may become fully saturated and from this point a $\phi = 0$ analysis would apply (Figure 44). The following function has often been used to describe the relationship between undrained strength and "total stress"

$$\tau_f = C_u + \sigma_f \tan \phi_u \qquad 23$$

where τ_f = shear stress at failure,
σ_f = normal stress at failure,
C_u = "total stress" cohesion, and
ϕ_u = "total stress" friction angle.

Values of C_u and ϕ_u depend largely upon the range of σ_f that is of interest, and care should be taken to duplicate field conditions when evaluating the undrained strength of a partially saturated material *(17)*. Therefore, it appears that the values of C_u and ϕ_u in Figure 43 can be used in a shear strength analysis if not extrapolated beyond the range of conditions used in this study.

Several creep tests were attempted on the dense-graded aggregate. There was a tremendous amount of scatter in the data and no trends were apparent. This, apparently, agrees with statements by others *(6, 7, 11)* that, for load durations and stresses typical of those experienced in-service, time-dependent effects during each load application do not appear to be significant. Although time or creep effects are not observed, some permanent deformation does occur with each load application. Also, others have shown *(9)* the response of dense-graded aggregate to be highly dependent on the state of stress. Consequently, a nonlinear elastic-plastic representation of behavior would appear to be appropriate. Therefore, the most important properties to be determined would be the elastic constitutive properties and the susceptibility to permanent deformation.

The test most often used to determine these properties is the repeated-load axial test. The permanent deformation as well as the resilient modulus can be found from these tests *(32)*. In this study, 27 axially repeated-load tests were performed at the same three moisture contents used in the triaxial testing program. The repeated-load specimens were prepared in exactly the same manner as the triaxial specimens. They were run at confining pressures of 5 psi (34 kPa), 10 psi (69 kPa), and 15 psi (103 kPa). In addition, at each confining pressure, deviator stresses of 10 psi (69 kPa), 20 psi (138 kPa), and 30 psi (207 kPa) were used. Again, the samples were run unconsolidated-undrained and partially saturated. Because time effects were not considered significant, only one pattern of loading and unloading was attempted for all tests. The load was on for 1 second and off for 1 second.

Figure 43. **Mohr's Failure Envelopes, Dense-Graded Aggregate.**

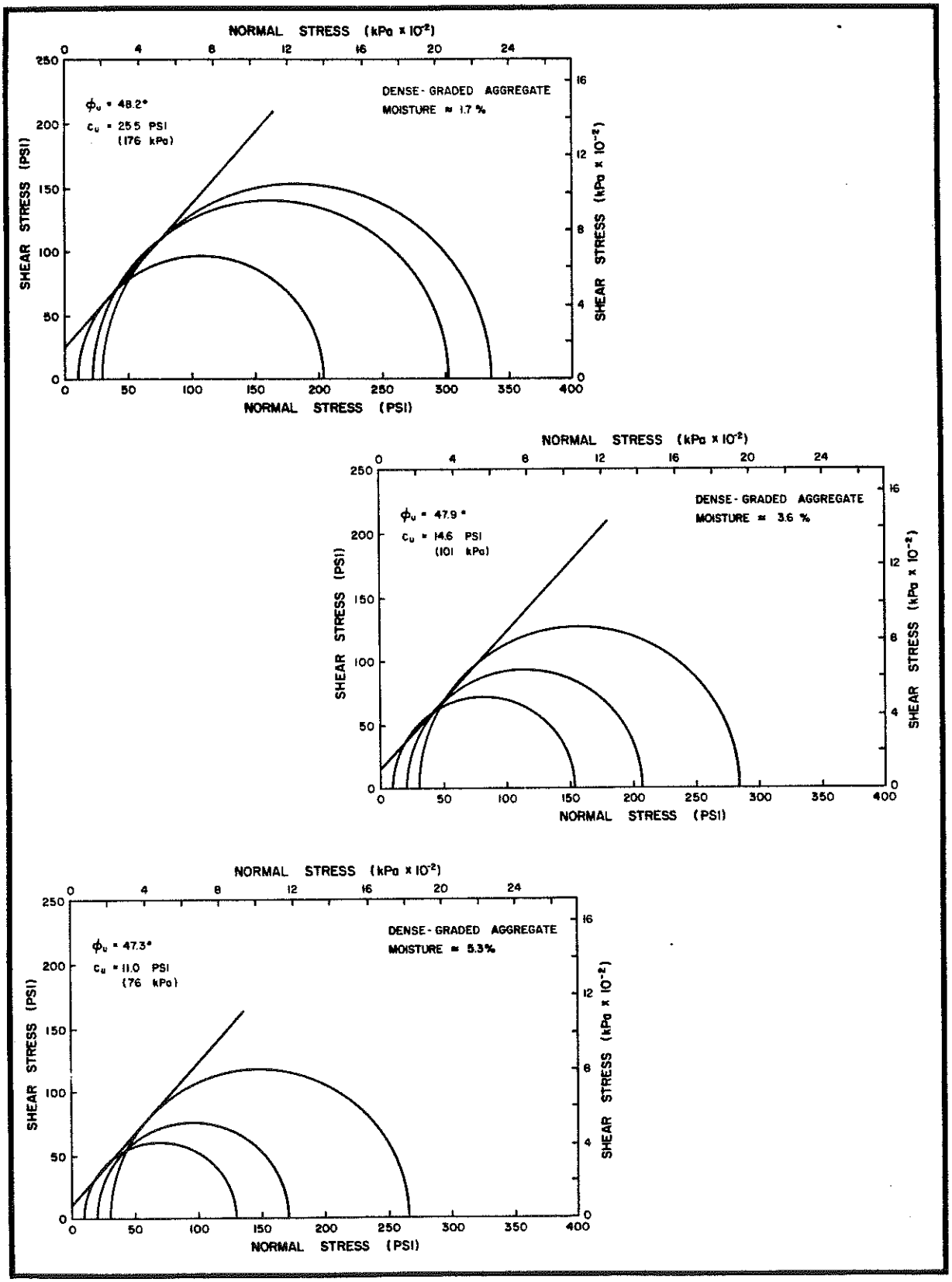

Figure 44. **Behavior of Unconsolidated-Undrained Triaxial Tests on Partially Saturated Material (Reference 17).**

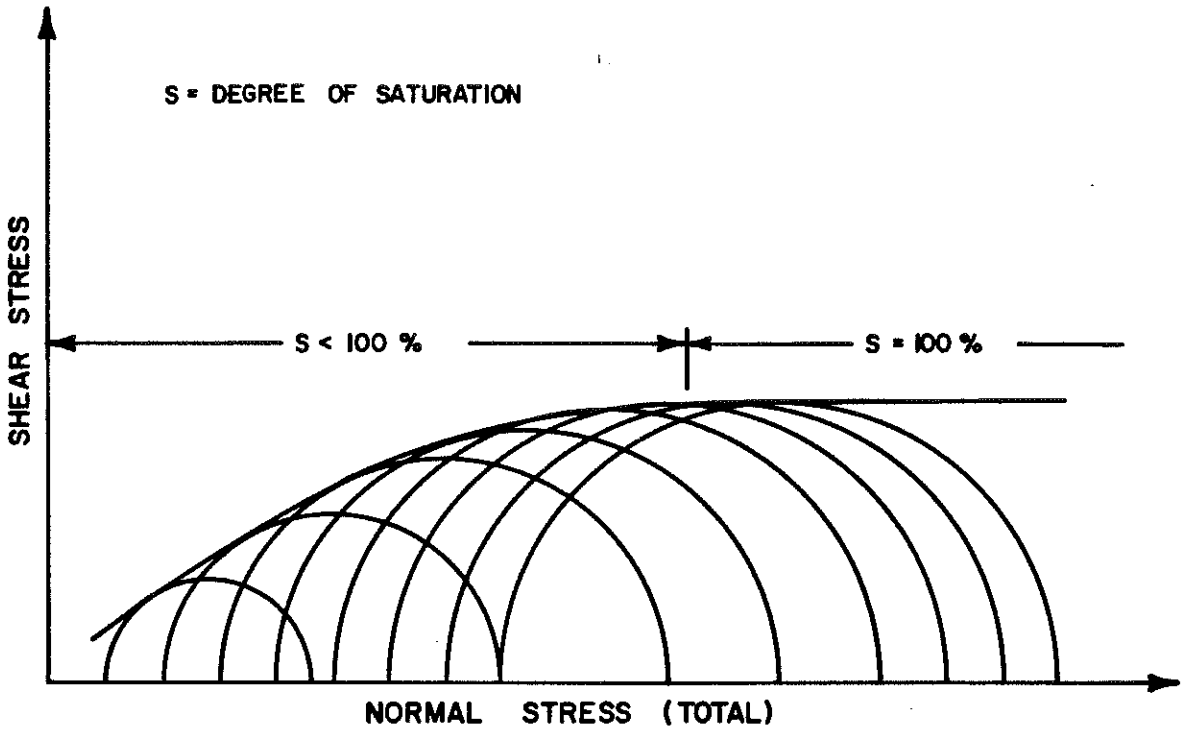

The results of the repeated-load tests are shown in Figures 45 through 47. It is interesting to note that the logarithmic slopes of the data increase with increasing moisture content or degree of saturation. This relationship was expected; however, the magnitude of the initial and early load cycles decreased with increasing moisture content. This was not expected. It appeared, however, that there was some pore-pressure build-up during the test in the "wetter" specimens. This residual pore pressure would (at short loading times) resist compression of the interparticle pores, making the sample appear more elastic in the early cycles of the test. However, the rate of accumulation of permanent deformation from cycle to cycle was greater for the "wetter" specimens (steeper slope) because of the "lubricating" effect of the pore fluid.

An empirical equation describes the data shown in Figures 45 through 47. The data for each test were analyzed using a least squares regression analysis to obtain a logarithmic slope for that particular test. The slope values for the nine tests run at each moisture content were averaged to give one slope value for each moisture content. These three average slope values were plotted as a function of moisture content, and an equation describing the change in slope with moisture content was derived. In addition, equations to determine the magnitude of the permanent strain after the initial load cycle was obtained in much the same way. The equation describing the slope and those describing the magnitude of strain after the initial load were then added to give the following:

$$\log \epsilon_p = \Big[\Big\{ [-3.27577 - 0.00042\ (10^{0.63\ W})] + [0.02356 + 0.0000265\ (10^{0.565\ W})]\,\sigma_1 \Big\} - \Big\{ (0.071\ W)\ (\log \sigma_3) \Big\} \Big] + \Big[\Big\{ [10^{(-1.699\ +\ 0.2478\ W)}] - [10^{(-4.1739\ +\ 0.4102\ W)_{(\sigma_3)}}] \Big\} \Big\{ \log N \Big\} \Big], \qquad 24$$

where ϵ_p = permanent strain (change in length/initial length),
log = logarithm to the base 10,
W = moisture content (percent),
σ_1 = deviator stress (psi),
σ_3 = confining pressure (psi), and
N = number of deviator stress repetitions (load cycles).

Figure 45. Relationship between Permanent Strain and Number of Deviator Stress Repetitions (Load Cycles) for Dense-Graded Aggregate, Moisture Content ≈ 1.7 percent.

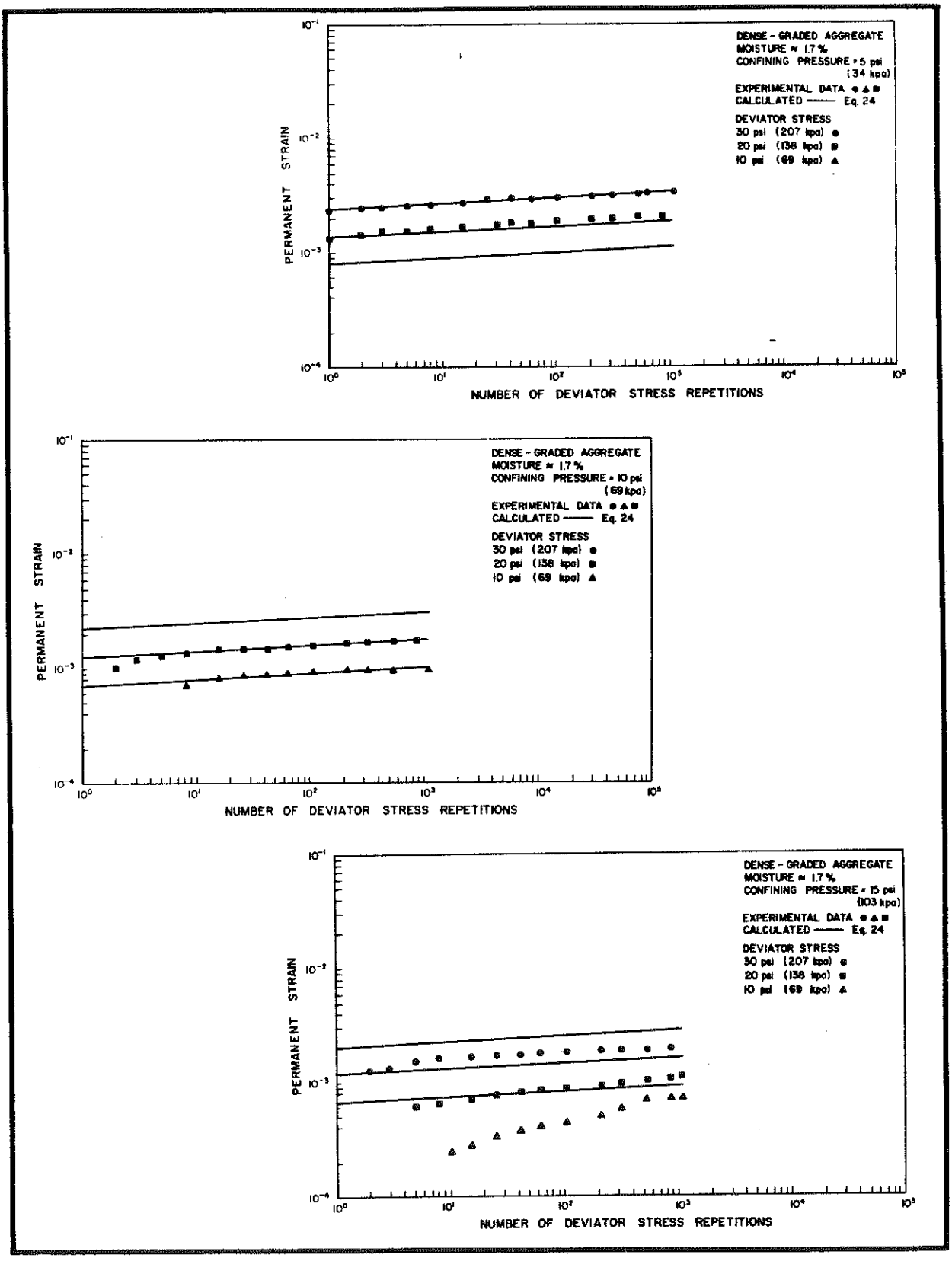

Figure 46. Relationship between Permanent Strain and Number of Deviator Stress Repetitions (Load Cycles) for Dense-Graded Aggregate, Moisture Content ≈ 3.6 percent.

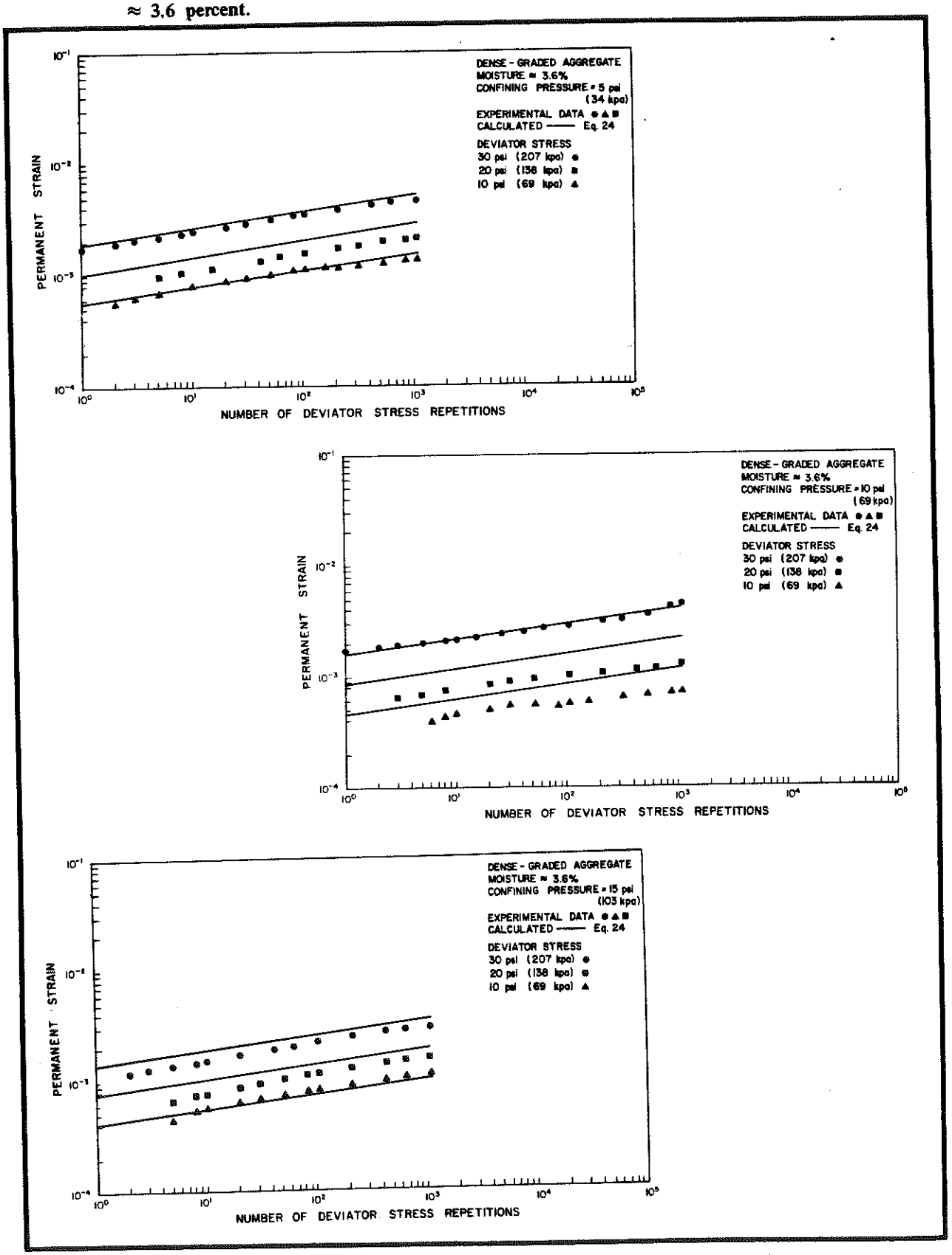

Figure 47. Relationship between Permanent Strain and Number of Deviator Stress Repetitions (Load Cycles) for Dense-Graded Aggregate, Moisture Content ≈ 5.3 percent.

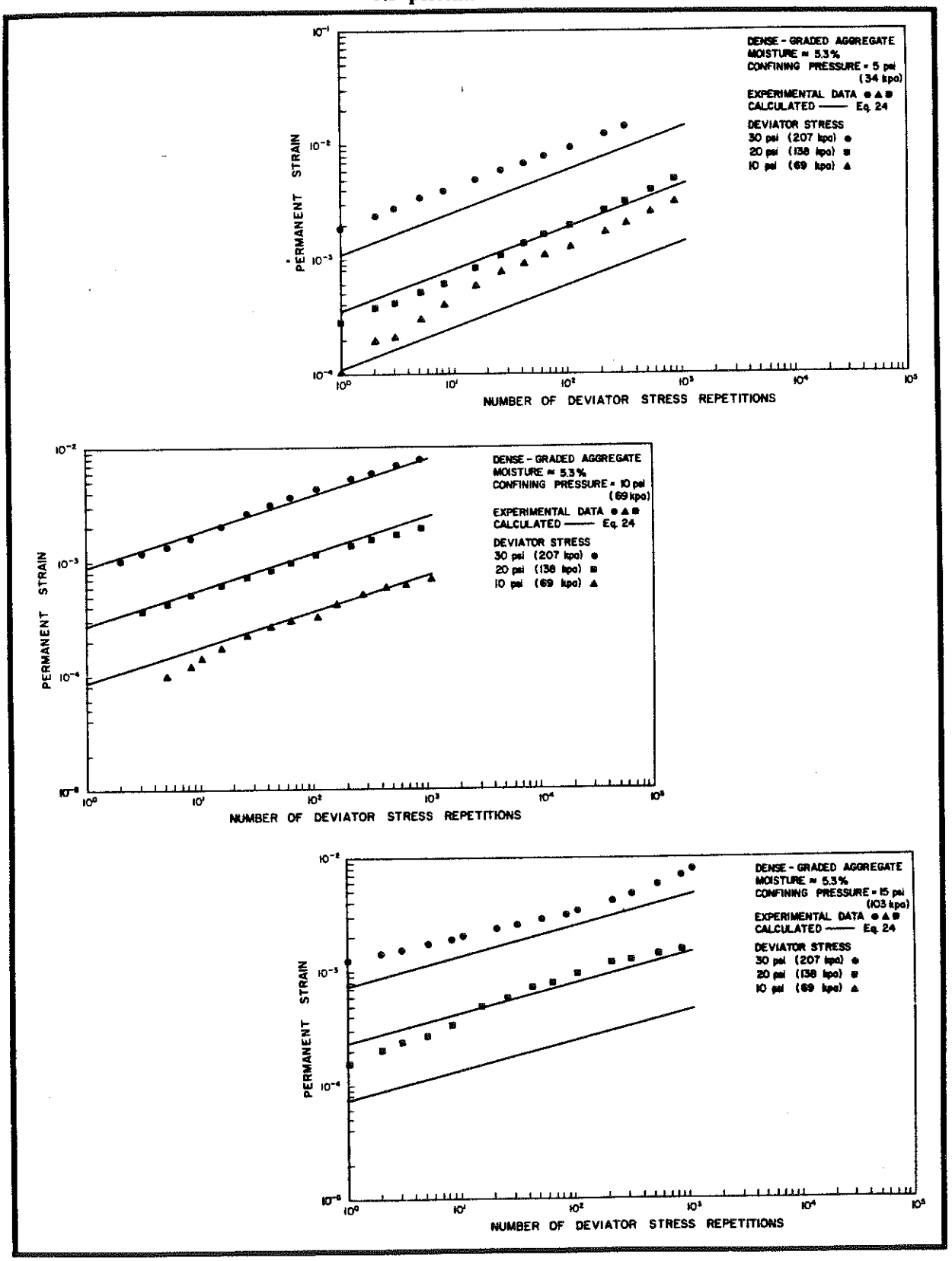

Therefore, given a unique set of conditions (moisture content or degree of saturation, deviator stress, confining pressure, and number of stress repetitions), the permanent strain may be estimated from Equation 24. In most cases, Equation 24 appears to adequately describe the relationship between permanent strain and number of deviator stress repetitions (slope); but in some cases, the permanent strain after the initial stress cycle is not as accurately predicted. Equation 24 has been programmed.

The resilient modulus for dense-graded aggregate is defined as the cyclic stress divided by the cyclic strain. The cyclic strain is defined as that portion of strain that is recovered after removal of each repetition of stress (Figure 48). The strains used in this analysis were taken from the repeated-load tests, previously described. Smith and Nair *(32)* reported that stress sequence, number of load cycles, and load duration have no significant effect on resilient modulus -- an additional reason for using only one loading sequence and pattern on the repeated-load tests in this study. Figure 49 shows the results. There is considerable scatter in the data; however, based on a total stress analysis, it is apparent that the resilient modulus is a function of confining pressure and moisture content or degree of saturation. This agrees with data reported by Hicks and Finn *(12)* and Seed, et al. *(31)* that the resilient modulus decreases with increasing degree of saturation, based on a total stress analysis. An estimate of the resilient modulus can be calculated from the following equation derived empirically from the data in Figure 49:

$$\log M_r = (5.4624 - 2.729 \log W) + (0.175 + 1.19 \log W)(\log \sigma_3) \qquad 25$$

where M_r = resilient modulus (psi),
log = logarithm to the base 10,
W = moisture content (percent), and
σ_3 = confining pressure (psi).

One resonant column test was run on a dense-grade aggregate specimen at four percent moisture content. The specimen was 5.35 inches (136 mm) in height and 2.79 inches (71 mm) in diameter and was tested at confining pressures of 5 psi (34 kPa), 10 psi (69 kPa), and 15 psi (103 kPa). The results are plotted in Figure 49. Again, because of extremely low stress values, Young's modulus from the resonant column is considerably higher than the resilient modulus for comparable conditions of moisture and confining pressure.

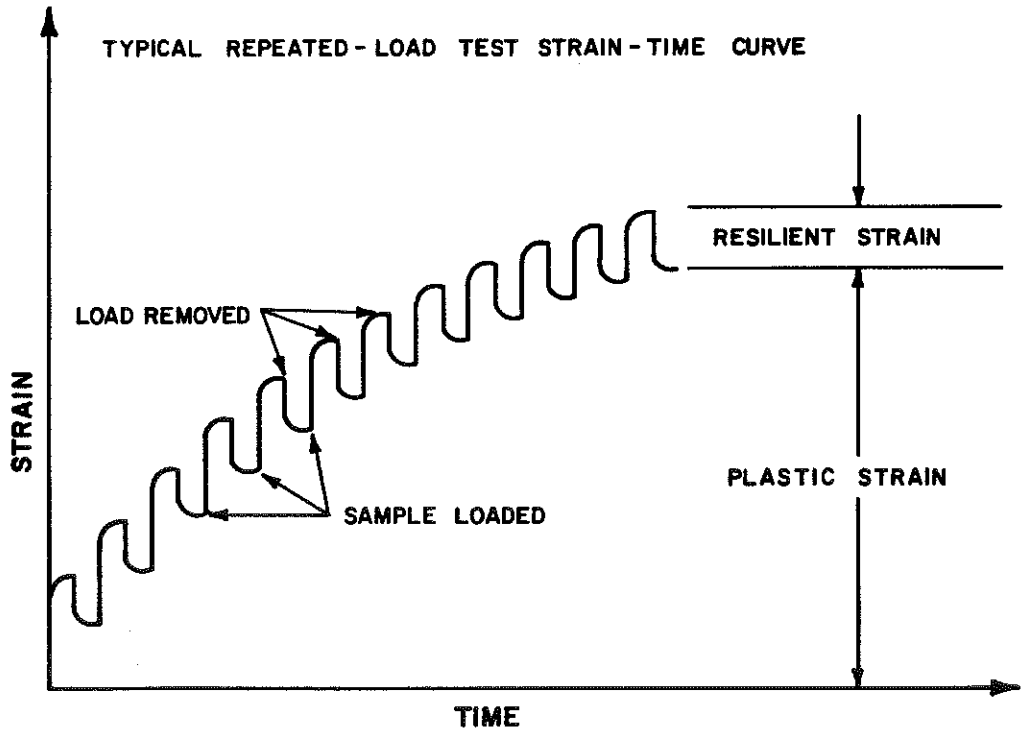

Figure 48. Typical Strain-Time Curve for Repeated-Load Tests.

Figure 49. Resilient Modulus as a Function of Confining Pressure and Moisture Content, Dense-Graded Aggregate.

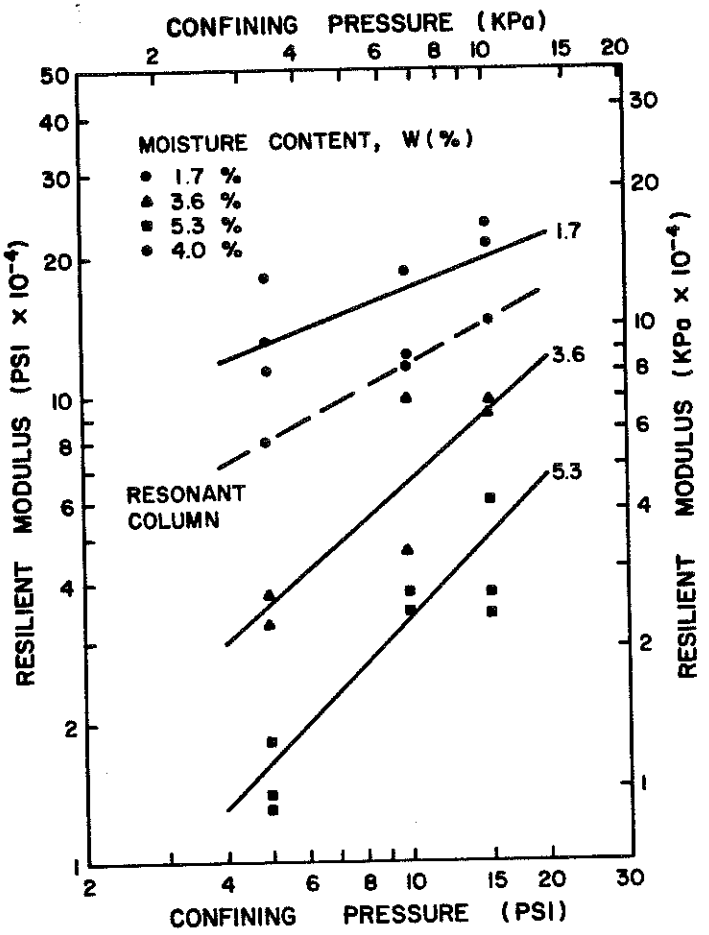

Subgrade Material

Samples of the subgrade were collected at Station 141 + 50. Figure 50 shows the gradation. Approximately 32 percent of the material was larger than 1 inch (25 mm). As in the case of the dense-graded aggregate, all particles larger than 0.75 inch (19 mm) were discarded and testing was performed on the minus 0.75-inch (19-mm) material. As previously stated, the subgrade contained 20 to 30 percent clay shales that were susceptible to "breakdown" under handling, wetting, and drying. This caused some problems in testing because mixing and compaction produced considerable "breakdown", thus changing the gradation. Although attempts were made to minimize this problem, some "breakdown" was assumed to be unavoidable.

Results of the moisture-density test (AASHTO T-180) are shown in Figure 51. The maximum dry density was 130.8 pounds per cubic foot (2,093 kg/m^3) at an optimum moisture of 9.7 percent. This was used in compacting all other subgrade test specimens.

The shear strength parameters were determined from nine triaxial tests that were run unconsolidated and undrained at three moisture contents (approximately 2, 10, and 14 percent). Three confining pressures of 5 psi (34 kPa), 10 psi (69 kPa), and 20 psi (138 kPa) were used at each moisture content. The specimens were strained at a rate of 0.03 percent per minute. All specimens were compacted at optimum conditions; however, those at 2 percent moisture were allowed to air dry seven days before testing; and those tested at 14 percent moisture were subjected to a back pressure for several minutes, to increase the degree of saturation, before testing. The tests at 10 percent moisture were run immediately after compaction.

Figure 50. Gradation of Subgrade Sample from Station 141 + 50 on KY 627, Clark County.

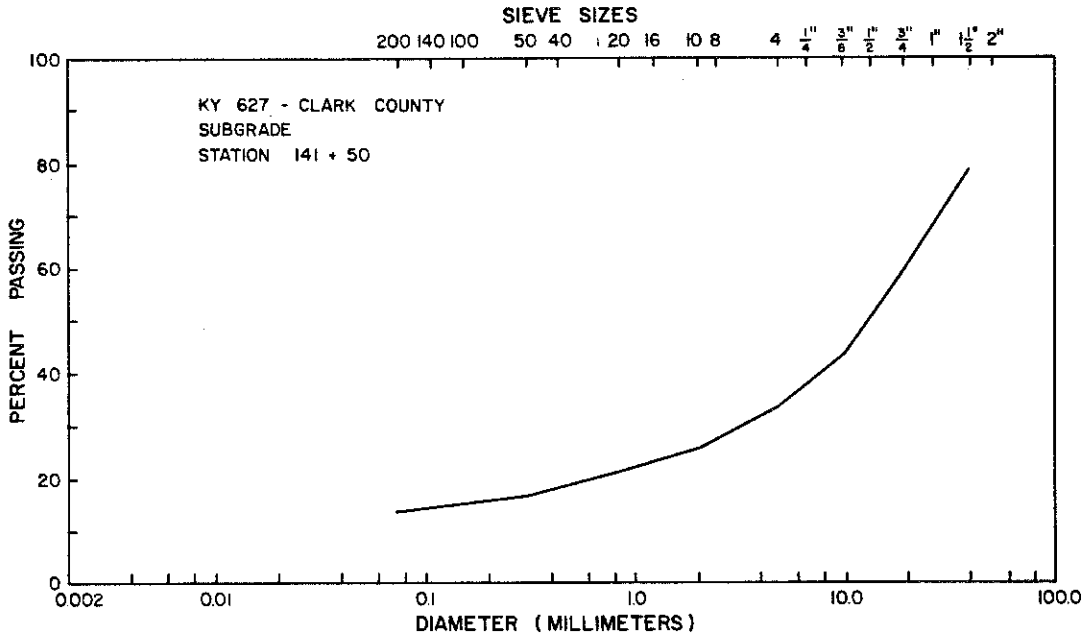

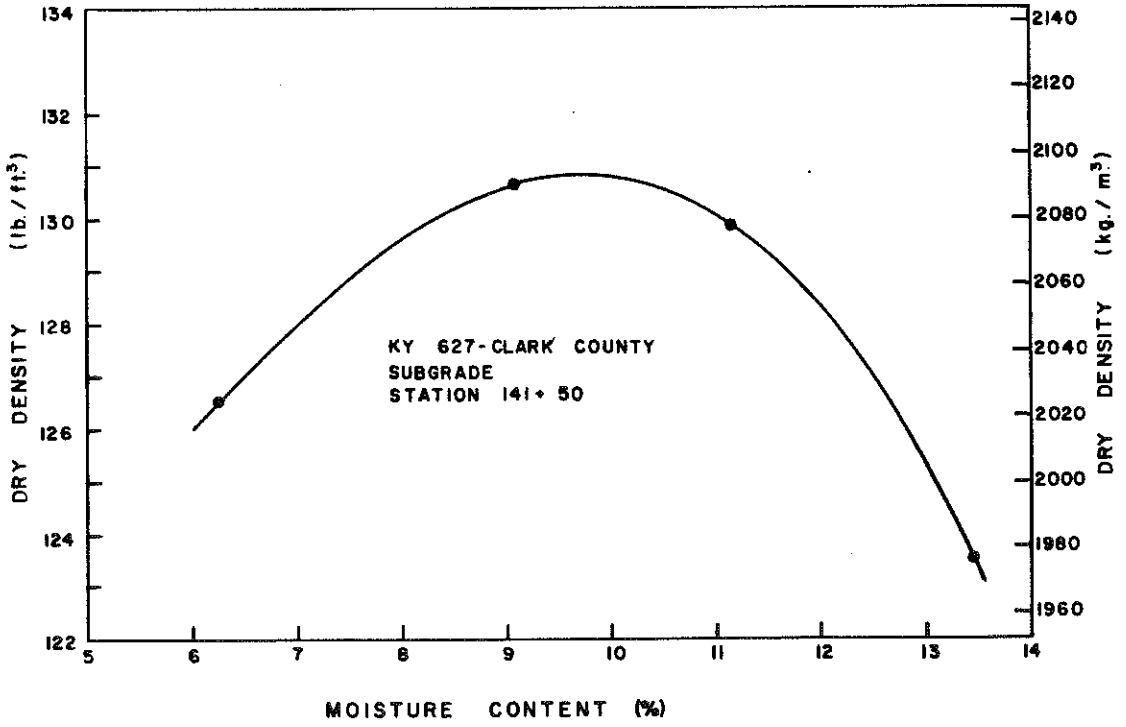

Figure 51. Moisture-Density Relationship, Subgrade.

The results of those triaxial tests are shown in Figure 52. The decrease in the internal friction angle, ϕ, with increasing moisture content indicates the specimens are approaching 100 percent saturation, where ϕ would be zero. However, because these specimens were also partially saturated, as in the case of the dense-graded aggregate, the results should not be extrapolated beyond the range of test conditions.

Approximately 100 creep tests were performed to determine the rheological behavior of the subgrade material. Figure 53 is an example of one set of data showing the relationship between permanent strain and time of loading. The material does not appear to exhibit time-dependent behavior; this seems so because there is, apparently, no correlation with loading time. Consequently, no further analysis was attempted.

To develop a permanent deformation model for the subgrade, a number of repeated-load, triaxial tests were attempted. Two series of specimens were tested: one at 8.2 percent moisture and the other at 9.4 percent. Three confining pressures [5 psi (34 kPa), 10 psi (69 kPa), and 15 psi (103 kPa)] were used in each series. At least three specimens were tested at each confining pressure with deviator stresses of 2.5 psi (17 kPa), 5 psi (34 kPa), and 10 psi (69 kPa). The rest of the procedure for the repeated-load tests is identical to that used for the dense-graded aggregate. There was considerable scatter in the data, and the results were not very repeatable. This was attributed largely to the high degree of variability of the material.

Results of the repeated-load tests are shown in Figures 54 and 55. Because of the scatter, each curve in these figures is an average of two or more tests; and, for this reason, no data points are shown. A permanent deformation model was derived for the subgrade material using a linear regression analysis on points taken from these average curves. The result is the following equation:

26

$$\log \epsilon_p = C_3 (\log N)^3 + C_2 (\log N)^2 + C_1 (\log N) + C_0$$

where
- ϵ_p = permanent strain (change in length/initial length),
- C_o = $[(-6.5 + 0.38\ W) - (1.1 \log \sigma_3)] + [1.86 \log \sigma_1]$,
- C_1 = $10^{(-1.1 + 0.1\ W)}$,
- C_2 = $-0.018\ W$,
- C_3 = $0.007 + 0.001\ W$,
- N = number of deviator stress repetitions,
- W = moisture content (percent),
- σ_1 = deviator stress (psi), and
- σ_3 = confining pressure (psi).

This model will provide only an estimate of permanent deformation, because of the variability of the original data. Caution should be used when strains approach failure (at approximately 10 percent). Equation 26 has been programmed.

The resonant column test was run on four specimens, each at a different moisture content (2, 6, 7.5, and 10 percent). The specimens were prepared in the same way as in the repeated-load tests. Each specimen was tested at three confining pressures: 5 psi (34 kPa), 10 psi (69 kPa), and 20 psi (138 kPa). The results are shown in Figure 56. Unlike the dense-graded aggregate, the subgrade material exhibited a wide range of values for Young's modulus as the moisture content varied. The specimens became overconsolidated as the moisture content decreased from the moisture content at compaction (9.7 percent). An estimate of Young's modulus can be obtained from the following empirical relationship:

27

$$E = C_3 W^3 + C_2 W^2 + C_1 W + C_0$$

where
- E = Young's modulus,
- C_0 = $266\ \sigma_3 + 214{,}900$,
- C_1 = $-38.3\ \sigma_3 + 9{,}315$,
- C_2 = $13.85\ \sigma_3 - 22$,
- C_3 = $0.04\ \sigma_3 + 103$,
- W = moisture content (percent), and
- σ_3 = confining pressure (psi).

Equation 27 was derived from a linear regression analysis performed on the data in Figure 56. This equation should not be used for values of moisture content above 10 percent; the calculated values of modulus will become negative.

Figure 52. Mohr's Failure Envelopes, Subgrade.

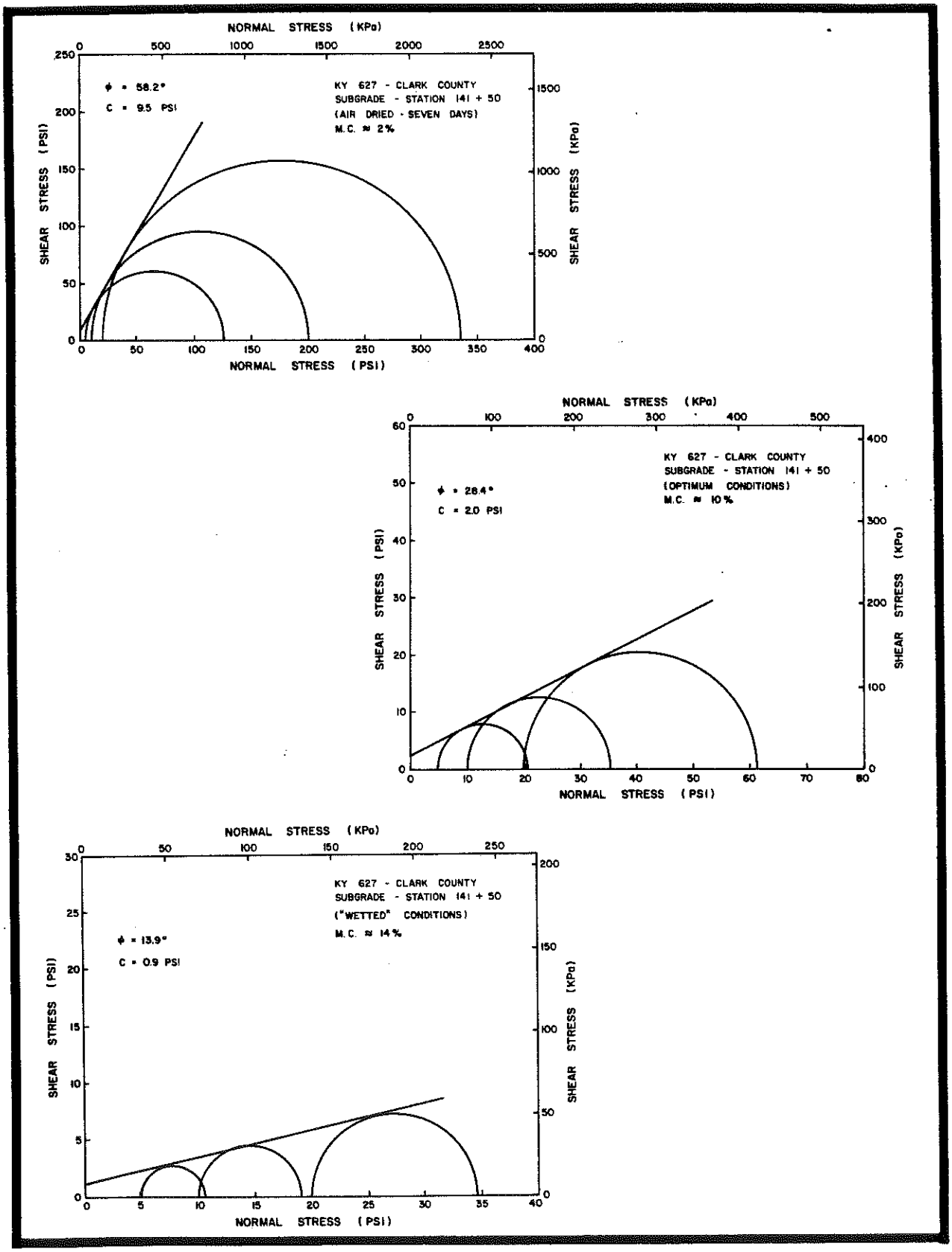

Figure 53. Relationship between Permanent Strain and Loading Time from the Creep Tests, Subgrade.

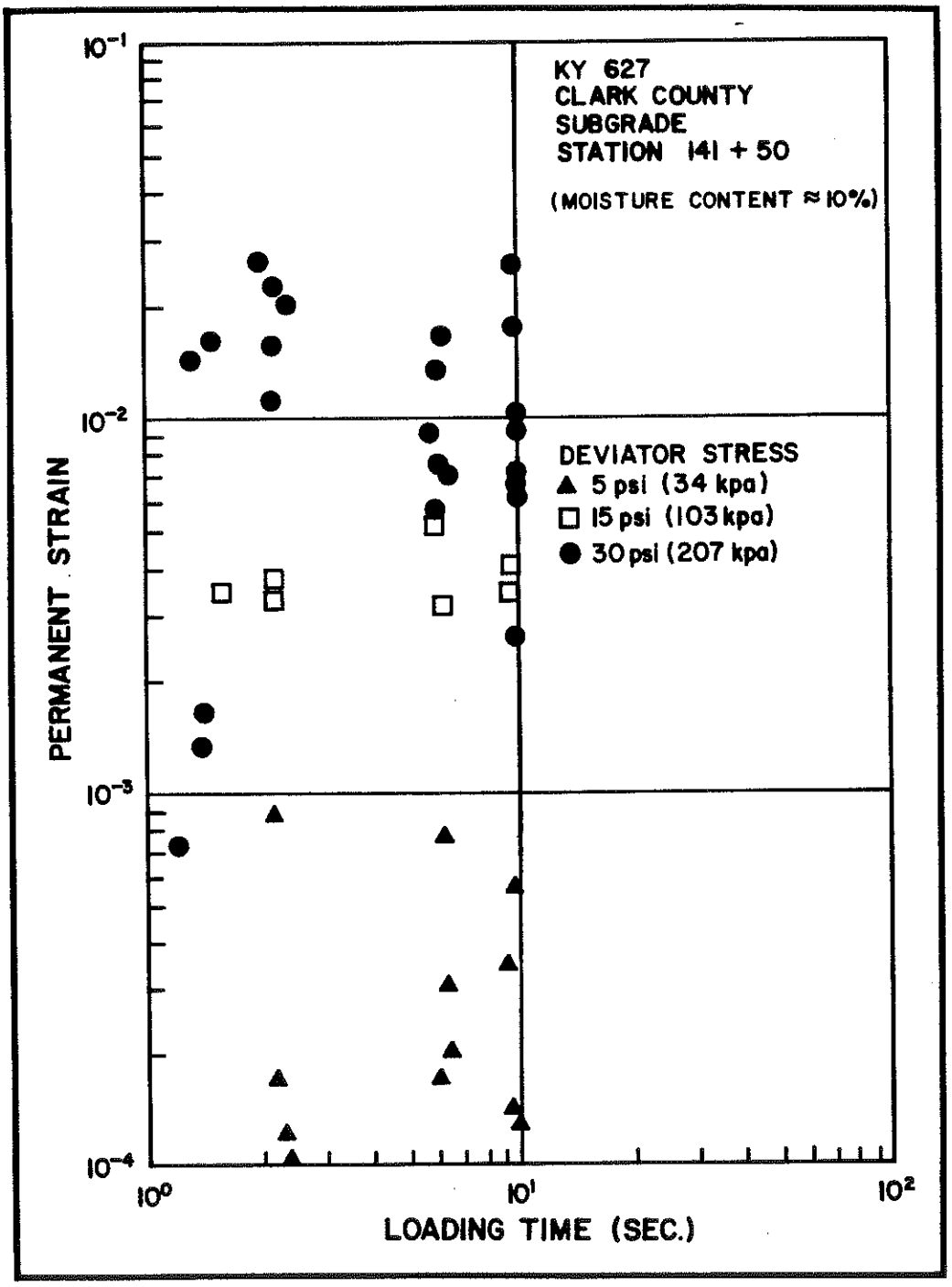

Figure 54. **Relationship between Permanent Strain and Number of Deviator Stress Repetitions (Load Cycles) for the Subgrade, Moisture Content ≈ 8.2 percent.**

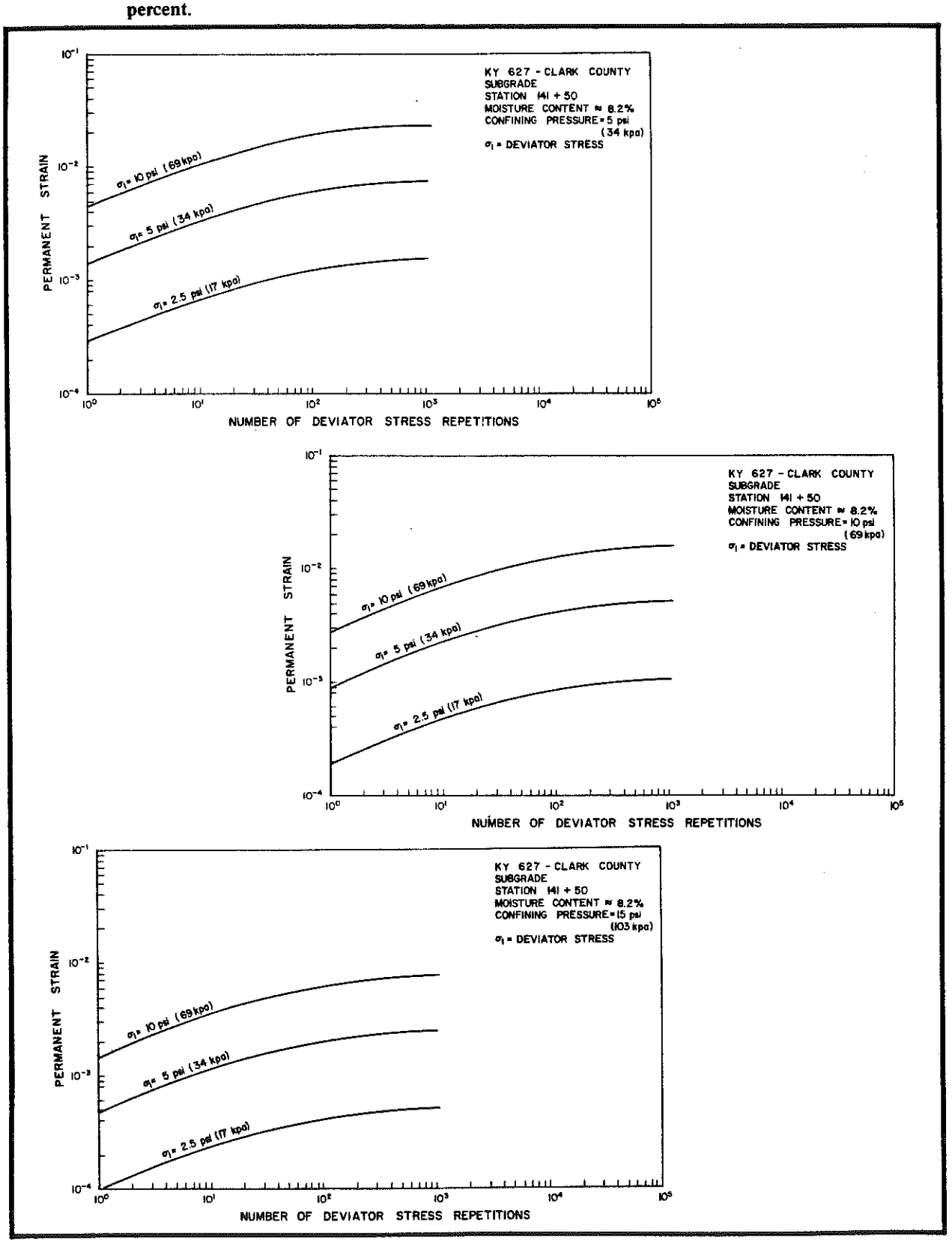

Figure 55. **Relationship between Permanent Strain and Number of Deviator Stress Repetitions (Load Cycles) for the Subgrade, Moisture Content ≈ 9.4 percent.**

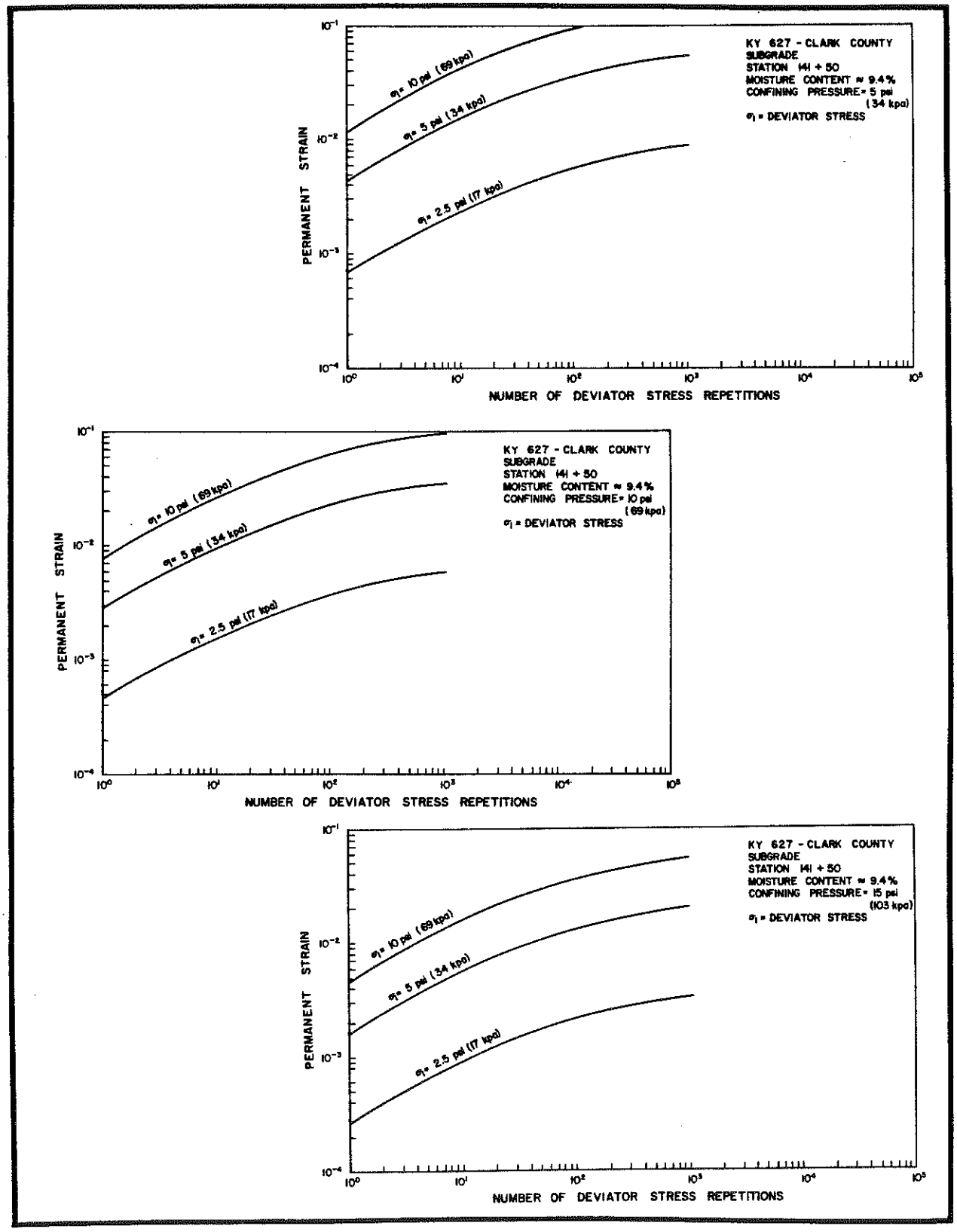

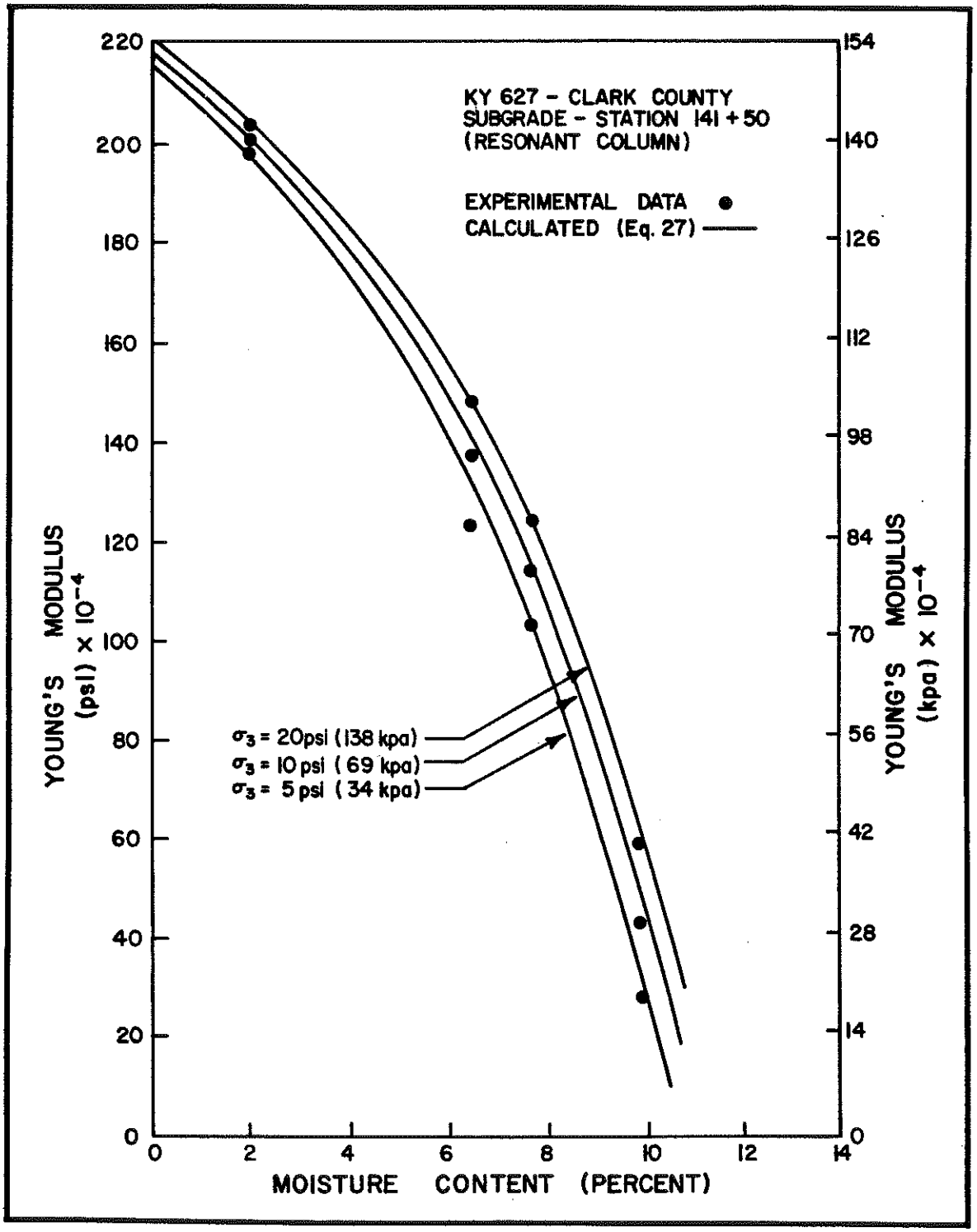

Figure 56. Young's Modulus, Calculated from the Resonant Column, as a Function of Moisture Content, Subgrade.

FUTURE RESEARCH AND IMPLEMENTATION

The models developed in this study (Equations 12, 24, and 26) will be used to construct rutting damage estimate for Station 141 + 50 in Clark County. Future work will require the development of traffic and environmental models from data obtained from temperature, weight, and traffic instrumentation installed in Clark County. The damage, traffic, and environmental models will be used with the CHEVRON computer program (using modulus values reported herein) to estimate rut depths. These will be compared to actual field measurements.

The pavement cross-section at Station 141 + 50 will be checked for stability against shear failure using the shear strength parameters included in this report. A computer program is presently under development.

A new instrumentation site in Taylor County is anticipated. This will provide data supplemental to that already available from the present site in Clark County. In addition, it is anticipated that some effort will be used to develop a behavioral model for asphaltic concrete using a somewhat more theoretical approach. This would be, to a degree, based upon work done previously by Allen *(2)*. If successful, attempts would be made to compare theoretical results with permanent strains reported herein. The permanent deformation models must be verified; they will doubtlessly be revised and refined; they must be more generalized; and their use must be simplified.

CONCLUSIONS

1. The deflection gages installed at Station 141 + 50 in Clark County appear to work well and provide reasonable results.

2. Creep tests may provide a reasonable approximation of complex modulus and a good approximation of permanent strain for asphaltic concrete base.

3. The asphaltic concrete base tested in this study exhibited nonlinear, plastic behavior.

4. The relationship between permanent strain and number of load cycles or total load time, for asphaltic concrete base, may be described by a third-degree polynomial.

5. The deformations of the dense-graded aggregate are not significantly time-dependent.

6. Apparently, the most influential factor affecting the relationship between permanent strain and number of load cycles, for dense-graded aggregate, is the quantity of moisture present.

7. The magnitude of the resilient modulus is largely dependent on moisture content and confining stress.

8. The subgrade material exhibited little or no time-dependent behavior.

9. The resonant column will not provide accurate values for Young's modulus when testing asphalts at low temperature.

REFERENCES

1. Allen, D. L.; *A Rheological Study of Cohesive Soils,* Division of Research, Kentucky Department of Highways, September 1972.

2. Allen, D. L.; *Stiffness of Solid-Liquid Mixtures: Theoretical Considerations,* Division of Research, Kentucky Bureau of Highways, January 1977.

3. Barenberg, E. J.; and Thompson, M. R.; *Behavior and Performance of Flexible Pavements Evaluated in the University of Illinois Test Track,* **Highway Engineering Series No. 36,** University of Illinois, January 1970.

4. Barksdale, R. D.; *Repeated Load Test Evaluation of Base Course Materials,* GHD Research Project No. 7002, Georgia Institute of Technology, 1972.

5. Barksdale, R. D.; and Miller, J. H.; *Development of Equipment and Techniques for Evaluating Fatigue and Rutting Characteristics of Asphalt Concrete Mixes,* Research Project No. 7305, Georgia Department of Transportation, 1977.

6. Coffman, B. S.; *Pavement Deflections from Laboratory Tests and Layer Theory,* **Proceedings,** Second International Conference on Structural Design of Asphalt Pavements, 1967.

7. Coffman, B. S.; Kraft, D. G.; and Tamayo, J.; *A Comparison of Calculated and Measured Deflections for the AASHO Test Road,* **Proceedings,** The Association of Asphalt Paving Technologists, 1964.

8. Drake, W. B.; and Havens, J. H.; *Re-evlauation of the Kentucky Flexible Pavement Design Criterion,* Division of Research, Kentucky Department of Highways, January 1959 (Published in **Bulletin No. 52,** Engineering Experiment Station, University of Kentucky, Vol 13, No. 4, June 1959).

9. Dunlap, W. A.; *A Report on a Mathematical Model Describing the Deformation Characteristics of Granular Materials,* Technical Report No. 1, Project 2-8-62-27, Texas Transportation Institute, 1963.

10. Ferry, J. D.; **Viscoelastic Properties of Polymers,** John Wiley and Sons, Inc., New York, 1961.

11. Hicks, R. G.; *Factors Influencing the Resilient Properties of Granular Materials,* Ph.D. Thesis, University of California, Berkeley, 1970.

12. Hicks, R. G.; and Finn, F. N.; *Analysis of Results from the Dynamic Measurements Program on the San Diego Test Road,* **Proceedings,** The Association of Asphalt Paving Technologists, 1970.

13. Hopkins, T. C.; and Deen, R. C.; *Mercury-Filled Settlement Gage,* Division of Research, Kentucky Department of Highways, December 1972.

14. Hopkins, T. C.; and Deen, R. C.; *Mercury-Filled Settlement Gage,* **Record No. 457,** Transportation Research Board, 1973.

15. Kallas, B. F.; and Riley, J. C.; *Mechanical Properties of Asphalt Pavement Materials,* **Proceedings,** Second International Conference on Structural Design of Asphalt Pavements, 1967.

16. Lai, J. S.; and Anderson, D.; *Irrecoverable and Recoverable Nonlinear Viscoelastic Properties of Asphalt Concrete,* **Record 468,** Transportation Research Board, 1973.

17. Lambe, W. T.; and Whitman, R. V.; **Soil Mechanics,** John Wiley and Sons, Inc., New York, 1969.

18. Lissajous, J. A.; *Memoire Sur L'etude Optique des Mouvements Vibratories,* **Annales de Chimie,** 3rd Ser., 51 (1857), pp. 147-231.

19. Lister, N. W.; and Mayo, A. P.; *A Gauge for the Measurement of Transient and Long Term Displacements in Road Pavements,* Road Research Laboratory, Ministry of Transport, Report LR 353, 1970.

20. McLean, D. B.; and Monismith, C. L.; *Estimation of Permanent Deformation in Asphalt Concrete Layers due to Repeated Traffic Loading,* **Record 510,** Transportation Research Board, 1974.

21. Monismith, C. L.; and Secor, K. E.; *Analysis of Triaxial Test Data on Asphalt Concrete Using Viscoelastic Principles,* **Proceedings,** Fortieth Annual Meeting, Highway Research Board, Vol 40, 295, 1961.

22. Monismith, C. L.; Hicks, R. G.; and Salam, Y. M.; *Basic Properties of Pavement Components,* Report No. FHWA-RD-72-19, Federal Highway Administration, September 1971.

23. Morris, J.; and Haas, R. C. G.; *Dynamic Testing of Bituminous Mixtures for Permanent Deformation Response,* **Fatigue and Dynamic Testing of Bituminous Mixtures,** STP 561, American Society for Testing and Materials, 1974, pp. 115-131.

24. Mossbarger, W. A.; *A Rheological Investigation of Asphaltic Materials,* Division of Research, Kentucky Department of Highways, January 1964.

25. Newberry, D. C.; *Gradation and Compaction Effects on Performance of Crushed Stone Base Courses,* (to be issued), Division of Research, Kentucky Bureau of Highways, 1978.

26. Pagen, C. A.; *Rheological Response of Bituminous Concrete,* **Bulletin 67,** Highway Research Board, 1965.

27. Papazian, H. S.; *The Response of Linear Viscoelastic Materials in the Frequency Domain,* Report No. 172-2, Transportation Engineering Center, Engineering Experiment Station, Ohio State University, 1961.

28. Saal, R. N.; and Labout, J. W. A.; *Rheological Properties of Asphalts,* **Rheology-Theory and Applications,** F. R. Eirich, Editor, Vol 2, Academic Press, Inc., New York, 1958.

29. Saraf, C. L.; and Majidzadeh, K.; *Dynamic Response and Fatigue Characteristics of Asphalt Mixtures,* **Fatigue and Dynamic Testing of Bituminous Mixtures,** ASTM STP 561, American Society for Testing and Materials, 1974, pp. 95-114.

30. Scott, G. D.; *Rheological and Ultimate Strength Properties of Cohesive Soils,* Division of Research, Kentucky Department of Highways, February 1969.

31. Seed, H. B.; Mitry, F. G.; Monismith, C. L.; and Chan, C. K.; *Prediction of Flexible Pavement Deflections from Laboratory Repeated Load Tests,* **NCHRP Report 35,** Highway Research Board, 1967.

32. Smith, W. S.; and Nair, K.; *Development of Procedures for Characterization of Untreated Granular Base Course and Asphalt-Treated Base Course Materials,* Report No. FHWA-RD-74-61, Federal Highway Administration, October 1973.

33. Southgate, H. F.; *An Evaluation of Temperature Distribution within Asphalt Pavements and Its Relation to Pavement Deflections,* Division of Research, Kentucky Department of Highways, April 1968.

34. Terrel, R. L.; Awad, I. S.; and Foss, L. R.; *Investigating Stress-Strain Characteristics of Asphalt-Treated Materials,* **Closed Loop,** MTS Corporation, Fall-Winter 1973, pp. 3-14.

35. Terrel, R. L.; Awad, I. S.; and Foss, L. R.; *Techniques for Characterizing Bituminous Materials Using a Versatile Triaxial Testing System,* **Fatigue and Dynamic Testing of Bituminous Mixtures,** STP 561, American Society for Testing and Materials, 1974, pp. 47-66.

36. Tons, E.; Goetz, W. H.; and Anderson, V. L.; *Flow in Aggregate-Binder Mixes,* **Proceedings,** The Association of Asphalt Paving Technologists, Vol 39, 1970.

37. Van de Loo, P. J.; *A Practical Approach to the Prediction of Rutting in Asphalt Pavements: The Shell Method,* **Record 616,** Transportation Research Board, 1976.

38. Van der Poel, C.; *Time and Temperature Effects on the Deformation of Asphaltic Bitumens and Bitumen-Mineral Mixtures,* **SPE Journal,** September 1955.

39. Witczak, M. W.; and Root, R. E.; *Summary of Complex Modulus Laboratory Test Procedures and Results,* **Fatigue and Dynamic Testing of Bituminous Mixtures,** STP 561, American Society for Testing and Materials, 1974, pp. 67-94.